UAV Communications: Spectral Requirements, MAV and SUAV Channel Modeling, OFDM Waveform Parameters, Performance and Spectrum Management

Jaber A. Kakar

Thesis submitted to the Faculty of the
Virginia Polytechnic Institute and State University
in partial fulfillment of the requirements for the degree of

Master of Science
in
Electrical Engineering

Vuk Marojevic, Chair
Carl B. Dietrich
Louis A. Beex

May 5, 2015
Blacksburg, Virginia

Keywords: Unmanned Aerial Vehicles, OFDM, Spectrum Management, Air-to-Ground Channels

UAV Communications: Spectral Requirements, MAV and SUAV Channel Modeling, OFDM Waveform Parameters, Performance and Spectrum Management

Jaber A. Kakar

(ABSTRACT)

Unmanned Aerial Vehicles (UAV) are expected to be deployed both by government and industry. Rules for integrating commercial UAVs into a nation's airspace still need to be defined, safety being the main concern. As part of this thesis, the communication needs of UAVs as important requirement for UAV integration into the national airspace is considered.

Motivated by recent prediction of UAV quantities, revealing the importance of Micro UAVs (MAV) and Small UAVs (SUAV), the thesis determines spectral requirements for control and non-payload communication (CNPC). We show that spectral efficiency, particularly in the downlink, is critical to the large-scale deployment of UAVs. Due to the limited range of small SUAV and MAV systems, communication between air and ground elements of these UAVs is established through radio Line-of-Sight (LoS) links. Ultimately, efficient LoS UAV systems are based on a better understanding of channels in the downlink, i.e. air-to-ground (A2G) channels, and also on efficient waveform as well as spectrum management implementation.

Because of limited research in wideband aeronautical channel modeling, we have derived an A2G channel prototype applicable to SUAV and MAV. As part of the research at Wireless@VT in designing and prototyping Orthogonal Frequency Division Multiplexing (OFDM) waveforms, this thesis derives the optimal parameters for SUAV and MAV A2G channels. Finally, the thesis discusses concepts that relate flight route with spectrum management as well as opportunities for a more dynamic spectrum allocation for UAV communication systems.

Contents

List of Figures

List of Tables

Abbreviations

A2G	Air-To-Ground
AC	Aircraft
ACI	Adjacent Channel Interference
ACL	Autonomous Control Level
AGL	Above Ground Level
ARQ	Automatic Repeat Request
ATC	Air Traffic Control
ATS	Air Traffic Service
BER	Bit Error Rate
BLoS	Beyond Line-of-Sight
C2	Command and Control
CFA	Controlled Firing Area
CIR	Channel Impulse Response
CNPC	Control and Non-Payload Communication
CoE	Center of Excellence
COA	Certificate of Waiver or Authorization
CP	Cyclic Prefix
CS	Cyclic Suffix
DDD	Dull, Dirty and Dull
DL	Downlink
DoD	Department of Defense
EtC	Edge-to-Center
FAA	Federal Aviation Administration
FEC	Forward Error Correction
FMT	Filtered Multi-Tone
FSPL	Free Space Path Loss
FY	Fiscal Year
GCS	Ground Control Station
GL	Ground Level
HALE	High Altitude, Long Endurance
HAP	High Altitude Platforms
ICAO	International Civil Aviation Organization

ICI	Inter-Carrier Interference
IFR	Instrument Flight Rules
IMC	Instrument Meteorological Conditions
INR	Interference to Noise
ISI	Inter Symbol Interference
ISR	Intelligence, Surveillance and Reconnaissance
ITAR	International Traffic in Arms Regulations
ITU-R	International Telecommunications Union Radiocommunication Sector
JUAS	Joint Unmanned Aircraft Systems
LA	Large Aircraft
LAA	Local Airport Advisory
LoS	Line-of-Sight
LP	Low Pass
MA	Medium Altitude Medium Aircraft
MALE	Medium Altitude, Long Endurance
MAV	Micro UAV
MOA	Military Operation Area
MPC	Multipath Components
MSL	Mean Sea Level
MTOW	Mean Takeoff Weight
MTR	Military Training Route
NavAID	Navigation Aid
NAS	National Airspace System
NBC	Nuclear Biological or Chemical
NLoS	Non-Line-of-Sight
NM	Nautical Mile
NSA	National Security Area
OFDM	Orthogonal Frequency Division Multiplexing
OLoS	Obstructed Line-of-Sight
OPEX	Operational Expenditure
PDF	Probability Density Function
PDP	Power Delay Profile
PMF	Probability Mass Function
PU	Primary User
px	Pixel
RC	Raised Cosine
S/P	Serial-to-Parallel
S&A	Sense and Avoid
SA	Small Aircraft
SAO	Special Area of Operation

SM	Statute Miles
SRC	Square-Root Raised Cosine
SU	Secondary User
TBD	To Be Determined
TFR	Temporary Flight Restriction
TI	Throughput Intensive
TRSA	Terminal Radar Service Area
UACS	Unmanned Aircraft Control Station
UAS	Unmanned Aerial System
UAV	Unmanned Aerial Vehicle
UL	Uplink
ULA	Ultralight Aircraft
VC	Virtual Carrier
VDL	VHF Digital Link
VFR	Visual Flight Rules
VHA	Very High Altitude
VHF	Very High Frequency
VLA	Very Low Altitude
VMC	Visual Meteorological Conditions
WRC	World Radiocommunication Conference

Chapter 1

Introduction

1.1 Motivation

An unmanned aerial vehicle (UAV), or sometimes simply UA, is an aircraft without a human pilot aboard. The employment of UAVs by the US DoD has ubiquitous presence. A recent DoD report [29] provides current unmanned aerial systems (UAS[1]), inventory for Air Force, Army, Marines and Navy. This data is then used to estimate future inventory up to fiscal year (FY) 2017. Irrespectively of the DoD branch, we can see increases in UAS inventory. For instance, the number of MQ-9A Reaper UAVs owned by the Air Force is expected to grow from 70 for FY 2012 to 256 for FY 2017. This explains why UAS in the military already outnumber traditional manned aircraft systems. The reason for such large-scale UAS deployment is because UAV technology is already fairly well-developed and development as well as maintenance costs are significantly lower than that of traditional manned aircraft systems [18].

Not only are UAVs cost-effective, the applications for government and commercial purposes are varied: transportation, communications infrastructure, humanitarian and public safety deployments, among others [39]. For instance, as part of Google Project Loon, high altitude and large-scale UAV LTE eNodeBs were proposed as alternatives for terrestrial eNodeBs [26]. Recent predictions, conducted by the US National Transportation Center, reflect the great range of UAS applications outside the military in predictions of UAV quantities. Unmanned aerial vehicles for non-military purposes will exceed DoD inventory already by 2020

[1]The UAS consists of the aircraft and its associated elements.

[47]. Economy of scale will likely happen for micro and small UAVs. Recognizing the potential of small UAVs, several companies, including GoogleX and Amazon Prime Air, have formed the small UAV (SUAV) coalition [33]. AeroVironment, for example, is examining the applicability of SUAVs to quickly re-establish critical communications infrastructure after a natural or man-made disaster [2].

The International Civil Aviation Organization (ICAO) decided that UAV control and non-payload communication (CNPC) links must operate over protected spectrum [50]. Such spectrum will be allocated through the International Telecommunications Union Radiocommunication Sector (ITU-R). ITU-R has computed bandwidth requirements of 34 MHz for LoS CNPC links and 56 MHz for BLoS satellite CNPC links to allow for future UAS CNPC spectrum allocation [39]. Internationally discussed frequencies for LoS CNPC on the World Radiocommunication Conference (WRC) in 2015 are, amongst others, 960–977 MHz and 5030–5091 MHz [50]. UAV spectrum in the 1755 MHz band is considered for relocation in the US. We can infer from the bandwidth requirement and the potential frequency ranges that future UAS operations are likely to occur on multiple, at least two, non-contiguous bands. Usually guard bands are required on both sides of each allocated band to reduce the effect of out-of-band interference making such solution less spectrally-efficient than a single, large bandwidth solution. Furthermore, propagation behavior for 960 MHz and 5030 MHz distinctly differs. The exchange of rich content data or streaming high-definition video, for example, requires a significant amount of spectrum, proportional to the desired throughput and quality. When the air becomes more congested, more bandwidth will be needed to accommodate the desired communication needs.

The aforementioned bandwidth calculations by the ITU-R are rather pessimistic because they only account for time-sparse video data exchange for sense and avoid (S&A) applications in environments with relatively low UAV densities. It is likely that future UAV links will be throughput-intensive and the above discussed dedicated CNPC spectrum will not be sufficiently available to carry payload data. New ways of spectrum management – apart from simply allocating more bandwidth – need to be considered. On the one hand spectrum sharing is an efficient concept to satisfy bandwidth demand in an opportunistic way, when and where needed. On the other hand, the search for a robust spectrally-efficient waveform is also necessary to utilize spectrum more efficiently.

1.2 Contribution

UAVs are operated in the National Airspace System (NAS). The use of UAS for intelligence, surveillance and reconnaissance (ISR) military applications is already standard practice. More recently, a number of *civilian* use cases for UAS have been identified in the agriculture, entertainment, and exploration domains, among others. The Federal Aviation Administration (FAA) as the US aviation authority tries to deploy policies, procedures and standards to integrate UAVs in the NAS. For instance, currently civil UAS cannot be operated in the NAS unless a valid airworthiness certificate, the Certificate of Waiver or Authorization (COA), is issued to that particular UAS [8]. For that reason, aircraft design standards and certification procedures need to be established to have similar reliability and safety as conventional aircraft [53].

Increasing UAV densities will bring along challenges in S&A, radio spectrum allocation [66] as well as UAV type-specific NAS integration [67]. The successful integration of unmanned aircraft in non-segregated airspace relies heavily on robust command and control communication links. Whereas UAV flight operation control signalling requires low throughput, and spectrum will likely be allocated for this purpose, the data rates for transmitting the information content that the UAV sensors gather can be significant and will grow with technology advancements. Recent predictions reveal that UAV quantities for the commercial and public sector will outnumber deployed UAVs for DoD. Today's and future missions of these aircraft increasingly rely on the information exchange of real-time payload data leading to a spectrum management problem. To alleviate this problem, one solution to the problem is the increase in spectral efficiency. Another solution is using higher frequencies (where there is more spectrum) or better spectrum management, in general.

Future designers of UAVs, in particular civil and public UAVs, need to be aware of intensified safety requirements and spectrum scarcity due to higher concentration in aircraft density. In this thesis, the spectral scarcity problem is addressed. In the beginning of this thesis, the UAV context is thoroughly established through an extensive literature analysis. Motivated by recent prediction of UAV quantities, revealing the importance of Micro and Small UAVs (MAV and SUAV), the thesis determines spectral requirements. It has been derived that spectral efficiency, particularly in the downlink, is critical to the large-scale deployment of UAVs. Hence, efficient UAV systems are based on a better understanding of channels in the downlink, i.e. air-to-ground (A2G) channels, and based on this an efficient waveform and

spectrum management implementation.

For that reason, in a literature survey, despite limited research in wideband aeronautical channel modeling, an A2G channel prototype applicable to SUAV and MAV has been determined. As part of the research of Wireless@VT in UAV Waveforms based on OFDM, parameters and the resulting performance of OFDM in SUAV and MAV A2G channels are extracted. The study of other waveforms in the UAV context is important, but is beyond the scope of this thesis. Finally, the thesis establishes some concepts of what future UAV spectrum management in a cellular system may look like. With this work, further research is enabled.

Chapter 2

Background

This chapter gives an overview of existing UAVs, their characteristics, communication types and applications. Due to the limited scope of this thesis, an historical outline of UAVs is not provided. For the interested reader, information about history related to the use of UAVs in the military can be found in [1, 19, 27, 34]. The reader may skip this chapter if he or she is familiar with the overall UAV context. The main contribution of this chapter is to combine relevant information in a comprehensive form.

2.1 Unmanned Aerial Vehicle Classification

Currently, military branches as one of the main operators of UAVs use different kind of UAVs. To differentiate UAVs, the most common factors for UAV classification in the literature are takeoff weight (MTOW), operational altitude, level of control autonomy as well as military-based and ownership-based UAV distinctions [74]. This section provides a brief summary of all UAV classifications based on the above criteria. The most relevant references for each way of classifying UAVs are included as well. The author recommends reference [27] for further details.

2.1.1 Weight-Based UAV Classification

UAVs of different types according to Table 2.1 are classified using MTOW as a metric. This metric in return is correlated to the expected kinetic energy. Hence, this metric is a good way to characterize the ground impact risk [74]. Other MTOW-based or MTOW derived classifications exist [10, 11].

Table 2.1: MTOW-based UAV classification derived from [11] "CARE innovative action preliminary study on integration of unmanned aerial vehicles into future air traffic management," Industrieanlagen-Betriebsgesellschaft mbH, Tech. Rep., February 2011. and [27] K. Dalamagkidis, K. Valavanis, and L. Piegl, On Integrating Unmanned Aircraft Systems into the National Airspace System: Issues, Challenges, Operational Restrictions, Certification, and Recommendations, Intelligent Systems, Control and Automation: Science and Engineering, 2nd ed. Dordrecht/New York: Springer, 2012, vol. 36. Used under fair use, 2015.

Name	**MTOW** [kg]	**Range Category**	**Notes**
Micro	< 1	Close Range	Regulation less restrictive
Mini	Up to 1 kg		
Small	< 13.5		
Light/Ultralight	< 242	Short Range	Airworthiness certification can be based on ultralight, light sport or normal aircraft.
Normal	$< 4,332$	Medium/Long Range	
Large	$> 4,332$	Long Range	Equivalent to transport airplanes.

2.1.2 Altitude-Based UAV Classification

Weight-based UAV classification (see Section 2.1.1) is indeed a way to classify the safety risk, but it is limited to risk assessment of direct ground impacts. Categorizing UAVs using their typical operational altitude is a way to determine airspace-specific aircraft densities and therefore determine the likelihood of collisions. In reference [27] four main altitude-based UAV types are defined. These are very low altitude (VLA[2]) LoS, VLA BLoS, medium altitude (MA) and very high altitude (VHA) UAVs. Table 2.2 assigns these UAV types to specific airspace classes (cf. Section 2.2.2). Based on the altitude of operation it might be necessary to avoid other aircraft by S&A and two-sided Air Traffic Control (ATC) communication links.

[2]Typical VLA altitudes are less than 400–500 ft or 120–150 m.

Table 2.2: Altitude-based UAV classification based on [27] K. Dalamagkidis, K. Valavanis, and L. Piegl, On Integrating Unmanned Aircraft Systems into the National Airspace System: Issues, Challenges, Operational Restrictions, Certification, and Recommendations, Intelligent Systems, Control and Automation: Science and Engineering, 2nd ed. Dordrecht/New York: Springer, 2012, vol. 36. Used under fair use, 2015.

Class	**Airspace Class**	**S&A**	**Transponder**	**2-way ATC Communication**
VLA/LoS	Class G	Not Required	Not Required	Not Required[3]
VLA/BLoS	Class G	Required	Required	Not Required[3]
MA	Class A–E	Required	Required	Required
VHA	Above FL 600[4]	Required	Required	Required

2.1.3 Autonomy-Based UAV Classification

Control of UAVs can range from the remotely piloted controlled case to the fully autonomous UAV case. In [25], the author defines 11 distinct autonomous control levels (ACL) taking requirements such as situational awareness, analysis, coordination, decision making and operational capability into account [25].

A rather simple classification based on autonomy is provided in [14]. Authors from reference [14] differentiate between remotely piloted, remotely operated (semiautonomous), and fully autonomous UAVs. The difference between remotely piloted and remotely operated UAVs is that for the latter case the actual flying is conducted by the UAV itself as opposed to the first case of remotely piloted UAVs.

2.1.4 Military-Based UAV Classification

Several military classifications of UAVs exists, amongst other, that of JAPCC [48] given by Table 2.4. Different classes as well as subclasses/subcategories of Class I differ from one another by distinct MTOW ranges. The distinction of subcategories is achieved through their operational role in potentially different altitudes.

[3]Communication with ATC before operation may still be necessary.
[4]Corresponds approximately 60,000 ft or 18,300 m.

Table 2.3: UAV ACLs retrieved from [25] B. Clough, "Unmanned Aerial Vehicles: Autonomous Control Challenges, A Researchers Perspective," in Cooperative Control and Optimization, R. Murphey and P. Pardalos, Eds. Dordrecht/Boston: Springer, 2002, ch. 3, pp. 35–53. Used under fair use, 2015.

ACL	**Description**
0	Remotely piloted vehicle
1	Execute preplanned mission
2	Changeable mission
3	Robust response to real-time faults/events
4	Fault/event adaptive vehicle
5	Real-time multi-vehicle coordination
6	Real-time multi-vehicle cooperation
7	Battlespace knowledge
8	Battlespace cognizance
9	Battlespace sware cognizance
10	Fully autonomous

Table 2.4: NATO UAV Classification [48] Joint Air Power Competence Centre (JAPCC), "Strategic Concept of Employment for Unmanned Aircraft Systems in NATO," 2010. Used under fair use, 2015.

Class	**Name**	**MTOW** [kg]	**Regular Operating Altitude**	**Regular Mission Radius**	**UAV Examples**
Class I	Micro	< 2	Up to 60 m AGL	5 km (LoS)	Black Widow
	Mini	$2 - 20$	Up to 915 m AGL	25 km (LoS)	Scan Eagle, Raven
	Small	> 20	Up to 1,525 m AGL	50 km (LoS)	Luna, Hermes 90
Class II	Tactical	$150 - 600$	Up to 3,050 m AGL	200 km (LoS)	Sperwer, Range
Class III	MALE	> 600	Up to 13,720 m AGL	Unlimited (BLoS)	Predator A, Predator B
	HALE		Up to 19,810 m AGL		Global Hawk
	Strike Combat				

In the report of the DoD [73], JUAV CoE subdivides FAA-based categories I, II and III from Table A.1 in [73] in six categories based on its usage for tactical, operational or strategic purpose. As opposed to many other classifications, JUAS CoE accounts for other factors such as the launch method (hand, mobile and conventionally launched) of UAVs.

2.1.5 Ownership-Based UAV Classification

UAVs can also be differentiated among each other in terms of ownership, whether the distinction between federal agencies and local agencies or the distinction between military branches (army, navy, air force, marines) [29].

2.1.6 Utilized UAV Classification

Sections 2.1.1 – 2.1.5 show that a commonly accepted UAS classification does not exist [47]. We use the UAS classification developed by Volpe National Transportation Systems Center [47]. The classification in [47] uses MTOW-based (cf. Table 2.1) and military-based classifications (cf. Table 2.4) to split UAVs into eight categories (plus the rest in category others), including five FAA-defined MTOW-based manned aircraft categories (ultralight, light sport, small, medium and large aircraft). The classification is shown in Table 2.5.

Table 2.5: Utilized UAV Classification for Report based on [47] John A. Volpe National Transportation Systems Center, "Unmanned Aircraft System (UAS) Service Demand 2015–2035," U.S. Department of Transportation, Tech. Rep. DOT-VNTSC-DoD-13-01, September 2013. Used under fair use, 2015.

Name	**MTOW** [kg]	**Operating Altitude** [m]	**Mission Radius** [km]	**UAV Examples**
Nano	< 0.5	< 120	1.6	Hummingbird
Micro	$0.5 - 2$	< 915	< 8	Raven A/B
Small	$2 - 25$	$< 3,050$	< 40	T-Hawk
Ultralight Aircraft	$25 - 115$	$< 4,570$	< 120	Integrator
Light Sport Aircraft	$115 - 600$	$< 5,500$	< 160	Shadow
Small Aircraft	$600 - 5,670$	$< 7,620$	< 320	Reaper
Medium Aircraft	$5,670 - 18,600$	$< 30,500$	TBD	Global Hawk
Large Aircraft	$18,600 - 136,000$	?	?	Pegasus

The classification in [47] also incorporates other characteristics such as size, mission speed and mission endurance that is not listed in Table 2.5 for the sake of simplicity.

2.2 Overview of the National Airspace System

The establishment of the FAA results from the Federal Aviation Act of 1958. The goal of the FAA is to provide a safe ground environment and efficient airspace system for civil, commercial and military aviation [31]. The NAS combines a network with air navigation facilities, ATC facilities, airports, personnel and technology with reasonable rules and regulations guaranteeing a well-functioning overall system [31].

2.2.1 Flight Rules and Weather Conditions

Poor weather conditions are a limiting factor directly influencing aircraft separation[5] and flight rules. Generally speaking, aircraft separation increases as weather conditions deteriorate leading to reduced airport capacities [31].

Categories of Flight Rules

Visual flight rules (VFR) and instrument flight rules (IFR) are the only two distinct operational flight rules that an aircraft can operate under.

Irrespective of weather conditions, the majority of commercial air traffic, operate under IFR [31]. In conditions of reasonable weather, ATC enhances efficiency by transferring responsibility of direct visual separation to the IFR aircraft itself.

Categories of Weather Conditions

VFR and IFR correlate to two weather conditions. These are visual meteorological conditions (VMC) and instrument meteorological conditions (IMC). VMC as the name says is a weather condition in case of fairly good weather as opposed to IMC which applies in cases of rain, low clouds or reduced visibility. Generally speaking, IMC applies if the range within sight is below 3 statute miles[6] (SM) or if the ceiling[7] falls below a value of 1000 ft (or 300 m) AGL.

Relationship Flight Rules and Weather Conditions

In case of VMC on the one hand, the aircraft *may* operate under VFR. Under VFR the pilot has to detect other aircraft and keep enough spacing to avoid accidents. An aircraft can also follow IFR principles in VMC. Nevertheless, the responsibility of safe operation still lies with the aircraft and not with ATC.

In case of IMC on the other hand, the aircraft operates under IFR. The main responsibility for meeting aircraft separation requirements lies with the ATC provided that the aircraft

[5]Corresponds to the physical distance between aircraft.

[6]A SM corresponds to 5,280 ft in length which in return equals approximately 1.6 km.

[7]The ceiling in aviations according to ICAO is defined as the height (in AGL) to the lowest layer of cloud that covers more than 50% of the sky. The height of the lowest cloud layer has to be less than 6,000 m.

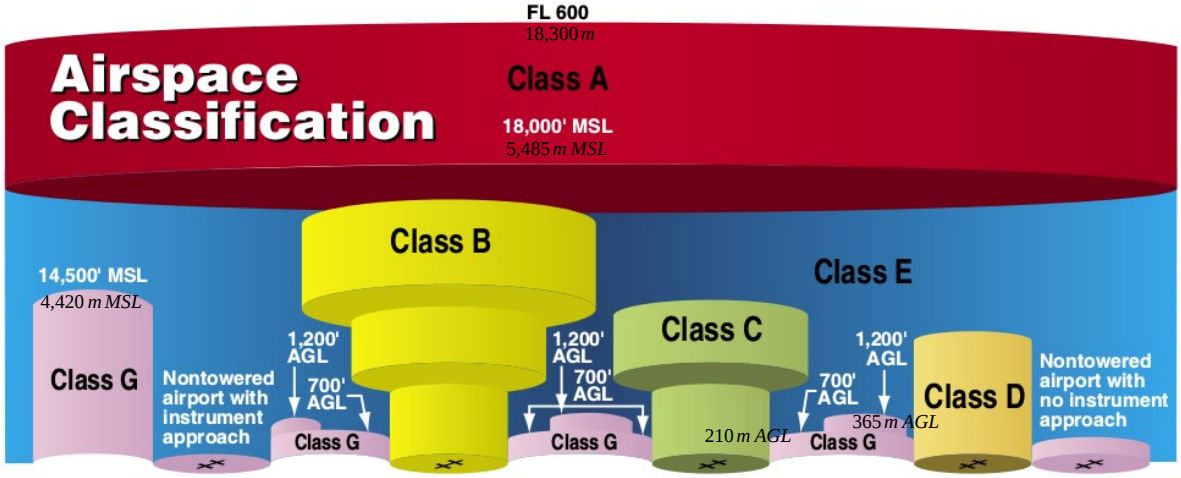

Figure 2.1: FAA Airspace Classes (modified from [3]) Airspace [Online]. Available: `http://www.faa.gov/regulations_policies/handbooks_manuals/aviation/pilot_handbook/media/PHAK-Chapter14.pdf`. Used under fair use, 2015.

complies with (minimum) equipment requirements and pilots meet proficiency requirements. Apart from using assigned routes and altitudes, IFR aircraft also have access to radio navigation aids (NavAID) and vectors from ATC to navigate [31].

2.2.2 Airspace

In accordance with ICAOs airspace classification, FAA has subdivided the US national airspace into six classes (see Figure 2.1). The altitude specifications in Figure 2.1 are all in ft and m. The airspace can be controlled by ATC or be uncontrolled [3]. Controlled airspace consists of classes A, B, C, D and E. Class F does not exist in the US and Class G is uncontrolled airspace.

In *controlled* airspace IFR service (ground-to-air radio communications, navigation aids and traffic separation services) is provided. This does not necessarily mean that *all* flights within the controlled airspace are subject to ATC control [31]. In uncontrolled airspace the aircraft is able to operate under IFR but IFR service might not be available.

The function of all classes is to allow for VFR coordination. In Class E, VFR traffic may operate without ATC control as long as weather conditions permit (i.e. in cases of VMC). VFR operating aircraft in close proximity to (busy) airports, i.e. airspace in class B, C or

D, are required to maintain ongoing contact with ATC. Table 2.6 lists and summarizes all (ICAO) airspace classes applicable to the US.

Table 2.6: Characteristics of Airspace Classes

Class	**Communications**	**Entry Requirements**	**Separation Provided**	**Notes**
A	Required	ATC Clearance	All Aircraft	- 18,000 ft MSL $\leq$ Altitude $\leq$ FL 600 - Usually IFR operation
B	Required	ATC Clearance	All Aircraft	- $\leq$ 10,000 ft MSL - Nation's busiest airport in Class B - Upside-down wedding shape with 3 or more layers
C	Required	Two-way Communication prior to entry	VFR from IFR	- $\leq$ 4,000 ft MSL - Outer radius 10 NM at $\geq$ 1,200 ft MSL Altitude - Inner radius 5 NM at surface level
D	Required	Two-way Communication prior to entry	Runway Operations	- $\leq$ 2,500 ft MSL
E	Not Required for VFR	None for VFR	None for VFR	- If not A, B, C, D, then E - Altitude $\leq$ 700 ft or $\leq$ 1,200 ft AGL in en-route environment - $\leq$ 18,000 ft MSL in offshore airspace areas - If no lower altitude specified, in the US $\geq$ 14,500 ft MSL holds
Class F does not exist in the US.				
G	Not Required	None	None	- From the surface until lower Class E altitude - VFR applies in Class G

Some specific airspaces that are not listed explicitly in Table 2.6 are special use airspaces in special areas of operation (SAO) and other airspace areas [3]. Special use airspaces, on the one hand, can be prohibited areas, restricted areas, warning areas, military operation areas (MOAs), alert areas and controlled firing areas (CFAs). Other airspace areas, on the other hand, include local airport advisory (LAA), military training route (MTR), temporary flight restriction (TFR), parachute jump aircraft operations, published VFR routes, terminal radar service area (TRSA) and national security area (NSA). For further details on each of these types as well as on all airspace classes in the US, the author recommends [3].

Utilizing the UAV classification from Table 2.5, we can deduce potential airspace classes of operation (see Table 2.7). In some classes, such as Class B, further standardization is required to justify actual UAV usage. The specified potential airspace classes in Table 2.7 take all five phases of aircraft operation into account: pre-flight, departure, en-route, arrival and post-flight. The phase duration relative to the total absolute flight operation by ITU [39] is estimated as follows:

- Pre-flight: 4%
- Departure: 8%

- En-route: 76%
- Arrival: 11%
- Post-flight: 1%

Table 2.7: Potential Airclasses of Operation

Name	**Potential Airspace Classes**
Nano	B–D, G
Micro	B–G
Small	
Ultralight Aircraft	
Lightsport Aircraft	
Small Aircraft	All
Medium Aircraft	
Large Aircraft	

2.3 Exchange of Information in Unmanned Aircraft Systems

ITU defines in [39] an unmanned aircraft system as the aggregation of multiple systems: unmanned aircraft subsystem, ground control station[8] (GCS) subsytem, ATC subsystem, S&A subsystem and payload subsystem (e.g. video camera, etc.).

The general information flow of a UAS divided in internal and external exchange of data is shown in Figure 2.2. Internally, command and control (C2) data is transferred among GCS and UAV. Externally, ATC is involved in the exchange of NavAID, air traffic services (ATS), ATC voice, S&A and non-payload data. The direct transfer of throughput-intensive payload data (e.g. HD video) is typically an internal downlink (UAV to GCS) information flow. Depending on the location of GCS and responsible ATC, information from GCS to ATC or vice versa need to be relayed through the UAV. In Figure 2.3, information exchange between UAV, GCS and ATC, in UL/DL are shown. CNPC is utilized in command and control, ATC relay and S&A information exchange between UAV and GCS *only*.

[8]Also known as unmanned aircraft control station (UACS).

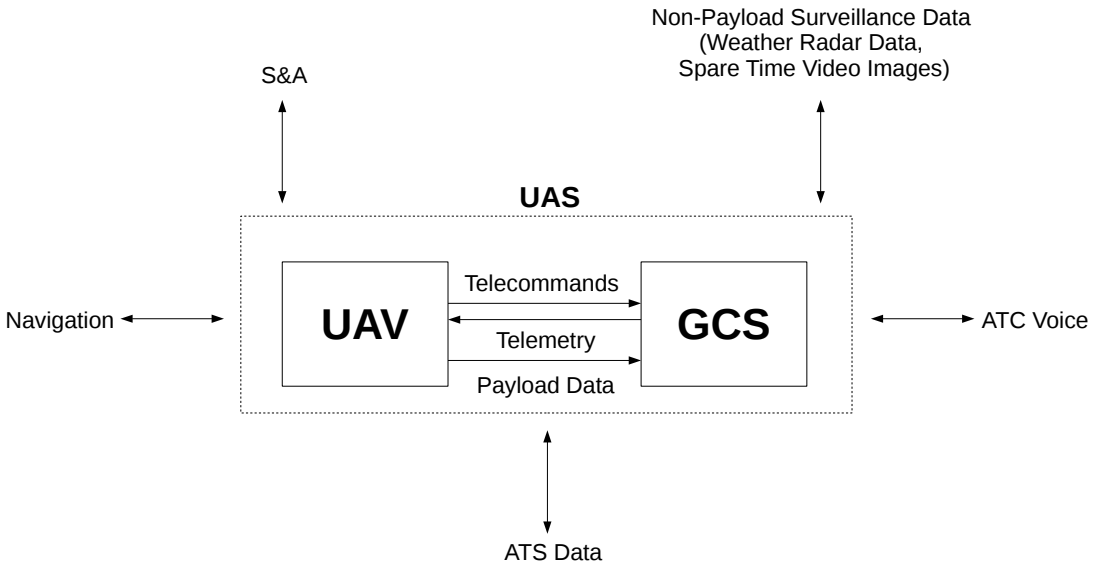

Figure 2.2: Internal and External Information Flow of a UAS (modified from [39]) ITU, "Characteristics of unmanned aircraft systems and spectrum requirements to support their safe operation in non-segregated airspace," International Telecommunication Union, Tech. Rep. M.2171, December 2009. Used under fair use, 2015.

C2 information encapsulates telecommands[9] in the UL for flight and navigational control of the aircraft and telemetry[10] data in the DL. In the presence of ATC, compliance with ICAO standards is required [39]. Data rates in UL and DL vary based on ACL, i.e. command and control data rates for ACL 10 are expected to be significantly lower than for ACL 1.

[9]For example, altitude commands, throttle commands and speed commands

[10]For example, latitude, longitude, altitude, (air) speed and engine information

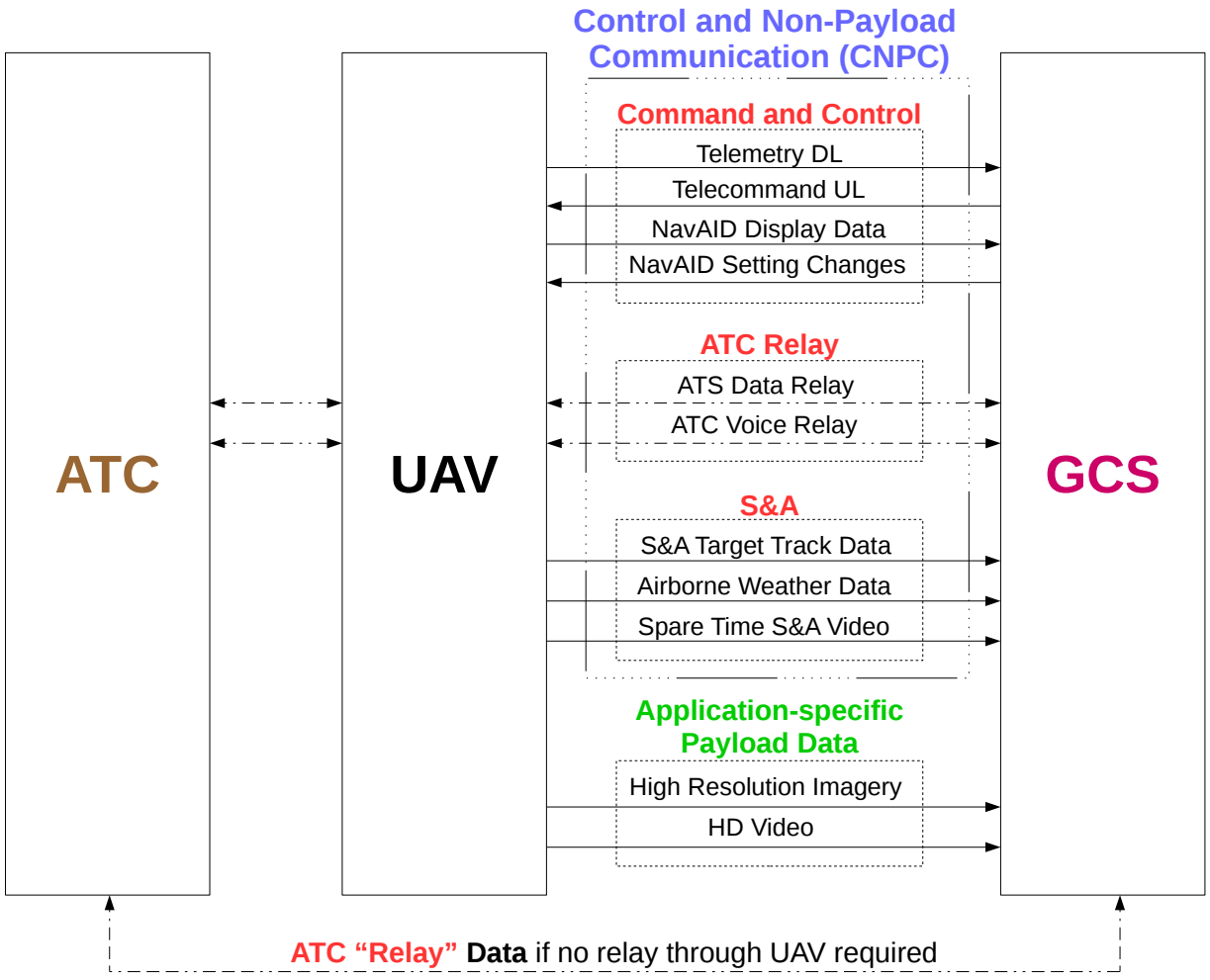

Figure 2.3: Detailed Information Flow (modified from [39]) ITU, "Characteristics of unmanned aircraft systems and spectrum requirements to support their safe operation in non-segregated airspace," International Telecommunication Union, Tech. Rep. M.2171, December 2009. Used under fair use, 2015.

Similar to command and control information, ATC relay data needs to meet future ICAO standards because it acts as a direct or indirect interface for GCS and ATC communication.

S&A data is deployed to ensure appropriate aircraft-to-aircraft separation and obstacle avoidance. Also S&A related links are expected to be ICAO compliant.

Payload data transfer motivates the use of UAV operation in future commercial and governmental applications. DL data-intensive links are the result of applications in movie making, industrial and federal inspection, airborne relay utilization, etc.

Future UAV missions will likely be operated in multi-UAV swarms or tiers working together [37]. In this case, the information flow graph from Figure 2.2 will further complicate requiring either UAV-UAV or additional GCS-UAV information exchange (or even both).

2.4 LoS and BLoS

UAS missions typically operate within RF line-of-sight (LoS) or beyond line-of-sight (BLoS) (cf. Figure 2.4). ITU defines LoS as "*the direct radio line of sight radiocommunication between the UA and UACS*" and BLoS as "*the indirect radio communication between the UA and a UACS using satellite communication services*" [39]. In this regard, the difference between non-line-of-sight (NLoS) and BLoS is that the latter refers to lack of visibility mainly caused by the curvature of the Earth's surface.

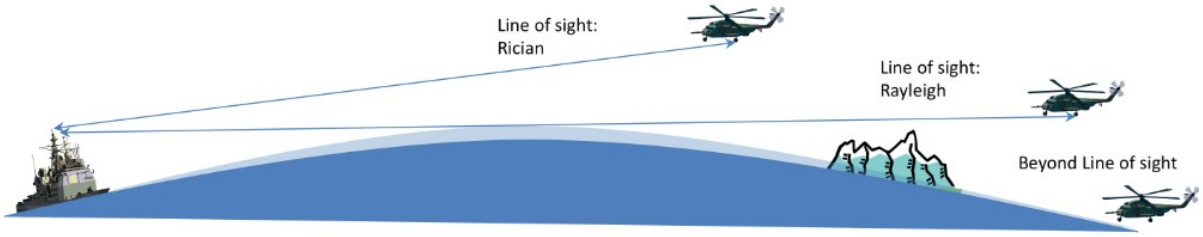

Figure 2.4: Difference between LoS and BLoS for ship-based Communications [58] J. H. W. Michael J. Luddy and A. Lackpour, "Beyond Line-of-Sight Communications with Smart Antennas (BLoSSA)." Used with permission from Michael J. Luddy, 2015.

LoS communication is limited by several factors, amongst others, link design. The maximum achievable distance, however, is impaired primarily by the radio horizon leading to typical values of 25–200 NM or 46–370 km depending on the operational altitude of the UAV [72]. Nevertheless, the actual distance through LoS can be considerably less than 370 km.

BLoS links as an "alternative" to LoS communication use geostationary satellites that have a turnaround link latency of 0.48 seconds or more [72]. In military terminology, BLoS is often used to characterize links with a range greater than 600 miles or 965 km. The footprint of satellite-based BLoS links depend for instance on deployed beamwidth (spot beam, wide beam, etc.), link margin and propagation impairments (ionospheric/atmospheric attentuation such as fading through rain).

LoS communication is applicable to three types of UAVs: low endurance, medium endurance

and high endurance [68]. In this context, it is important to note that low endurance UAVs almost exclusively operate under LoS [68]. Medium and high endurance UAVs, however, are usually operable in both LoS and BLoS. UAV types in Table 2.4, for instance, are implicitly classified based on their way of establishing communication to GCS – LoS or BLoS. Based on the classification of UAVs (see Section 2.1), the author of this report concludes that UAVs classified as Nano, Micro, Small, Ultralight Aircraft (ULA) and Light Sport Aircraft (LSA) are typically LoS-based whereas UAVs of type Small Aircraft (SA), Medium Aircraft (MA) and Large Aircraft (LA) utilize BLoS technology.

In terms of security, ITU states that the "*impact of latency on UAS command and control systems is a prime factor when considering the safety of operations* [39]. For that reason, irrespective of the UAV type, all unmanned aircraft should ideally be capable of LoS communication.

2.5 Application of UAS

UAVs are deployed in applications where their assigned roles fit to task requirements. UAV aptitude tests may also involve a benefit assessment over a manned aircraft approach [18]. Traditional military large-scale UAV deployment originated from usage in dull, dirty and dangerous (DDD) tasks [18].

Nowadays, the take-over of DDD tasks by UAVs is not the only reason for public and federal interest in UAVs. A more important factor in favor of UAVs is their small size compared to manned aircraft used for the exact same task [18]. This leads to first cost savings of about 20–60% of first costs of manned aircraft [18]. Moreover, expected operating costs (maintenance, fuel, hangarage, labor and insurance) amount to 40–80% of manned aircraft operational expenditure (OPEX) [18].

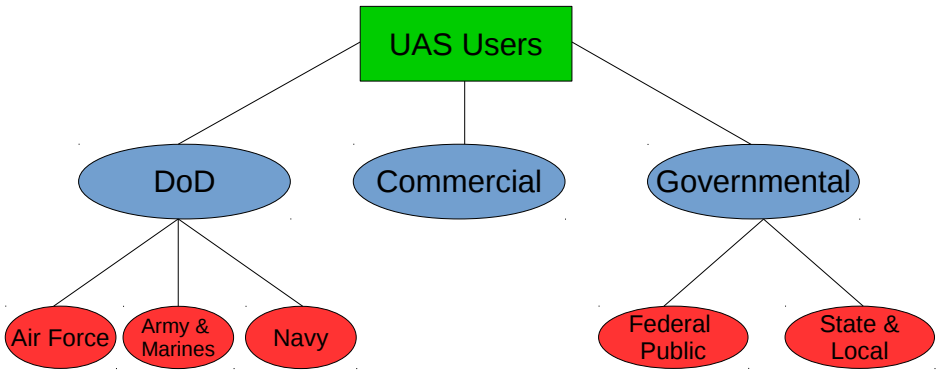

Figure 2.5: Main expected Users of UAS in the US

Table 2.8: DoD UAS Applications [5] "Military UAS Applications," `https://www.uavs.org/military`, accessed: 2014-12-22. [34] S. Gupta, M. Ghonge, and P. Jawandhiya, "Review of Unmanned Aircraft System (UAS)," International Journal of Advanced Research in Computer Engineering and Technology, vol. 2, no. 4, pp. 1645–1658, 2014. Used under fair use, 2015.

Role	**DoD**		
	Air Force	**Army/Marines**	**Navy**
Intelligence	- Electronic intelligence		
Surveillance & Reconnaissance	- Long-range, high-altitude surveillance - Damage assessment	- Surveillance of enemy activity - Monitoring of NBC contamination - Target monitoring - Location of mines	- Shadowing enemy fleets - Monitoring of sonar buoys
Combat & Security	- Elimination of unexploded bombs - Airfield base security	- Destruction of land mines	- Warfare - Protection of ports from offshore attacks
Communications	- Radar system jamming		- Relaying radio signals

UAS are typically deployed by military, the commercial and the governmental/public sector (see for example 2.5). UAS missions in miltary are typically either ISR or direct combat missions. Specific tasks for Air Force, Army, Marines and Navy are provided in Table 2.8.

UAS can broadly be utilized to serve domestic purposes – either commercial or governmental (cf. Table 2.9). Commercial UAV roles considered are in economic fields of (news) media,

transportation, communications, agriculture and site monitoring. Governmental/public applications are considered to be related to science, security or humanitarian support. Some examples of specific tasks in each of these categories are specified in Table 2.9. There are many other applications, but the aforementioned table lists the most relevant ones.

Table 2.9: Commercial and Governmental UAS Applications [5] "Military UAS Applications," `https://www.uavs.org/military`, accessed: 2014-12-22. [34] S. Gupta, M. Ghonge, and P. Jawandhiya, "Review of Unmanned Aircraft System (UAS)," International Journal of Advanced Research in Computer Engineering and Technology, vol. 2, no. 4, pp. 1645–1658, 2014. [39] ITU, "Characteristics of unmanned aircraft systems and spectrum requirements to support their safe operation in non-segregated airspace," International Telecommunication Union, Tech. Rep. M.2171, December 2009. Used under fair use, 2015.

Role	**Commercial**	**Role**	**Governmental**	
			Federal	**State & Local**
Media	- Event filming - Aerial photography - Information services	**Science**	*Earth & Environment* - Pollution and land monitoring - Meteorological services - Biological services - Research	
Transport	- Cargo planes			
Monitoring	*Security* - Pipeline *Inspection* - Power and rail line	**Security**	- Coast line - Border patrol - Anti-terror fight - Search & Rescue - Disaster and catastrophe management	- Police support - Fire fighting - Traffic spotting - Forest fire avoidance
Communications	- Relay - Remote sensing - Disaster eNBs			
Agriculture	- Crop spraying/dusting - Forestry operations	**Humanitarian Support**	- Famine relief - Medical support - Emergency relief	

Chapter 3

Spectrum Requirements

3.1 Projection of UAS Growth

Predicting the numbers of UAVs is an important step to determine spectrum requirements. A UAS consist of a GCS and one or several UAVs. To address the spectrum requirements for CNPC, ITU and NASA have conducted projections on the evolution of UAVs [35, 39]. In comparison to recent projections (cf. [47]), projection by ITU and NASA are rather conservative. For this thesis, references [29] and [47] are used to quantify national UAV-type specific numbers from 2015 until 2035. The UAVs are classified according to Table 2.5. The UAS users are given by Figure 2.5. The aforementioned reference predicts future demand of UAVs for DoD, public/governmental sector and commercial sectors. Reference [47] suggests an s-curve shaped functional relationship for characterizing the number of UAVs between 2015 and 2035 for commercial and public sectors. Using this source, the author of this thesis estimates the number of UAVs between 2015 and 2035 ($t_{year} = \{2015, 2016, ..., 2035\}$) by

$$f(x) = p_1 + \frac{(p_2 - p_1)}{1 + 10^{p_4(p_3 - x)}}, \tag{3.1}$$

where $x = t_{year} - 2015$. The curve fitting results for commercial UASs and total governmental/public agencies (including DoD) are shown in Table 3.1.

In this thesis, the UAS differentiation applied is based on Section 2.1.6. Figure 5.7 shows the evolution of UAV numbers per type distinguishing between public agency owned (5.8a) and commercial UAVs (5.8b). For the public (commercial) case in Figure 5.7, it is assumed that

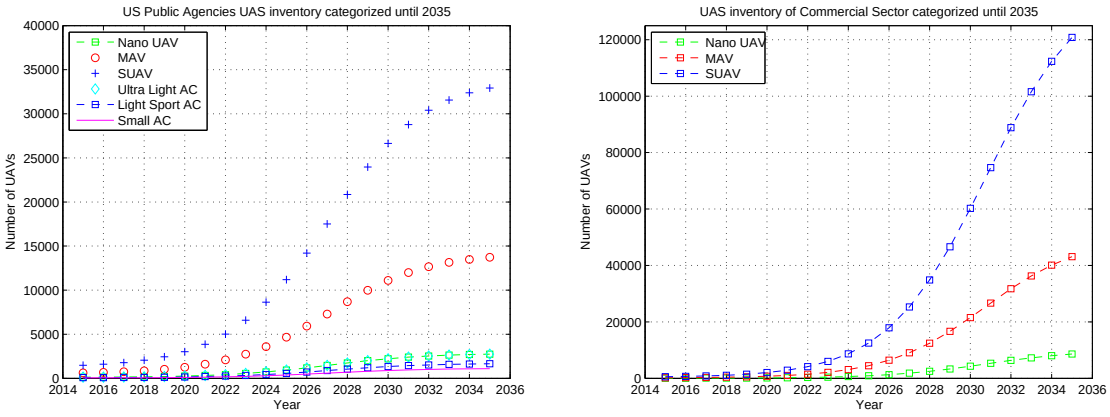

(a) Projection of public agency UAV quantities (without DoD)

(b) Projection of commercial UAV quantities

Figure 3.1: Projection of UAV numbers

Table 3.1: Modeling Parameters for Equation (3.1) (2 digit precision)

	p_1	p_2	p_3	p_4
Commmercial	487.95	$2.03{\cdot}10^5$	15.75	0.18
Federal Agencies	207.22	$1.02{\cdot}10^4$	9.73	0.18
State and Local Agencies	$1.87{\cdot}10^3$	$4.64{\cdot}10^4$	12.49	0.19

60% (70%), 25% (25%) and 5% (5%) of all deployed UAVs, will be of type Small UAV, Micro UAV (MAV) and Nano UAV, respectively. The subfigures show that commercial UAVs will outnumber public agency UAVs. (The DoD expects a linear increase of their UAV fleets, which will be outnumbered by commercial UAVs within the next 10 years.)

The total numbers for each type (including estimates for DoD-owned UAVs) are used to determine the probability mass function (PMF) of UAV types. The time-dependent PMF for 2015-2035 can be seen in Figure 3.2. It shows that SUAVs and MAVs are expected to dominate the UAV market. Because of their low cost, around 22% and 67% will be of type MAV and SUAV by 2035. According to Table 2.7, this results in higher airspace densities for *controlled* airspace classes B through E and uncontrolled airspace of class G. One question, however, that remains to be answered is how "tolerable" these UAVs are in airspaces in close proximity to airports, i.e. classes B, C and D, particularly class B.

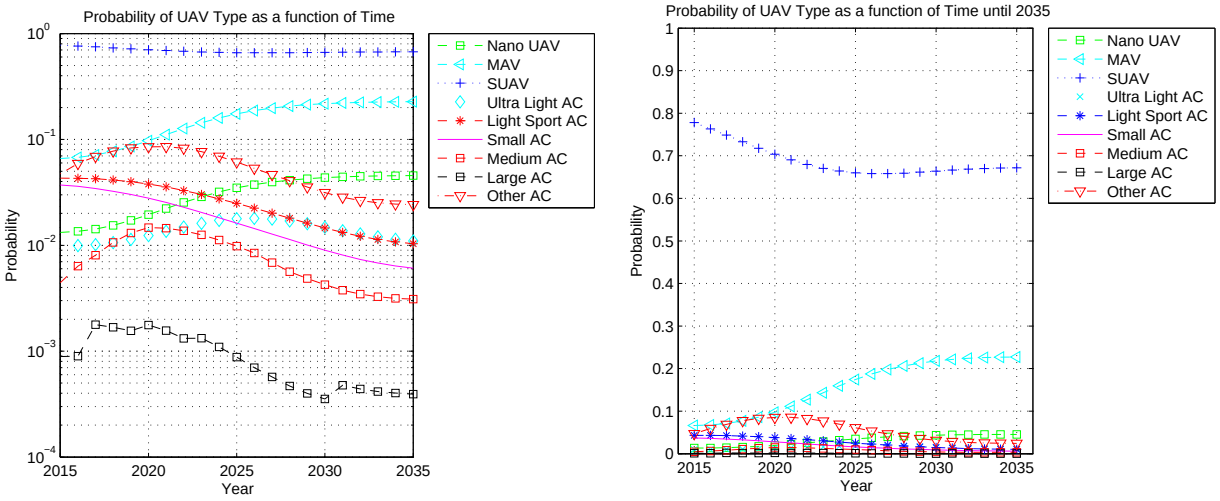

(a) Log-scaled PMF of UAV types (b) Linear-scaled PMF of UAV types

Figure 3.2: PMF of UAV types over time

3.2 Type-specific Data Rate Requirements

ICAO decided that UAV CNPC links must operate over protected spectrum [50]. Figure 2.3 summarizes the information flow between UAV and GCS in the absence (existence) of a satellite as relay for CNPC and payload LoS (BLoS) communication. This section addresses the data rate requirement for each information link indicated in Figure 2.3. Most numbers used in this section are obtained from [39][11]. In many cases, reference [39] provides different data rates for distinct phases of a flight (pre-flight, departure, en-route, arrival, post-flight) for UL and DL in both automatic and manual mode (AM and MM). AM and MM are introduced in [39] to account for distinct ACLs (cf. Section 2.1.3). Furthermore, overhead (through coding, etc.) is accounted.

3.2.1 Command and Control

Telemetry and Telecommand Link

Table 3.2 lists the data rate requirement for telemetry and telecommand links in bps *without overhead*, i.e. the raw data rate requirement. The data rate requirement for en-route is far

[11]This report computes the expected CNPC spectrum requirement for UAS in 2030 in non-segregated airspace.

lower than for the departure and arrival flight phase because the repetition/retransmission rate for departure and arrival is typically twice as high as for the en-route phase. Moreover, additional information (such as the state of lights) are transmitted during departure and arrival but not during the en-route flight phase. In AM, the data rate requirement is lower than for MM, because reporting frequency (such as latitude position reporting in DL) occur less frequently (up to 20 times less).

Table 3.2: Data Rate Requirement for Telemetry and Telecommand Links in bps [39] ITU, "Characteristics of unmanned aircraft systems and spectrum requirements to support their safe operation in non-segregated airspace," International Telecommunication Union, Tech. Rep. M.2171, December 2009. Used under fair use, 2015.

	Flight Phase					
	Departure		**En-route**		**Arrival**	
	AM	MM	AM	MM	AM	MM
DL: **Telemetry**	480	3,008	280	1,240	672	4,008
UL: **Telecommand**	408	1,256	152	632	656	2,424

NavAID

Table 3.3 summarizes the data rate requirement of NavAID for both UL and DL *without overhead*. The UAV navigation receivers can be controlled through the provided NavAID UL. In the DL, navigation data from the UAV is transmitted to the GCS.

Table 3.3: Data Rate Requirement for NavAID Links in bps [39] ITU, "Characteristics of unmanned aircraft systems and spectrum requirements to support their safe operation in non-segregated airspace," International Telecommunication Union, Tech. Rep. M.2171, December 2009. Used under fair use, 2015.

	Flight Phase					
	Departure		**En-route**		**Arrival**	
	AM	MM	AM	MM	AM	MM
DL: **NavAID Display Data**	98.4	440	98.4	440	123.2	600
UL: **NavAID Setting Changes**	74.4	352	74.4	352	74.4	352

3.2.2 ATC Relay

ITU estimates that transmission of ATC voice messages, on the one hand, will require FEC with code rate of 0.86[12] leading to a rate of 4,800 bps. This throughput corresponds to ICAO VDL Mode 3. ATC voice messages do not require any encryption.

The data rate requirement for ATS data relay, on the other hand, *accounting for overhead* as well, is shown in Table 3.4.

Table 3.4: ATS Data Relay Bit Rate in bps [39] ITU, "Characteristics of unmanned aircraft systems and spectrum requirements to support their safe operation in non-segregated airspace," International Telecommunication Union, Tech. Rep. M.2171, December 2009. Used under fair use, 2015.

	Flight Phase									
	Pre-flight		**Departure**		**En-route**		**Arrival**		**Post-flight**	
	DL	UL	DL	UL	DL	UL	DL	UL	DL	UL
Total	173	113	59	49	28	23	32	16	22	15
Total by Phase	286		108		51		48		37	

3.2.3 Sense and Avoid

Target Track Data

Target track data incorporates, amongst others, 3D target position information, 3D target velocity data and level of accuracy. The number of bits required to transmit a single target message after data compression equals approximately 80 bits [39]. In ITU's computation, the number of tracks is limited to 60 tracks and messages are updated at a 1 Hz pulse. An upper bound on the data rate of target track data for a single UAV corresponds to 4,800 bps.

Airborne Weather Data

The purpose of airborne weather radar data is to provide the GCS with meteorological information. A radar with a beamwidth of 3.5° in weather/turbulence detection mode,

[12]The overhead factor contributed to FEC is 1.16.

requiring 4 s to scan a 180° sector, serves as a basis to calculate the underlying data rate requirement. It is assumed that an update occurs after every 3.5° radial sweep leading to an effective update frequency of $180/(3.5 \cdot 4) = 12.86$ Hz. Each data frame consists of 1,600 bits, including 1,536 data bits plus header. This results in a required DL data rate (*without FEC overhead*) of 20,571 bps. If latency for this particular DL "channel" is not an issue (typically the case for the en-route phase), on-board data compression techniques in the UAV can be applied. For a 4 s delay, ITU believes weather radar data can be compressed by a factor of 7, i.e. reducing the data rate to 2,939 bps (*without FEC overhead*).

This link will not be packetized limiting overhead to FEC only. ITU deploys an overhead factor of 1.35 increasing the data rate requirement to 27,771 and 3,968 bps, respectively.

Spare Time S&A Video

In the calculation of the CNPC bandwidth requirement, ITU introduces a spare time video link in DL for situational awareness. Provided that a video resolution of 720 x 480 pixels (px) is used, the expected data rate requirement *without overhead* for low-altitude (medium and high altitude) operation is 200,000 (20,000) bps.

S&A video DL will not be packetized limiting overhead to FEC only. ITU deploys an overhead factor of 1.35 increasing the data rate requirement to 270,000 and 27,000 bps, respectively.

3.2.4 Overhead through Packetization of C2 and S&A Target Track Data

ITU suggest to packetize telemetry, telecommand messages (Section 3.2.1) , NavAID messages (Section 3.2.1), and S&A target track messages (Section 3.2.3) into a 576 byte long package (including overhead) (cf. Figure 3.3). For this particular case due to packetization and encryption, 42.5% redundancy is added into the system. 3/4 FEC will introduce an additional increase in overhead by 33%. As a consequence, the overall overhead factor is $1.425 \cdot 4/3 = 1.9$.

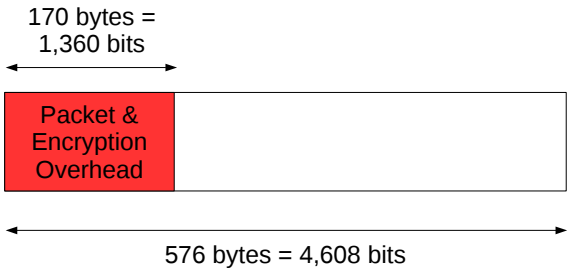

Figure 3.3: Packetizing C2 and Non-Video S&A Data

3.2.5 Overall CNPC Data Rate Requirement

In fully MM, spectrum computation will produce an upper bound (as opposed to using data rates for AM). Data rate requirements in MM are shown in Table 3.5.

Table 3.5: CNPC Throughput Requirement including Overhead [39] ITU, "Characteristics of unmanned aircraft systems and spectrum requirements to support their safe operation in non-segregated airspace," International Telecommunication Union, Tech. Rep. M.2171, December 2009. Used under fair use, 2015.

	Flight Phase	**Percentage Flight Phase**	**Command & Control**				**ATC Relay**				**S&A**		
			Control		**NavAID**		**ATC Voice**		**ATC Data**		**Target Track**	**Airborne Weather**	**Spare Time Video**
			UL	DL	UL	DL	UL	DL	UL	DL	DL	DL	DL
Airport Surface and Low Altitude	Departure	42%	2,386	5,715	669	839	4,800	4,800	49	59	9,120	27,771	270,000
			=9,606				UL: =4,849 DL: =4,859						
	Arrival	58%	4,606	7,615	669	1,140	4,800	4,800	16	32	9,120	27,771	270,000
			=14,030				UL: =4,816 DL: =4,832						
	Average		$0.42 \cdot 9,606 + 0.58 \cdot 14,030$ **=12,167**				UL, DL $\approx$ **4,855**				**9,120**	**27,771**	**270,000**
Medium and High Altitude	En-route	100%	1,201	2,356	669	839	4,800	4,800	23	28	9,120	3,968	27,000
			=5,062				UL: =4,823 DL: =4,828 UL, DL $\approx$ **4,855**				**9,120**	**3,968**	**27,000**

The column "percentage flight phase" in Table 3.5 is derived by considering that low-altitude and airport operations happen during departure and arrival, whereas higher altitude operations happen during the en-route phase. The percentage is computed by accounting for the phase duration of departure/arrival and en-route relative to the phase duration at a specific altitude (airport surface, low altitude and medium, high altitude).

3.3 Computation of Spectrum Requirements

In this section, the bandwidth requirement on CNPC for LoS communication is calculated. Because UAVs in the future will mainly be of type SUAV and MAV (cf. Section 3.1) having a finite range (cf. Section 2.4), the computation of bandwidth requirements is limited to LoS communication. According to Figure 2.3, CNPC information is divided into three classes of traffic. The bandwidth requirement W for any traffic link (e.g. ATC relay) can be computed as follows [39]:

$$W = K \cdot B \cdot M \cdot R/(U \cdot E), \tag{3.2}$$

where:

- K: Cellular cluster size
- B: Data rate requirement from Table 3.5
- M: M is the number of UAVs per cell. This number is a derived quantity generated from expected UAV quantities.
- R: Redundancy factor ($R \geq 1$) to account for higher reliability through backup links. If an equivalent second link exists, then R=2, otherwise $1 \leq R < 2$ holds.
- U: Utilization factor ($U \leq 1$) to guarantee sufficient bandwidth availability in case of traffic surges.
- E: E is the spectral efficiency set to 0.75 bps/Hz. This value is comparable to the performance of VDL Mode 3.

All parameters (except of the cluster size K[13]) are either known or can be selected based on link requirements. To account for Automatic Repeat Request (ARQ) in an explicit manner, it is possible to either slightly increase (decrease) the redundancy factor R (utilization factor U) by ϵ. Depending on the desired delay for retransmission, ϵ can be easily calculated. The next section explains how ITU calculated the frequency reuse factor for altitude-dependent cells.

[13]The frequency reuse factor is often said to equal K, but throughout this thesis 1/K is specified as the frequency reuse factor.

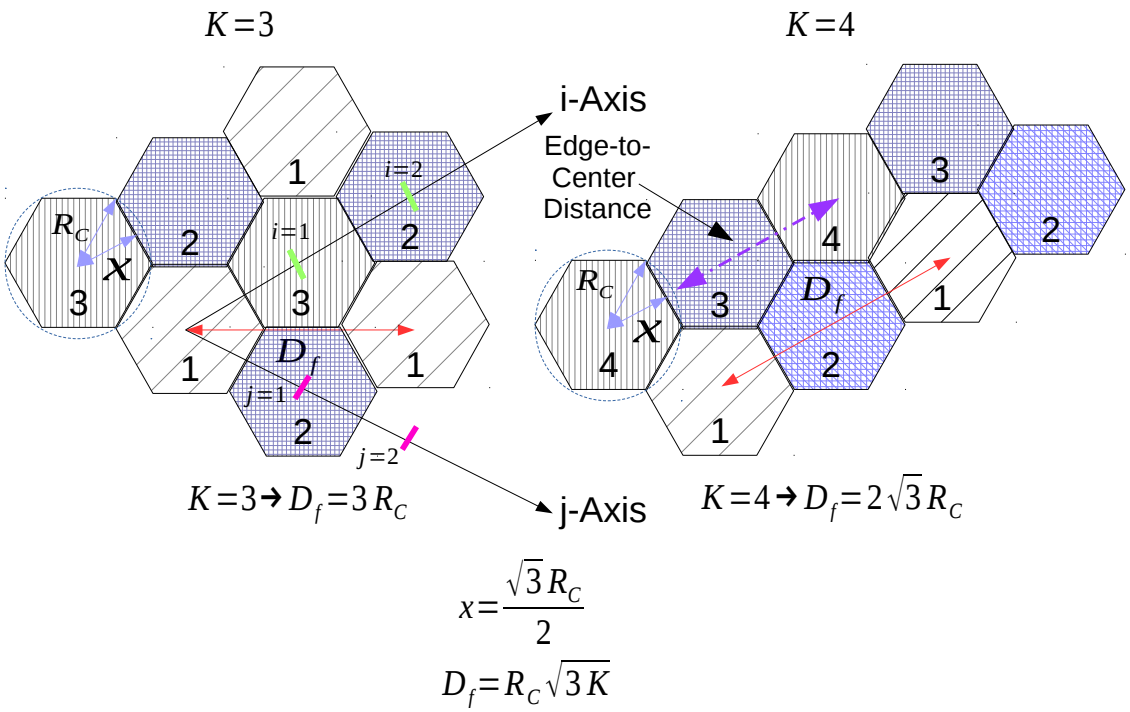

Figure 3.4: Cell Pattern for $K = 3$ and $K = 4$

3.3.1 Cluster Size for Altitude-Dependent Cells

Equation (3.2) is based on the concept of a terrestrial cellular network – spatial frequency reuse. In a cellular network N_W duplex channels are distributed among K neighboring cells known as cluster [64]. The *same* frequency is reused every D_f distance units. D_f is the frequency reuse distance. D_f depends on the cell radius R_C and the cluster size K (cf. Figure 3.4). Provided that a regular hexagon cell structure exists (which is the case for the cells in Figure 3.4), then it is easy to show that $D_f = R_C\sqrt{3K}$. D_f is always a multiple of $2x = R_c\sqrt{3}$. Centers of regular hexagons that use the same frequency can always be reached by walking integer increments of $R_c\sqrt{3}$ along i and j-axis[14]. For example, a cell center with index 1 can be reached by an other cell with index 1 in Figure 3.4 for $K = 3$ ($K = 4$) if $i = j = 1$ ($i = 2, j = 0$). This example shows that the relationship $K = i^2 + j^2 + ij, i, j \in \mathbb{N}_0^+ \backslash \{i, j = 0\}$ applies [64, 71]. The set that contains potential cluster sizes starts as follows (cf. Table 3.6): $\{1, 3, 4, 7, 9, 12, 13, 16, 19, 21, ...\}$

In case of UAVs, cells have to be regarded in all three dimensions. ITU defined in [39] four

[14]One can describe each cell center as a linear combination along i and j-axis in integer multiples of $2x$.

Cell Name	Configuration	Notes
A	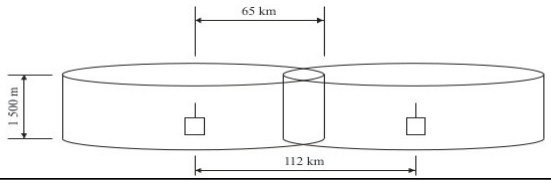	$R_C = 65\,km, d_R \approx 160\,km$ $K=1 \rightarrow D_f \approx 113\,km$ $K=3 \rightarrow D_f = 195\,km$ $K=4 \rightarrow D_f \approx 225\,km$ $K=7 \rightarrow D_f \approx 298\,km$ $K=12 \rightarrow D_f = 390\,km$
B	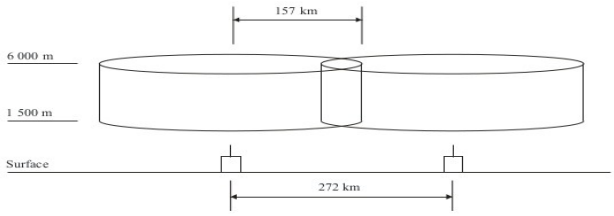	$R_C = 157\,km, d_R \approx 319\,km$ $K=1 \rightarrow D_f \approx 272\,km$ $K=3 \rightarrow D_f = 471\,km$ $K=4 \rightarrow D_f \approx 544\,km$ $K=7 \rightarrow D_f \approx 719\,km$ $K=12 \rightarrow D_f = 942\,km$
C	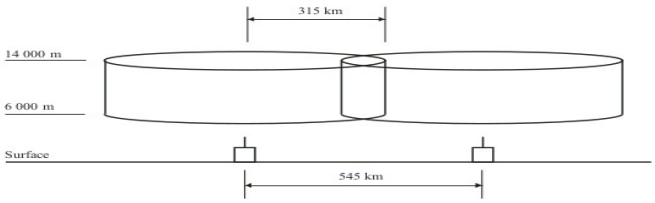	$R_C = 315\,km, d_R \approx 487\,km$ $K=1 \rightarrow D_f \approx 546\,km$ $K=3 \rightarrow D_f = 945\,km$ $K=4 \rightarrow D_f \approx 1{,}091\,km$ $K=7 \rightarrow D_f \approx 1{,}444\,km$ $K=12 \rightarrow D_f = 1{,}890\,km$
D	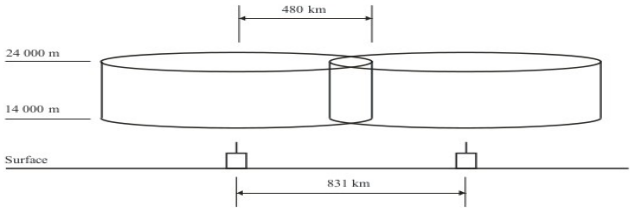	$R_C = 480\,km, d_R \approx 638\,km$ $K=1 \rightarrow D_f \approx 831\,km$ $K=3 \rightarrow D_f = 1{,}440\,km$ $K=4 \rightarrow D_f \approx 1{,}663\,km$ $K=7 \rightarrow D_f \approx 2{,}200\,km$ $K=12 \rightarrow D_f = 2{,}880\,km$

Figure 3.5: 3D cells at distinct altitude ranges and varying cell radii R_C

different LoS "3D cells" that accomodate UAVs at differential operational altitudes. All four classes of 3D cells are summarized in Figure 3.5.

The question that remains unanswered is what cluster size needs to be assigned to all four 3D cells. Under ideal conditions (same cell size and same transmission power) co-channel interference is independent of transmit power and only depends on R_C and D_f. The co-channel reuse ratio $Q = D_f/R_C = \sqrt{3K}$ [64] is a metric that describes the trade-off involved in the design of cellular systems. A small (large) value of Q results in greater capacity (in a lower level of co-channel interference) than it is the case for a large (small) value of Q. ITU suggests in [39] to balance the interference level with capacity for all four LoS 3D UAV cells in the following manner: *Find the* ***smallest*** *cluster size* K^* *such that the edge-to-center*

Table 3.6: Cluster Size K for $i, j \leq 4$

i \ j	0	1	2	3	4
0	–	1	4	9	16
1	1	3	7	13	21
2	4	7	12	19	28
3	9	13	19	27	37
4	16	21	28	37	48

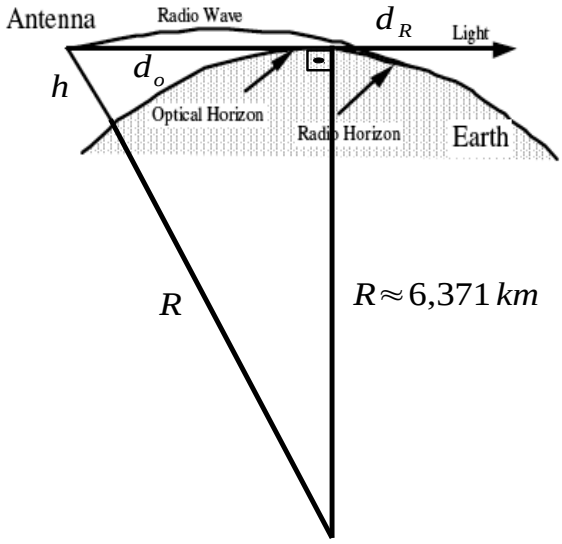

Figure 3.6: Radio and Optical Horizon (modified from [4]) "Communication Systems/Wave Propagation," `https://upload.wikimedia.org/wikibooks/en/b/b7/Surface_wave.gif`, accessed: 2014-12-27. Used under fair use, 2015.

distance [purple line in Figure 3.4] *between two distinct cells using the* ***same*** *radio frequency channel is greater than the radio horizon* d_R or mathematically:

$$\min K \tag{3.3}$$

subject to

$$D_f - R_C > d_R. \tag{3.4}$$

This approach keeps capacity high while limiting co-channel interference. The edge-to-center (EtC) distance uses cells shapes in the form of circles that intersect all six vertices of a regular

hexagon (cf. Figure 3.4). The EtC distance is a function in K and is given by $D_f - R_C$.

The optical horizon can be easily verified to be $d_o = \sqrt{2Rh}$ by using the Pythagorean theorem and assuming $R \gg h$ (cf. Figure 3.6). This derivation, however, does not consider refractive effects of atmospheric layers. Typically, to account for that, a constant k is inserted to above equation, i.e. $d = \sqrt{2kRh}$. Under normal weather conditions k equals $4/3$ to consider for the four-third Earth effect meaning that the actual radio wave refraction behaviour is described by an earth with an extended radius of $4/3 \cdot R$ [6]. All together, this leads to a radio horizon of $d_R \approx 4.12 \cdot \sqrt{h}$ for h in m and d_R in km. The proposed cell radii for 3D cells A, B, C and D all are dimensioned for LoS communication based on lower altitude limits using aforementioned equation for the radio horizon.

With the remarks under the "Notes" column in Figure 3.5, it is easy to compute K^*. The results for all four cells are given in Table 3.7.

Table 3.7: Resulting K^*

Cell Name	**EtC** [km]	$\mathbf{d_R}$ [km]	$\mathbf{K^*}$
A	233	160	7
B	387	319	4
C	630	487	3
D	960	638	3

3.3.2 Aggregating Bandwidth Requirements

Equation (3.2) is used to compute bandwidth requirements for traffic-specific channels in 2030. Traffic with challenging requirements on reliability and overload resiliency (e.g. C2 links in Table 3.9) are assigned a redundancy factor of $R = 2$ and a utilization factor of $U = 0.5$. For these links, reliability is highly important. Values for R and U in case of ATC Relay, C2 and S&A account partially for ARQ overhead. In Table 3.9, the S&A link is categorized in low and medium latency by varying R and U. A link is usually of low latency if sufficient spectral resources ($U \downarrow$) and a back-up link ($R \uparrow$) in case of issues with the communication link exist. Table 3.5 specifies the data rate requirements in bps for command & control, ATC relay, S&A (including video and weather radar data) based on altitudes of the UAVs.

Table 3.8: Estimation of average UAV densities in 2030.

			ITU UAV Definition		
			Small	Medium	Large
Effective Number of UAVs in operation by 2030			6,492[15]	8,919	760
UAV Density [UAV/10000km^2]	Low Altitude	$<$ 1500 m	6.59[16]	–	–
	Medium Altitude	$>$ 1500 m and $<$ 6000 m	–	9.05	–
	High Altitude	$>$ 6000 m	–	–	0.77

Estimates for commercial and public agency UAVs for 2030 due to Figure 5.8a and 5.8b are used to determine M. It is assumed that around 88% of commercial UAVs in Figure 5.8b belong to the agricultural sector that are mainly applied in ground operations (e.g. crop spraying/dusting) [47]. This percentage is not considered for CNPC bandwidth computation. Furthermore, it is assumed that about 15% of all public UAVs will be used on a regular basis. Using the probability of Figure 3.2 and the typical altitude of operation of small, medium and large UAV, the altitude-specific UAV densities (using the US total area of around 9.8 Mio. km^2) are computed. The results are shown in Table 3.8. Note that small, medium and large in Table 3.8 is used to classify the altitude of operation and should not be confused with the UAV type definitions from Section 2.1.6. For further details see Table 33 of [39]. The UAV densities that are computed differ from ITU's results by a factor of approximately 1.02[17] for the small and large cases and by a factor of 5.8 for the medium case.

Table 3.9: Computation of Ratio $R/(U \cdot E)$

	C2	**ATC Relay**	**S&A Low Latency**	**S&A Medium Latency**	**Video/Weather Radar**
R	2	2	2	1.5	1
U	0.5	1	0.5	0.75	1
E [bps/Hz]	0.75				
Ratio $R/(U \cdot E)$	5.33	2.66	5.33	2.66	1.33

The results of spectrum requirements for UL/DL as well as UL AND DL for LoS communication without video and without weather radar (with video and without weather radar) is given in Table 3.10 (Table 3.11). In ITU's computation, it is claimed that their figures account for weather radar and video. However, in the computation they do not explicitly

[15]When considering Nano UAVs, the number increases to 7,229. 25% of all SUAVs from Figure 5.7 are accounted in this number.

[16]The number would be 7.33 if Nano UAVs are also considered.

[17]If Nano UAVs are accounted, then the ratio is 1.14.

Table 3.10: Spectrum Requirement for LoS UAV Communication without Video/Weather Radar

Cell Type	**M**	**K**	$\mathbf{B \cdot R/(U \cdot E)}$ [kHz]			**Spectrum Need** [MHz]		
			DL	UL	Overall	DL	UL	Overall
Surface	3	1	91.2	36.1	127.3	0.27	0.11	0.38
A	5	7	91.2	36.1	127.3	3.19	1.26	4.45
B	70	4	66.5	22.9	89.4	18.61	6.42	25.02
C	24	3	66.5	22.9	89.4	4.79	1.65	6.43
D	8	3	66.5	22.9	89.4	1.60	0.55	2.14
Total						28.46[19]	9.99[20]	38.44[21]

consider data rates for airborne weather radar (27.77 and 3.97 kbps) given in Table 3.5. They use 270 kbps for both video and weather radar, which is actually only the data rate requirement for spare time video.

3.4 Overall Bandwidth Requirement for CNPC

CNPC bandwidth estimates are 65.7 MHz for a terrestrial communications infrastructure with video and 38.4 MHz without video and weather radar data. (Spectral requirements if Nano UAVs are included are provided in the footnotes.) For comparison, ITU's values are 33.9 (UL: 4.6 MHz, DL: 29.4 MHz) and 15.9 MHz, respectively. Note that all links are considered to have a spectral efficiency of 0.75 bps/Hz.

In order to cover the CNPC bandwidth requirement (including video) according to estimates (from this thesis) with the designated bandwidth of 34 MHz *only*, the overall spectral efficiency needs to improve to about 1.45 bps/Hz[18]. Therein included is an improvement in spectral efficiency for DL (UL) to 1.42 (1.63) bps/Hz. The CNPC links are not supposed to carry throughput-intensive payload videos of 1–2 Mbps [9] (cf. Section 2.3) and neither would the designated 34 MHz be sufficient to consider video data transmission.

[18]If Nano UAVs are considered, the spectral efficiency needs to increase to 1.53 bps/Hz
[19]The number would be 29.19 if Nano UAVs are also considered.
[20]The number would be 10.28 if Nano UAVs are also considered.
[21]The number would be 39.46 if Nano UAVs are also considered.

Table 3.11: Spectrum Requirement for LoS UAV Communication with Video and without Weather Radar

Cell Type	**M**	**K**	$\mathbf{B \cdot R/(U \cdot E)}$ [kHz]			**Spectrum Need** [MHz]		
			DL	UL	Overall	DL	UL	Overall
Surface	3	1	451.2	36.1	487.3	1.35	0.11	1.46
A	5	7	451.2	36.1	487.3	15.79	1.26	17.05
B	70	4	102.5	22.9	125.4	28.69	6.42	35.10
C	24	3	102.5	22.9	125.4	7.38	1.65	9.03
D	8	3	102.5	22.9	125.4	2.46	0.55	3.01
Total						55.67[22]	9.99[20]	65.65[23]

As a result it is important that future UAS communications systems need to be more spectrally efficient. In addition, a more effective spectrum management is needed to enable real-time video streaming, among others, from UAVs to GCSs. Furthermore, more spectrum for payload data needs to be allocated.

[22]The number would be 59.28 if Nano UAVs are also considered.
[23]The number would be 69.55 if Nano UAVs are also considered.

Chapter 4

UAV-To-Ground Communication Channel

The simplest communications system for a UAV operating in *segregated* airspace consists of the UAV and the GCS with exclusive frequency assignment for the direct UAV-to-GCS and GCS-to-UAV links, i.e., downlink and uplink. Such links can be LoS or BLoS. As in Section 3.3, this chapter will focus on LoS communication, particularly the underlying communication channel, given that SUAV and MAV with limited operational range will dominate the future airspace.

The situation changes in non-segregated airspace as UAVs and manned aircrafts will need to share airspace. In addition to the GCS and UAV link, communication between ATC and GCS – a direct link or a relay link through the UAV – is required. Critical for UAV airworthiness in NAS are in particular C2 links due to high requirements on reliability and latency. It was shown in Section 3.3 that spectrum demand for CNPC communication in UL and DL is far away from being balanced: 85% of the CNPC spectrum demand is attributed to DL and only 15% to UL. Adding throughput-intensive payload DL data (e.g. real-time video broadcast) in addition to CNPC will intensify the importance of DL. For that reason, this chapter, as part of a comprehensive literature review, is used to study the air-to-ground (A2G) channel in further detail.

Wireless communication is typically subject to *fading*, i.e. amplitude fluctuations over time and frequency [23]. Fading is broadly classified into large-scale fading and small-scale fading (cf. Figure 4.1) [71]. Note that in strict sense, distance-based path loss is not considered

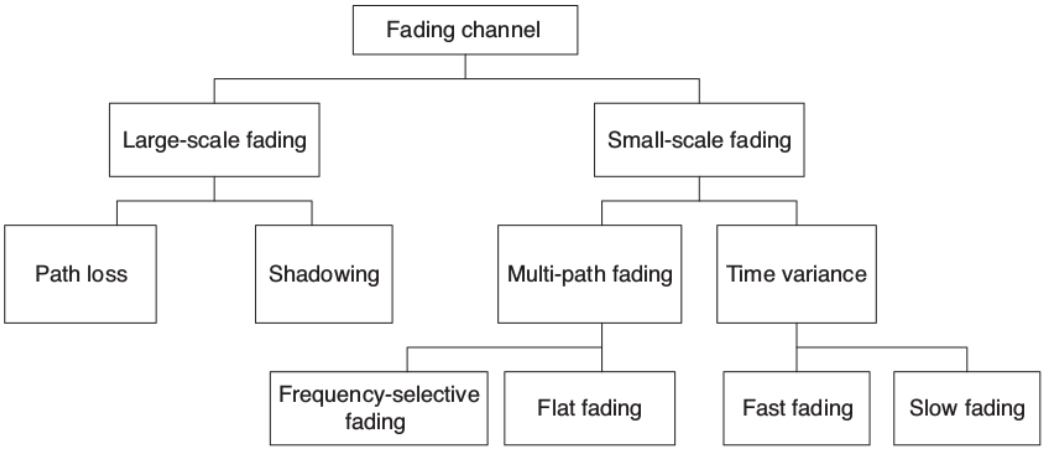

Figure 4.1: Classification of Fading Channels [23] Y. S. Cho, J. Kim, W. Y. Yang, and C. G. Kang, MIMO-OFDM Wireless Communications with MATLAB. Wiley, October 2010. Used with permission from John Wiley and Sons, 2015.

as part of large-scale fading. Large-scale fading through shadowing accounts for shadowing losses in addition to the mean path loss. Nevertheless, we keep the structure of this chapter in agreement with Figure 4.1 for the sake of conformity. Path loss and shadowing models and the time and frequency-selectivity behavior of A2G channels is subject of this chapter.

4.1 Large-Scale Fading

The path loss in dB of direct LoS communication is mainly driven by free space path loss (FSPL) [41]

$$L_{\text{FSPL}} = 20\log(d_{\text{km}}) + 20\log(f_{\text{MHz}}) + 32.45 \tag{4.1}$$

and additional losses (losses due to atmospheric gases, rain attenuation, diffraction losses, multipath fading, etc.) [44]. In the following subsections, the author readdresses all additional losses based on ITU-R Recommendation P.530-11 [44]. Path loss models and shadowing models for A2G channels in built-up areas for LAP and HAP are provided in Appendix A.

4.1.1 Attenuation due to Atmospheric Gases

In [44], the attenuation A_a (in dB) due to absorption by oxygen and water vapor is calculated by

$$A_a = \gamma_a \cdot d_{\mathrm{km}}, \tag{4.2}$$

where γ_a is the specific attenuation in dB/km obtained by Annex 2 of Recommendation ITU-R P.676 [43]. In this thesis, γ_a is computed for a propagation path slightly inclined, i.e. low elevation angles θ, assuming a temperature of 15°C, an air pressure of 1,013 hPa and a water-vapour density of 7.5 g/m^3 for a standard atmosphere. For the two discussed LoS bands (960–977 $\approx$ 1,000 MHz and 5030–5091 $\approx$ 5,000 MHz), γ_a equals $5.4 \cdot 10^{-3}$ dB/km and $7.4 \cdot 10^{-3}$ dB/km, respectively. Attenuation due to atmospheric gases for Cell A (Cell B) with radius $R_C = 65$ km ($R_C = 157$) km equals 0.351 (0.848) dB if $f_{\mathrm{MHz}} = 1,000$ MHz and 0.481 (1.162) dB if $f_{\mathrm{MHz}} = 5,000$ MHz.

4.1.2 Rain Attenuation

The specific rain attenuation γ_R in dB/km as a function of the rain rate R (mm/h) and the carrier frequency is obtained by Recommendation ITU-R P.838 [42] for low, medium and high rain rates ($R = \{1.25, 30, 150\}$ mm/h). The results are shown in Figure 4.2.

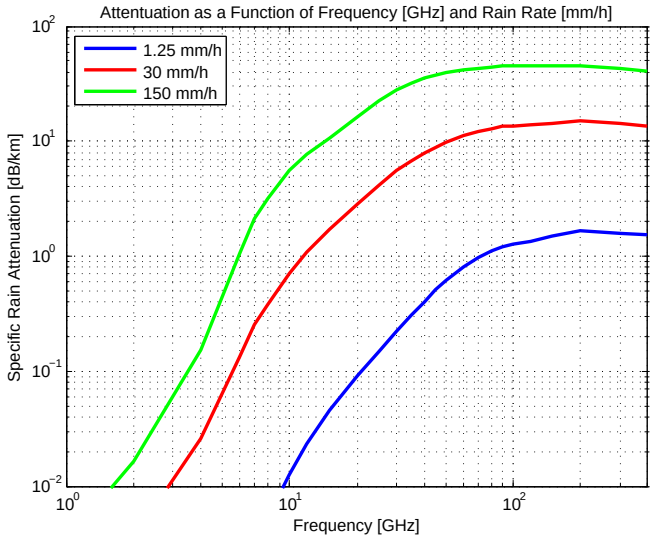

Figure 4.2: Specific Rain Attenuation as a Function of Frequency and Rain Rate

Table 4.1: Specific Rain Attenuation γ_R for Circular Polarization

Specific Rain Attenuation [dB/km]	1.0 GHz	5.0 GHz
$R = 1.25$ mm/h	$4.51 \cdot 10^{-5}$	$1.4 \cdot 10^{-3}$
$R = 30$ mm/h	$7.80 \cdot 10^{-4}$	0.063
$R = 60$ mm/h	$1.14 \cdot 10^{-3}$	0.15
$R = 150$ mm/h	$3.3 \cdot 10^{-3}$	0.45

In the south-east of the US, the rain rate $R_{0.01} = 60$ mm/h is exceeded 0.01% of the time [45]. Using the procedure described in Section 2.4 of [44], the rain path attenuation $A_{0.01}$ for Cell A (Cell B) corresponds to 0.013 (0.015) dB if $f_{\text{MHz}} = 1,000$ MHz and 1.75 (1.96) dB if $f_{\text{MHz}} = 5,000$ MHz. This value is exceeded 0.01% of the time.

4.1.3 Consideration of Additional Losses

In this section fading due to multipath, beam spreading and scintillation is considered. Scintillation fading caused by turbulent irregularities in the atmosphere is negligible for frequencies below 40 GHz [44]. Multipath fading can be caused by refractive atmospheric layers or through surface reflections. In this thesis, the method of small percentages of time [44, 62] is used to compute the fade depth A in dB. The percentage p_w is introduced to control the percentage of time that fade depth A is exceeded. The equations for this particular method were initially introduced by Olsen et al. in [62] and have been further generalized by ITU in [44]. A is given by:

$$A = 10\log(K) + 30\log(d_{\text{km}}) - 12\log(1 + |\epsilon_p|) + 0.33 f_{\text{GHz}} - 0.01\min(h_{\text{UAV}}, h_{\text{GCS}}) - 10\log(p_w), \quad (4.3)$$

where $h_{\text{UAV}}, h_{\text{GCS}}$ correspond to the altitude of the UAV and the GCS antenna in m above sea level. K is the geoclimatic factor that can be estimated by Equation (5) of [44]. $|\epsilon_p|$ is the path inclination in mrad and it can be computed by the trigonometric relation

$$|\epsilon_p| = 1000 \arctan[|h_{\text{UAV}} - h_{\text{GCS}}|/1000 d_{\text{km}}] \approx |h_{\text{UAV}} - h_{\text{GCS}}|/d_{\text{km}}. \quad (4.4)$$

For $h_{\text{GCS}} = 30$ m, $K = 9.12 \cdot 10^{-4}$ and $p_w = 0.2\%$, Table 4.2 lists fade depth values A for both Cell A and Cell B.

Table 4.2: Fade Depth A at Cell Edges for Cell A and Cell B

			Frequency [GHz]	
			1.0	5.0
Cell A	$R_C = 65$ km	$h_{UAV} = 500$ m	20.0 dB	21.3 dB
		$h_{UAV} = 750$ m	18.0 dB	19.3 dB
		$h_{UAV} = 1,000$ m	16.6 dB	17.9 dB
Cell B	$R_C = 157$ km	$h_{UAV} = 2,000$ m	28.9 dB	30.2 dB
		$h_{UAV} = 3,000$ m	26.9 dB	28.2 dB

4.1.4 Link Budget

Combining the impairments discussed in Subsections 4.1.1–4.1.3, it is possible to compute a UL/DL link budget (Table 4.3) for MAV and SUAV at operating frequencies $f_c = 1.0(5.0)$ GHz for 12.5 (37.5) kHz channels. The position 'Additional Losses' accumulates all losses. The transmit power is fixed to reasonable values based on the dimension of the underlying UAV and its GCS. The theoretical SNR is determined based on a theoretical minimum SNR of 6 dB. The procedure is also repeated for DL interference analysis with an interference to noise (INR) level of -5 dB (Table 4.4).

Table 4.3: LoS Link Budget for MAV and SUAV 12.5/37.5 kHz Channels at $f_c = 1.0/f_c = 5.0$ GHz

Parameter	Units	MAV		SUAV	
		UL	DL	UL	DL
TX Power	dBm	20		27	
TX Antenna Gain	dBi	8	0	8	0
TX Cable Loss	dB	1	2	1	2
TX EIRP	dBm	27	18	34	25
Path Distance	km	30.0		23.8	
FSPL (1 GHz)	dB	122		120	
Additional Losses	dB	20		29	
RX Antenna Gain	dBi	0	8	0	8
RX Cable Loss	dB	2	1	2	1
RX Power	dBm	-117			
Noise SPD (T=290 K)	dBm/Hz	-174			
Noise Figure	dB	2			
RX Bandwidth (12.5 kHz)	dB/Hz	41			
RX Noise Power	dBm	-131			
RX SNR	dB	14			
Theoretical SNR	dB	6			
Implementation Losses	dB	2			
Aviation Safety Margin	dB	6			
Required SNR		14			
Excess Margin	dB	0			

Parameter	Units	MAV		SUAV	
		UL	DL	UL	DL
TX Power	dBm	23		30	
TX Antenna Gain	dBi	18	0	18	0
TX Cable Loss	dB	1	2	1	2
TX EIRP	dBm	40	21	47	28
Path Distance	km	10.1		7.1	
FSPL (5 GHz)	dB	126.5		123.5	
Additional Losses	dB	23.5		33.5	
RX Antenna Gain	dBi	0	18	0	18
RX Cable Loss	dB	2	1	2	1
RX Power	dBm	-112			
Noise SPD (T=290 K)	dBm/Hz	-174			
Noise Figure	dB	2			
RX Bandwidth (37.5 kHz)	dB/Hz	46			
RX Noise Power	dBm	-126			
RX SNR	dB	14			
Theoretical SNR	dB	6			
Implementation Losses	dB	2			
Aviation Safety Margin	dB	6			
Required SNR	dB	14			
Excess Margin	dB	0			

Table 4.4: DL LoS Interference Budget for MAV and SUAV 12.5/37.5 kHz Channels at $f_c = 1.0/f_c = 5.0$ GHz

Parameter	Units	MAV	SUAV
		DL	DL
TX Power	dBm	20	27
TX Antenna Gain	dBi	0	0
TX Cable Loss	dB	2	2
TX EIRP	dBm	18	25
Interference Distance	km	106.5	84.6
FSPL (1 GHz)	dB	133	131
Additional Losses	dB	20	29
RX Antenna Gain	dBi	0	0
RX Cable Loss	dB	1	1
RX Interference Power	dBm	-136	
Noise SPD (T=290 K)	dBm/Hz	-174	
Noise Figure	dB	2	
RX Bandwidth (12.5 kHz)	dB/Hz	41	
RX Noise Power	dBm	-131	
Required INR	dB	-5	

Parameter	Units	MAV	SUAV
		DL	DL
TX Power	dBm	23	30
TX Antenna Gain	dBi	0	0
TX Cable Loss	dB	2	2
TX EIRP	dBm	21	28
Interference Distance	km	11.3	8
FSPL (5 GHz)	dB	127.5	124.5
Additional Losses	dB	23.5	33.5
RX Antenna Gain	dBi	0	0
RX Cable Loss	dB	1	1
RX Interference Power	dBm	-131	
Noise SPD (T=290 K)	dBm/Hz	-174	
Noise Figure	dB	2	
RX Bandwidth (37.5 kHz)	dB/Hz	46	
RX Noise Power	dBm	-126	
Required INR	dB	-5	

The range of the link is typically longer for 1.0 GHz (30.0 and 18.9 km) than for 5.0 GHz (10.1 and 7.1 km). The same effect applies for the interference distance.

4.2 Small-Scale Fading

Small-scale fading, or often simply fading, is the rapid variation of the received signal level in the short term. Fading is caused by multipath signal propagation leading to the subsequent arrival of multipath components (MPC) with varying phases [23, 52]. Relative phase differ-

ences of these components can cause constructive and destructive interference. The speed of the TX/RX and surrounding objects causes changes in MPCs [23].

4.2.1 Parameters for Small-Scale Fading

A multipath fading channel is often characterized by its power delay profile (PDP) (cf. Figure 4.3) – a description of MPCs[24] by their relative delay and average power [71]. The average power for each MPC is typically normalized by that of the strongest path.

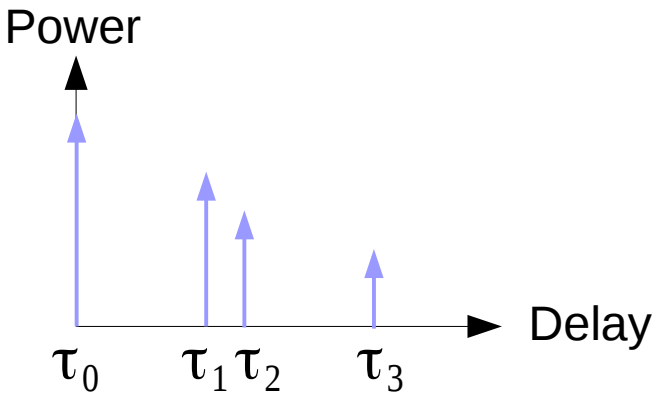

Figure 4.3: Example of a Power Delay Profile

A PDP gives information about the channel delay τ_k, the amplitude a_k and the power $P(\tau_k)$ of the kth path. it is possible to compute the mean excess delay $\bar{\tau}$ by [23, 64]

$$\bar{\tau} = \frac{\sum_k a_k^2 \tau_k}{\sum_k a_k^2} = \frac{\sum_k P(\tau_k)\tau_k}{\sum_k P(\tau_k)}. \tag{4.5}$$

Note that τ_k is measured relative to the first detectable signal at the receiver at $\tau_0 = 0$ [64]. One can think of $\bar{\tau}$ as a mean in delay where each tap k is weighted by its contributing power $P(\tau_k)$ relative to the overall power of all paths $\sum_k P(\tau_k)$.

The RMS delay spread σ_t can be thought of as a power-weighted standard deviation in delay, i.e.

$$\sigma_t = \sqrt{\overline{\tau^2} - \bar{\tau}^2}, \tag{4.6}$$

[24]Sometimes also called path tap.

where $\overline{\tau^2}$ is the second moment

$$\overline{\tau^2} = \frac{\sum_k a_k^2 \tau_k^2}{\sum_k a_k^2} = \frac{\sum_k P(\tau_k)\tau_k^2}{\sum_k P(\tau_k)}. \tag{4.7}$$

The coherence bandwidth, denoted as B_c, is inversely-proportional to the RMS delay spread [23]. The coherence bandwidth is a statistical measure of the frequency range over which the channel has approximately equal gain and linear phase [64]. Typically, the coherence bandwidth is derived from a normalized (cross) correlation function (i.e. a correlation coefficient) of two fading signals at two frequencies f_1 and f_2 [52]. The frequency spacing $\Delta f = |f_2 - f_1|$ leading to a desired value of the correlation coefficient gives an estimate $\hat{B}_c$ of the coherence bandwidth. For a correlation of 0.9 or above, the coherence bandwidth estimate is given by [23, 71]

$$\hat{B}_c = \frac{1}{50\sigma_t} \tag{4.8}$$

and for correlation 0.5 or above by

$$\hat{B}_c = \frac{1}{5\sigma_t}. \tag{4.9}$$

The Doppler effect – a shift in frequency by $\pm f_D$ – comes into place if radio units or obstacles involved in multipath propagation are in motion. In Figure 4.4, the mobile station moves with velocity $\vec{v}$. The Doppler shift f_D can be computed by

$$f_D = \frac{|\vec{v}|}{\lambda} \cos\varphi, \tag{4.10}$$

where λ is the wavelength and φ is the enclosed in Figure 4.4. The maximum positive and minimum negative shift in Doppler, denoted as $f_{D,\max}$ and $f_{D,\min}$, occurs for $\varphi = 0°$ and $\varphi = 180°$, respectively. As multipath propagation φ may vary, a so-called Doppler spectrum evolves. The range of the spectrum is limited by $[f_{D,\min}, f_{D,\max}]$ with resulting maximum bandwidth $B_d = 2f_{D,\max}$.

The coherence time T_c – the counterpart of B_c in the time domain – is estimated by [23, 71]

$$\hat{T}_c = \sqrt{\frac{9}{16\pi f_{D,\max}^2}} \approx \frac{0.423}{f_{D,\max}}. \tag{4.11}$$

T_c is a statistical measure of the time duration over which the channel impulse response (CIR) is invariant, i.e. the duration in time in which two received signals have high amplitude

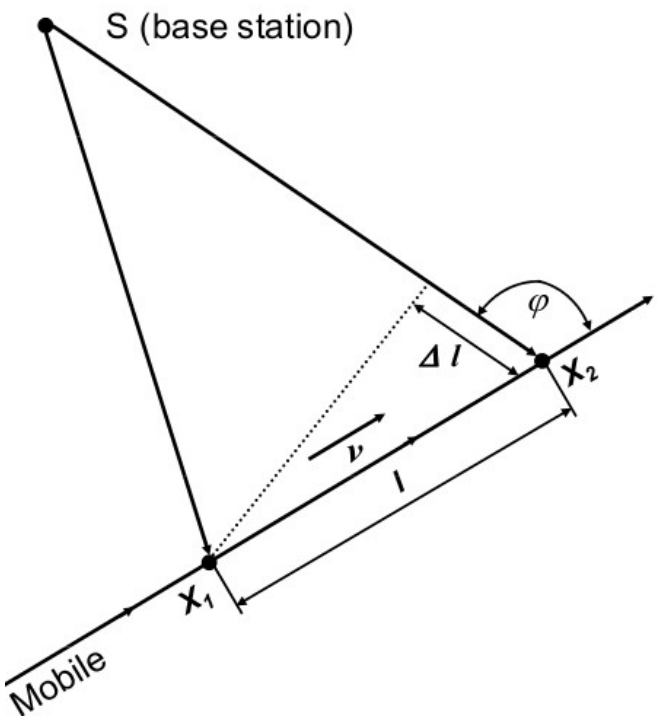

Figure 4.4: Illustration of the Doppler Effect

correlation [64].

4.2.2 Classification of Channels

Dispersive channels, in both frequency and time domain, cause fading. In dispersive channels, two kind of spreads exist [52]: Delay and Doppler spread. Based on the relation of waveform parameters, particularly signal bandwidth and symbol period, and channel parameters described in Section 4.2.1, the fading channel can undergo four possible fadings effects: Flat Fading, Frequency Selective Fading, Fast Fading and Slow Fading [64].

Selective and Non-Selective Channels in Frequency

Due to time dispersion (effectively measured by σ_t), a signal is subject to frequency-selective or frequency-non-selective fading (=flat fading).

Figure 4.5 illustrates how these two types of fading channels differ. For a signal bandwidth B

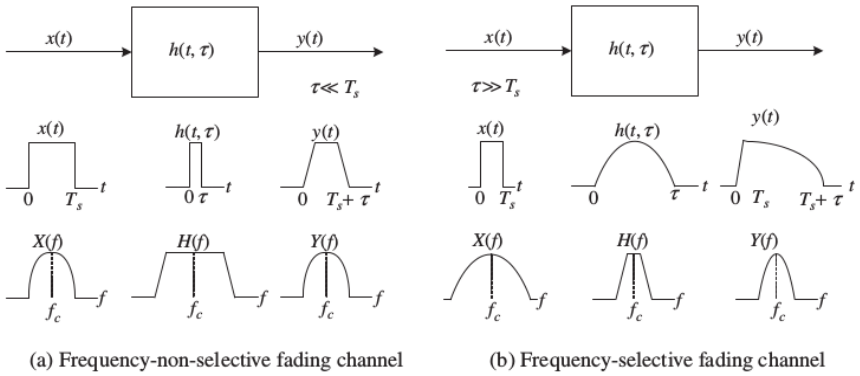

Figure 4.5: Characteristics of Fading due to Time Dispersion [64] T. S. Rappaport, Wireless Communications: Principles and Practice, 1st ed. Piscataway, NJ, USA: IEEE Press, 1996. Used under fair use, 2015.

that is wide enough relative to the bandwidth of the wireless channel, frequency-non-selective fading is typically present (assuming a constant amplitude and linear phase of the wireless channel in its passband). A narrowband signal relative to the channel bandwidth, on the other hand, is equivalent to a symbol period T_s that is greater than the delay spread. This criteria in time implies that consecutive symbols have low inter-symbol-interference (ISI).

In the frequency-selective fading case, the opposite holds true. In summary, we have

$$\begin{cases} B \ll B_c \text{ and } T_s \gg \sigma_t & \text{if Flat Fading} \\ B > B_c \text{ and } T_s < \sigma_t & \text{if Frequency-Selective Fading.} \end{cases} \tag{4.12}$$

Slow and Fast Fading

Depending on the extent of the Doppler spread, RX signals are either subject to fast or slow fading. In fast fading, the CIR changes within a symbol period, (i.e. the coherence time T_c is smaller than the symbol period T_s or) leading to distortion. In the fast fading case, the opposite holds true. In summary, we have

$$\begin{cases} T_s > T_c \text{ and } B < B_d & \text{if Fast Fading} \\ T_s \ll T_c \text{ and } B \gg B_d & \text{if Slow Fading.} \end{cases} \tag{4.13}$$

4.3 Air-to-Ground Channel Model

The A2G channel with time-variant baseband channel impulse response (CIR) $h(t,\tau)$ in its most general form for a single-input single-output (SISO) antenna case is given by [54]

$$h(t,\tau) = \sum_{p=0}^{L(t)-1} \Big[z_p(t)\alpha_p(t) \underbrace{e^{j2\pi f_{D,p}(t)(t-\tau_p(t))}}_{\text{Doppler Effect}} \underbrace{e^{-j2\pi f_c(t)\tau_p(t)}}_{\text{Phase Shift}} \delta(\tau-\tau_p(t)) \Big], \tag{4.14}$$

where $L(t)$ is the number of multipaths, $\alpha_p(t)$ is the amplitude of the p-th multipath, $z_p(t) \in \{0,1\}$ is a persistence process to quantify the duration of MPCs, $f_c(t)$ is the carrier frequency (usually constant over time) and $f_{D,p}(t) = v(t)f_c(t)cos(\phi_p(t))/c$ is the Doppler-shift of the p-th multipath. The parameters $v(t), c$ and $\phi_p(t)$ are the relative aircraft-to-ground velocity, speed of light and the average angle of arrival for multipath component p. Typically we can observe that $f_c \gg |f_D|$, which means that exponential terms in Equation (4.14) change with significantly different rates.

4.3.1 Typical A2G Channel Parameters

We are interested in wideband channel models for A2G in order to derive suitable OFDM waveform parameters in the next chapter. Table 4.5 summarizes the main measurement campaigns and their parameters. Several references from Table 4.5 do not explicitly specify the utilized bandwidth. The campaigns differ in deployed frequency, antenna configuration (including altitude) as well as the ground environment. Table 4.6 (parts based on [54]) summarizes the results for each measurement campaign in terms of the number of MPCs, RMS delay spread as well as the Doppler spectrum. Using the last two parameters, we are able to provide an estimate for coherence bandwidth and coherence time using Equation (4.9) and Equation (4.11). A2G channel measurements in VHF frequency range (30 MHz to 300 MHz) have for example been conducted in Aspen and Dulath [30] leading to (maximum) RMS delay spreads of about 4μs ($\hat{B}_{c,min} = 50$kHz). The RMS value in this case is more than 10 times higher than delay spreads for frequencies in L- and C-bands (see Table 4.6).

The results from Table 4.6 reveal that the RMS delay spread is a function of the aircraft and GCS altitude [57] or elevation angle [60]. The ground environment has an impact on the number of MPCs ([65] vs. [60]). This is in agreement with recent estimates for non-

LOS (NLoS) probabilities for different ground environments [17, 36]. UAVs that operate at higher altitudes will usually produce greater Doppler shifts than SUAVs and MAVs. The different phases (parking, taxiing, take-off, landing, en-route) lead to different A2G channels. Measurements in [20] identify take-off and landing as the most critical phases because maximum delay spread (up to 34μs) as well as large Doppler spread (up to 2.5 kHz) are encountered.

4.3.2 Power Delay Profile

SUAVs and MAVs typically operate at altitudes of less than 3,000 m (cf. Table 2.5). Commercial applications will predominantly take place in built-up areas (cf. Table 2.9). Out of those conducted wideband measurement campaigns and the availability of information, it is believed that measurement results available in [60] best describe fading characteristics of SUAV and MAV channels during the en-route phase. Issues in using results available in [60] are on the one hand that no information about the Doppler spread is available. On the other hand, the utilized frequency of 2.05 GHz and the position of the ground station at ground level (GL) are not typical configurations under which future SUAVs and MAVs will operate. Nevertheless, in this thesis this model is used due to lack of other feasible alternatives.

In [60], four measurements, i.e. four distinct elevation angles (7.5, 15, 22.5 and 30°) have been conducted to determine elevation-specific PDPs. The RMS delay spread typically decreases when the elevation angle increases because the probability of scattered NLoS components increases for small elevation angles. In [60], the mean RMS delay spread varies from 98.1 ns to 18.3 ns for elevation angle 7.5° and 30°, respectively. Table 4.7 lists the average number of MPCs per delay bin.

Table 4.7 is utilized to determine the per delay bin probability. The per belay bin probability is computed by $n_i^\tau / \sum_i n_i^\tau$, where n_i^τ corresponds to the average number of signal components der delay bin i. A uniform random variable is introduced to assign how often a signal component falls into a particular delay bin with specific delay. The power per delay bin is assumed to follow a normal distribution with appropriate mean and standard deviation

Table 4.5: Wideband Configuration for Air-to-Ground Measurements (Vertical Polarization)

Reference	**Frequency** [MHz]	**Antenna** (Elevation Beamwidth)				**(Antenna) Height** [m]		**Ground Environment**
		Aircraft		Ground Station		Aircraft	Ground Station	
		Omni.	Direc.	Omni.	Direc.			
[65]	1,510.5 1,460.5 2,344.5 2,360.5	√	×	×	6° 6° 3° 6°	1,525/ 3,050 AMSL	2.5 (Antenna) + 700 AMSL 4.5 (Antenna) + 700 AMSL	Mountainous Desert
[51]	5,120	√	×	√	×	5,000/ 8,000/ 11,000 AMSL	18 (Antenna) + 750 AMSL	Sonthofen (Germany)
[57]	5,700	√	×	×	2 25° Antennas	370/970/ 1,830	2.10 + ? 7.65 + ?	Sea Surface
[60]	2,050	√	×	4-Array	×	$450 \leq h \leq 950$ AGL	GL	College Campus
[20]	5,135	√	×	×	Dish (d=2.4 m)	Taxiing, Take-off, En-route	Airbus Saint- Martin site	Saint-Martin (Airbus)
[55]	960-977 5,000-5,100	×	Cosine	×	2 x 81° Antennas 2 x 35° Antennas	$h_{\max} = 12,500$	3.5-18.3 + ?	Cleveland & Oxnard

Table 4.6: Resulting (Estimated) Channel Parameters

Reference	$L(t)$		σ_t [μs]		**Doppler Spectrum** [kHz]	$\hat{B}_{c,min}$ [kHz]	$\hat{T}_c$ [μs]	**Comments**
	min	max	average	max				
[65]	3		0.074	–	–	–	–	–
[51]	1 (mainly LoS)		0.0384	0.398	$[-5; 5]$	$\approx$ 500	$\approx$ 85	v=±293 m/s,B=20 MHz STD(σ_t) $\approx$0.021 μs
[57]	2 or 3	7	–	0.480	–	$\approx$420	–	Max RMS for Channel 2 (GCS Height: 2.10 m) and altitude 370 m
[60]	$\approx$8		0.098^{25}	0.485	–	$\approx$410	–	Use of elevation angles θ: 7.5, 15, 22.5, 30°
[20]	1		–	–	$[-3.6; 4.1]$	–	$\approx$105	Time Delay MPC for en-route not considered.
[55]	$\approx$3		–	0.050	–	4000	–	For Oxnard C-band measurement case

Table 4.7: Average Number of Signal Components per Delay Bin for an Elevation Angle of 7.5° [60] W. G. Newhall, R. Mostafa, C. Dietrich, C. R. Anderson, K. Dietze, G. Joshi, and J. H. Reed, "Wideband air-to-ground radio channel measurements using an antenna array at 2 GHz for low-altitude operations," Military Communications Conference, vol. 2, pp. 1422–1427, October 2003. Used under fair use, 2015.

Delay Range [ns]	**Average Number of Signal Components per Delay Bin**	**Delay Range** [ns]	**Average Number of Signal Components per Delay Bin**
0–97	2.98	778–875	0.167
97–195	1.53	875–973	0.180
195–292	1.19	973–1,070	0.107
292–389	0.620	1,070–1,167	0.0664
389–486	0.404	1,167–1,264	0.0389
486–584	0.253	1,264–1,362	0.0228
584–681	0.163	1,362–1,459	0.00265
681–778	0.167	1,459–1,556	0.00139

based on provided example PDPs in [60]. This simulation is done 10,000 times resulting in a PDP prototype defined by the delay vector $\tau = [0\ 33\ 70\ 115\ 175\ 262\ 405\ 682]$ ns and the normalized power vector $P_{dB} = [0\ -8.7\ -9.6\ -11.3\ -13.4\ -15.2\ -17.0\ -20.2]$. The resulting RMS delay spread for the prototype equals $\sigma_t = 87.5$ ns.

Chapter 5

Analysis of OFDM-based Waveform for UAS

OFDM is a technique of modulating digital data on multiple carriers. This technique is used in broadband digital communications systems, such as 4G systems and digital video broadcasting.

Advantages of OFDM include tight channel packing when compared to conventional multi-carrier systems, resource allocation and sharing flexibility and ease of implementation when compared to single-carrier systems. In practical terms this typically leads to higher spectral efficiencies. The use of a cyclic prefix (CP) makes it possible to effectively eliminate inter symbol interference (ISI). Each OFDM subcarrier is an unfiltered waveform whose spectral sidelobes decay slowly. This brings along other challenges that are discussed in continuation. In conclusion, its suitability based on performance is discussed.

5.1 Single-Carrier vs. Multi-Carrier Transmission

In this chapter, single and multi-carrier systems are briefly compared at baseband level. We denote transmit symbols as $\{a_k\}$ that have a symbol period of T_s seconds. A transmit symbol is typically described in an I/Q constellation diagram by $a_k = A_k e^{j\Phi_k}$, implying amplitude modulation schemes ($\Phi_k = \text{const}, \forall k$), phase modulation schemes ($A_k = \text{const}, \forall k$) or both. Without loss of generality, we assume (average) unit symbol energy, i.e. $\mathrm{E}[|a_k|^2] = \mathrm{E}[|A_k|^2] =$

1.

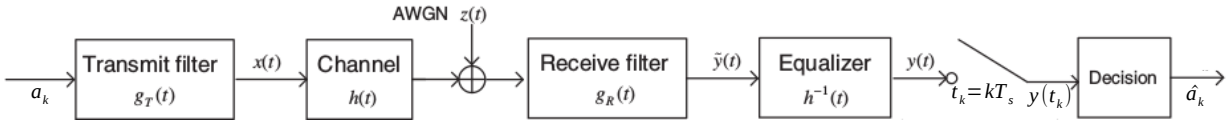

Figure 5.1: Single-Carrier Baseband Communication System Model (modified from [23]) Y. S. Cho, J. Kim, W. Y. Yang, and C. G. Kang, MIMO-OFDM Wireless Communications with MATLAB. Wiley, October 2010. Used under fair use, 2015.

(Baseband) Processes that occur in *single-carrier* systems on both transmitter and receiver side are depicted in Figure 5.1. The overall (system) impulse response is $g(t) = g_T(t) * h(t) * g_R(t) * h^{-1}(t)$ [23]. In the ideal case, channel impairments are fully compensated through the Equalizer $h^{-1}(t)$, i.e. $h(t) * h^{-1}(t) = \delta(t)$. The input to the Decision block (without filtered noise) is given by [23, 63]

$$y(t_k) = \sum_{m=-\infty}^{\infty} a_m g((k-m)T_s). \tag{5.1}$$

Equation (5.1) can be rewritten as

$$y(t_k) = a_k g(0) + \sum_{m=-\infty, m\neq k}^{\infty} a_m g((k-m)T_s). \tag{5.2}$$

The goal is to find a band-limited $g(t)$ such that different symbols at the receiver are isolated avoiding ISI (i.e. Nyquist's zero ISI criteria: $g((k-m)T_s) = 0, \forall m \neq k$) [63]. In thoery, Nyquist's zero ISI criteria can be achieved by a non-causal low pass (LP) filter with *base-band* bandwidth $W = 1/(2T_s)$. The set of physically realizable Nyquist filters $G_{RC}(f)$ are raised-cosine (RC) filters[26], where the so-called roll-off factor r governs the total *baseband* bandwidth ranging from $1/(2T_s)$ for $r = 0$ to $1/(T_s)$ for $r = 1$ [23]. Typically the transmit and receive filter are matched to each other, that is $G_R(f) = G_T^*(f)$ leading to a square-root raised cosine (SRC) filter $G_T(f) = \sqrt{G_{RC}(f)}$. SRC filters guarantee zero ISI *at the receiver* in case of matched filtering.

The minimum required *baseband* bandwidth is $1/(2T_s)$ achieved by a LP Nyquist filter. This bandwidth can be expressed by the symbol rate R_s as $R_s/2$. To increase the data rate a wider bandwidth needs to be utilized. A wider bandwidth, however, leads to dispersion

[26]For further detail, references [23, 63] are recommended.

through ISI resulting in the design of more complex, adaptive equalizers (typically) through FIR filters making high rate wireless transmission less practicle [23].

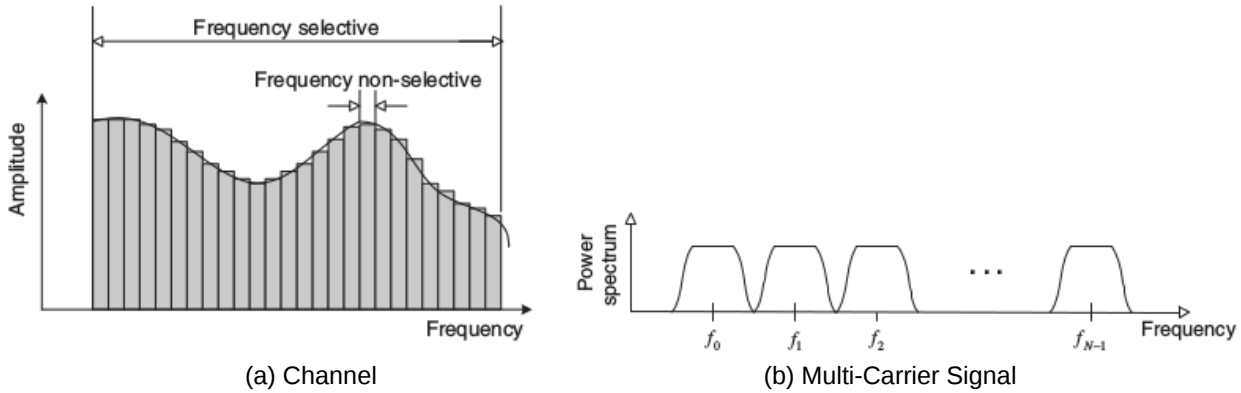

Figure 5.2: Channel and Multi-Carrier Signal in the Frequency Domain [23] Y. S. Cho, J. Kim, W. Y. Yang, and C. G. Kang, MIMO-OFDM Wireless Communications with MATLAB. Wiley, October 2010. Used with permission from John Wiley and Sons, 2015.

In multi-carrier systems, the frequency selectivity of a wideband channel is transformed to N frequency non-selective, flat subchannels according to Figure 5.2. For that, N narrowband subchannels with subcarrier frequency f_k $(k = 0, 1, 2, ..., N-1)$ are utilized. In the most general case, baseband filters at the transmitter side $G_0^{TX}(f), ..., G_{N-1}^{TX}(f)$ and receiver side $G_0^{RX}(f), ..., G_{N-1}^{RX}(f)$ are deployed for shaping subchannels to suppress inter-carrier interference (ICI).

The subchannels in Figure 5.2 are orthogonal subchannels of equal bandwidth centered at $f_k, k = 0, 1, ..., N-1$. If each subchannel is *bandlimited* as in Figure 5.2, the transmission is known as filtered multi-tone (FMT) transmission [23]. OFDM, also a multi-carrier system is similar to FMT with the difference that no (individual) subcarrier-specific bandlimited filters and oscillators are used causing non-negligible adjacent channel interference (ACI). ACI in OFDM is limited by using virtual subcarriers as guard band. FMT implementation is far more complex and challenging than OFDM. In OFDM as opposed to FMT, subcarrier signals overlap in frequency preserving orthogonality. In terms of spectral efficiency FMT is advantageous over OFDM only in a case where the number of subcarriers N is less than 64 [23]. All in all, it is believed that the study of OFDM for UAS is useful due to the ease of implementation and flexibility. Details about OFDM implementation is discussed in consecutive sections.

5.2 Mathematical Description of OFDM

OFDM is based on the concept of orthogonality. Two signals are said to be orthogonal if the integral of the signal products over their common fundamental period T_{sym} is zero, i.e.

$$\frac{1}{T_{\text{sym}}}\int_0^{T_{\text{sym}}} e^{j2\pi\frac{m}{T_{\text{sym}}}t}e^{-j2\pi\frac{i}{T_{\text{sym}}}t}dt = \begin{cases}1, & \forall m=i, m,i\in\mathcal{N}\\ 0, & \text{otherwise.}\end{cases} \tag{5.3}$$

Analogously, for the time-discrete case at sampling instances $t = kT_s = kT_{\text{sym}}/N, k = 0,1,...,N-1$, Equation (5.3) can be reformulated as follows:

$$\frac{1}{N}\sum_{k=0}^{N-1} e^{j2\pi\frac{m}{\cancel{T_{\text{sym}}}}\frac{k\cancel{T_{\text{sym}}}}{N}}e^{-j2\pi\frac{i}{\cancel{T_{\text{sym}}}}\frac{k\cancel{T_{\text{sym}}}}{N}} = \begin{cases}1, & \forall m=i, m,i\in\mathcal{N}\\ 0, & \text{otherwise}\end{cases} \tag{5.4}$$

It can be inferred from the previous two equations that complex exponentials can be orthogonalized over a symbol period T_{sym} if their frequency spacing Δf is integer multiple of $1/T_{\text{sym}}$. OFDM uses this concept to allow OFDM signals to be free from ICI [23].

5.2.1 OFDM Modulation and Demodulation

In an OFDM transmission the transmit symbols $\{a_{k'}\}$[27] are converted into N parallel streams through serial-to-parallel (S/P) conversion. Through S/P N modulation symbols are mapped to N subcarriers. N complex modulation symbols fed through an N-point IFFT to generate N samples (OFDM symbol without cyclic prefix extension) of $NT_s = T_{\text{sym}}$ duration. In this context, the notation $X[s,k]$ is often introduced to denote the modulated data symbol on the kth subcarrier of the sth OFDM symbol. The OFDM signal $x(t)$ is given by:

$$x(t) = \frac{1}{\sqrt{T_{\text{sym}}}}\sum_{s=0}^{\infty}\sum_{k=0}^{N-1} X[s,k]e^{j2\pi f_k(t-sT_{\text{sym}})} \tag{5.5}$$

[27]Without the use of virtual subcarriers, the relationship $s = \lfloor k'/N \rfloor$ and $k = \text{mod}(k'/N) - 1$ holds.

Figure 5.3 shows the OFDM signal in a time-frequency lattice grid. Sampling $x(t)$ at time instances $t = sT_{\text{sym}} + nT_s, n = 0, 1, ..., N-1$ will produce the signal of the sth OFDM symbol

$$x_s(n) = \frac{1}{\sqrt{N}} \sum_{k=0}^{N-1} X[s,k] e^{j2\pi f_k n T_s} = \frac{1}{\sqrt{N}} \sum_{k=0}^{N-1} X[s,k] e^{j2\pi kn/N} \tag{5.6}$$

Equation (5.7) can be effectively realized through an N-point IFFT of modulated data symbols $\{X[s,k]\}_{k=0}^{N-1} = \{a_{k'}\}_{k'=sN}^{N(s+1)-1}$. Assuming no distortion, the data symbols can be perfectly reconstructed at the receiver side by an N-point FFT (as shown below).

$$Y[s,k] = \frac{1}{\sqrt{N}} \sum_{n=0}^{N-1} x_s(n) e^{-j2\pi kn/N} = \frac{1}{N} \sum_{n=0}^{N-1} \sum_{i=0}^{N-1} X[s,i] e^{j2\pi (i-k)n/N} = X[s,k] \tag{5.7}$$

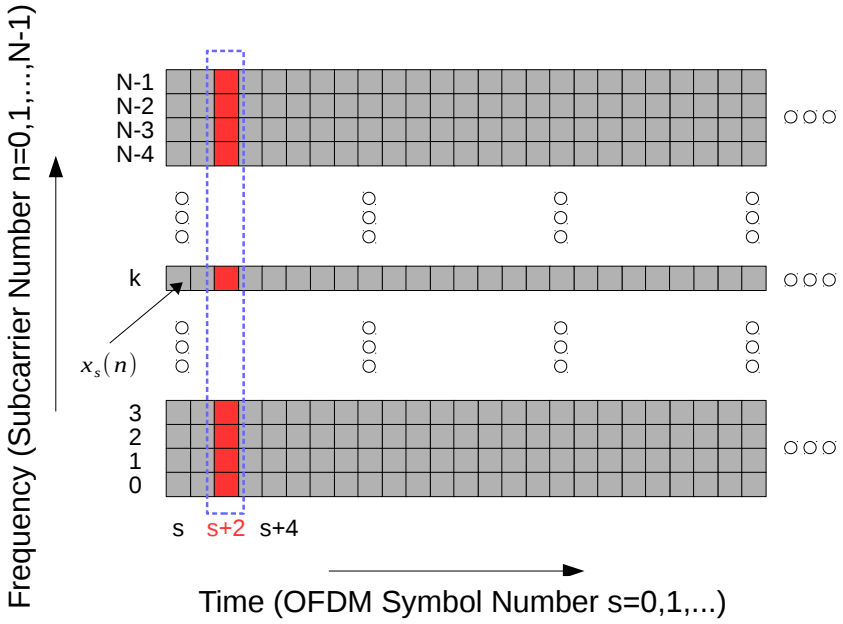

Figure 5.3: OFDM Time-Frequency Resource Grid

5.2.2 Cyclic Prefix Extension

The A2G channel has been identified to be subject to multipath (see Section 4.3). The multipath channel output (plus noise) in OFDM notation for the sth symbol is the convolution

of the transmitted signal with the CIR of length L_h samples. That is:

$$y_s(n) = \sum_{m=0}^{L_h-1} h_s(m)x_s(n-m) + z_s(n) \tag{5.8}$$

It is important to understand that in (5.8), $x_s(-p) = x_{s-1}(N-p)$ for $p \geq 1$. This explains the effect of ISI between consecutive OFDM symbols for $L_h - 1$ samples. This is the reason a guard interval between two consecutive OFDM symbols is required [75, 23]. Guard bands, as opposed to guard intervals, are needed only at the edge of the OFDM spectrum.

The guard interval is typically filled by cyclic extension of the OFDM symbol with cyclic prefix (CP) or cylic suffix (CS). The reason why CP or CS is to be preferred over silent intervals is that Doppler spread and other frequency impairments in an OFDM system can be reliably estimated through the existence of redundant CP/CS intervals using the autocorrelation function of the received signal (cf. reference [22]). In case of CP, for instance, the CP-inserted OFDM symbol at the transmitter side is given by

$$\tilde{x}_s(k) = [\underbrace{\underbrace{x_s(N-N_{CP})\cdots x_s(N-1)}_{\text{CP insertion}}, \quad \underbrace{\{x_s(n)\}_{n=0}^{N-1}}_{\text{Initial OFDM Symbol}}}_{\text{Overall Length } N+N_{CP}} \quad]. \tag{5.9}$$

The overall symbol length after CP insertion is $T_{\text{sym}}^{CP} = T_{\text{sym}} + N_{CP}T_s = (N + N_{CP})T_s$. It can be shown that ISI is completely eliminated if $N_{CP} \geq L_h$, which means that at least L_h samples of $y_s(k)$ will be discarded before the OFDM demodulation [69]. The main disadvantage of CP insertion is that the transmit energy has to be increased by $\gamma_{CP} = (N + N_{CP})/N$ to achieve a desired Signal-to-Noise Ratio (SNR) [75]. In other words, CP insertion results in power loss as well as throughput loss since these samples are discarded at the receiver. This power or throughput loss is usually acceptable and perfect ISI/ICI elimination is usually weighted against excessive power/bandwidth/throughput loss.

The PDP specified in the previous chapter is similar to 3GPPs specified Rural Area channel model (for default velocities of $v = \{120, 180\}$ km/h and classical Jakes Doppler Spectrum) [12]. For 3GPPs PDP, the RMS delay spread equals $\sigma_t = 100$ ns (as opposed to $\sigma_t = 87.5$ ns for the specified A2G PDP). The A2G performance is expected to be similar to that of the Rural Area model.

5.2.3 Guard Bands

From previous subsections, we know that bits are mapped to modulation symbols which are directly modulated to subcarriers without pulse shaping (rectangular pulse). T_{sym} is the effective OFDM modulation symbol period. The rectangular or unfiltered pulse has a sinc-type spectrum, characterized by side lobes that extent to $\pm\infty$ with first-null (baseband) bandwidth of $2/T_{\text{sym}}$ [23]. It is well known that rectangular windows cause large out-of-band power transmission leading to relatively high ACI if not RF filtering were performed. Two main ways to alleviate the effect of ACI in OFDM are time-domain windowing (such as RC windows) and/or the use of $N - N_{\text{used}}$ so-called virtual carriers (VCs), i.e. subcarriers that are not used at both ends of the transmission band. In 4G-LTE, for instance, in most cases (except of 1.4 MHz LTE) the spectral efficiency is reduced by $1 - N_{\text{used}}/N$ which is about 10%. Guard bands are also needed because filtering strong side lobes would modify the spectrum of the subcarriers and significantly compromise the orthogonality among them, leading to ICI.

5.2.4 Receive Diversity for OFDM

Receive diversity (signal processing included) can improve the SNR by using N_{RX} antennas at the receiver and some processing. Out of the three main receive diversity techniques – selection combining, equal gain combining and maximal ratio combining (MRC) – we only consider MRC for simulation due to its superior performance in SNR improvement [15]. MRC weights the different signal components according to the signal quality or SNR before combining them. At the ith receiver front end (after CP detachment and FFT operation), the received symbol (without ISI/ICI distortion) can be written as

$$Y_i[s,k] = H_i[s,k]X[s,k] + Z_i[s,k], \quad i = 0,1,...,N_{RX}-1, \tag{5.10}$$

or in vector form

$$\mathbf{Y}[s,k] = \mathbf{H}[s,k]X[s,k] + \mathbf{Z}[s,k], \tag{5.11}$$

where the bold terms in Equation (5.11) are $N_{RX} \times 1$ vectors. To simplify notation in this section, we sometimes simply write $\mathbf{H}, X, \mathbf{Z}$ instead of $\mathbf{H}[s,k], X[s,k]$ and $\mathbf{Z}[s,k]$. Note that $()^H$ is the Hermitian and $()^*$ is the conjugate complex. The vector $\mathbf{W}^H$ is introduced to

weight each component Y_i to maximize the instantaneous SNR γ, i.e.

$$\gamma = \frac{|\mathbf{W}^H\mathbf{H}X|^2}{E\{|\mathbf{W}^H\mathbf{Z}|^2\}} \overset{|X|^2=1}{=} \frac{|\mathbf{W}^H\mathbf{H}|^2}{\mathbf{W}^H E[\mathbf{Z}\mathbf{Z}^H]\mathbf{W}} \overset{E[\mathbf{Z}\mathbf{Z}^H]=\sigma^2}{=} \frac{|\mathbf{W}^H\mathbf{H}|^2}{\sigma^2||\mathbf{W}||^2} \overset{||\mathbf{W}||^2=1}{=} \frac{|\mathbf{W}^H\mathbf{H}|^2}{\sigma^2}. \tag{5.12}$$

From the Cauchy-Schwarz inequality, we know that γ can be maximized if $\mathbf{W} = \mathbf{H}$. Hence, for 1×2 diversity schemes using MRC, we know that $\mathbf{W}^H = [H_0^*, H_1^*]$ and the MRC combining of $Y_i[s,k]$ becomes:

$$R[s,k] = H_0^*[s,k]Y_0[s,k] + H_1^*[s,k]Y_1[s,k]. \tag{5.13}$$

In summary, in MRC signal components after CP detachment and FFT operation are all weighted by the conjugate complex of the (known) frequency response.

5.3 Subcarrier Spacing and Performance Figures

In this section a suitable subcarrier spacing is chosen and the metric we use is spectrum efficiency. The BER performance of an OFDM signal (using the determined subcarrier spacing) over the defined A2G channel is provided.

5.3.1 Selection of Subcarrier Spacing

Doppler spread or frequency offsets lead to ICI, which becomes more significant when the subcarrier spacing is low. Higher subcarrier spacing can tolerate more frequency offset, but, on the other hand, compromises the assumption of a flat channel. In the previous chapter, an A2G channel applicable to UAVs operating in Cell A and B (during their en-route phase) has been identified. During this flight phase, different UAVs operate under different maximum mission speeds, for example MAVs at 40 km/h, SUAVs at 120 km/h and ULAs at 240 km/h [47]. It is important to alleviate the effect of ICI (Doppler shift, carrier frequency offset, etc.) by selecting the OFDM subcarrier spacing Δf appropriately. Based on the link budget calculations (cf. Table 4.3) the minimum SNR at the receiver is set to 14 dB and the following optimization problem is solved [28]:

$$\Delta f^* = \underset{\Delta f_j}{\operatorname{argmax}} \frac{1}{\mathrm{BW}\left(\frac{1}{\Delta f_j} + N_{CP}T_s\right)} \sum_{k \in A_{\text{eff}}^j} b_L(k, \Delta f_j)(1 - \mathrm{BER}_{\mathrm{AWGN}}(k, \Delta f_j) \tag{5.14}$$

subject to

$$\Delta f_j < \hat{B}_c, \tag{5.15}$$

$$\frac{1}{\Delta f_j} + N_{CP}T_s < \hat{T}_c, \tag{5.16}$$

where $A^j_{\text{eff}} = \{0 \leq q \leq N-1 | q \notin \text{virtual carrier}\}$ is the set of all subcarriers except of VCs. A^j_{eff} is fixed such that $|A^j_{\text{eff}}|\Delta f_j \leq \text{BW}_\alpha$, where $\text{BW}_\alpha = \alpha \cdot \text{BW}$ for $0 \leq \alpha \leq 1$. The FFT-size N is chosen to be the "closest" radix-2 FFT size to the number $\lfloor \text{BW}_\alpha / \Delta f_j \rfloor$. The available bandwidth and the effective bandwidth are fixed to BW = 5.0 MHz and $\text{BW}_\alpha \approx 4.5$ MHz, respectively. $b_L(k, \Delta f_j)$ is the associated per subcarrier QAM bit load given by [24]

$$b_L(k, \Delta f_j) = \text{round}_2\left\{ \frac{1}{c_3} \log_2 \left[c_4 - \frac{c_2}{\ln(\text{BER}_{\text{fixed}}/c_1)} \text{SINR}_{\Delta f_j}(k) \right] \right\}. \tag{5.17}$$

In this case, the $\text{round}_2(x)$ function rounds the (positive) real value x to the even (bit load) integers $\{0, 2, 4\}$ corresponding to no transmission, 4-QAM and 16-QAM. $\text{BER}_{\text{fixed}}$ is the target bit error rate (BER) which we set to 10^{-3}. The *actual* BER in an AWGN channel for M-QAM ($M = 2^{b_L}$) at subcarrier k for a subcarrier spacing Δf_j is approximated by the Chernoff bound through the expression [24]

$$\text{BER}_{\text{AWGN}}(k, \Delta f_j) = c_1 \exp\left[- \frac{c_2 \cdot \text{SINR}_{\Delta f_j}(k)}{2^{c_3 \cdot b_L(k, \Delta f_j)} - c_4} \right], \tag{5.18}$$

where $c_1 = 0.2$, $c_2 = 1.6$, $c_3 = 1$ and $c_4 = 1$ are constants estimating QAM BER performance in an AWGN channel [24]. The SINR[28] at subcarrier k for a selected subcarrier spacing Δf_j is estimated by [28]

$$\text{SINR}_{\Delta f_j}(k) \approx \frac{E[|X[k]|^2]|H[k]|^2 \text{sinc}\left(\pi \frac{\delta f_c}{\Delta f_j}\right)^2}{\sigma_z^2 + \frac{1}{2}\left(\pi \frac{\delta f_c}{\Delta f_j}\right)^2 E[|X[k]|^2]|H[k]|^2}. \tag{5.19}$$

Parameter δf_c incorporates frequency offsets caused by the Doppler effect and local oscillator drifts. For the PDP (using Jake's Doppler Spectrum) defined in the previous chapter and a CP length of $N_{CP}T_s = 2$ μs[29], the (average) SINR per subcarrier at 5 GHz is shown in

[28]This estimate does not account for inter-cell interference and inter-symbol interference.

[29]The CP length is chosen to be 2 μs as the maximum excess delay spread (at 30 dB level) in [60] is

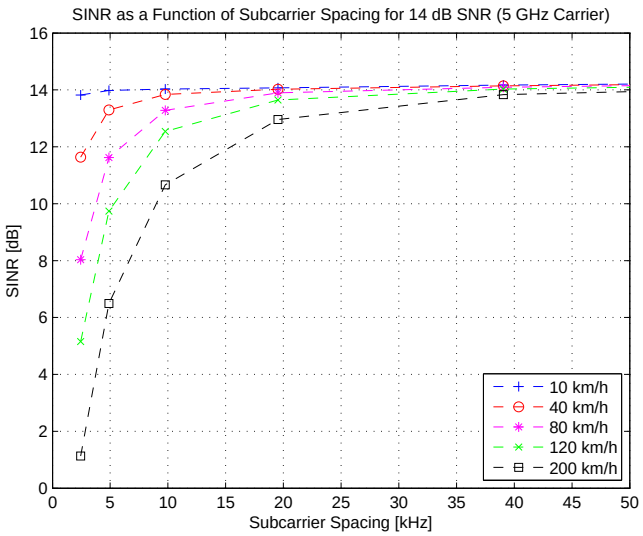

Figure 5.4: SINR as a Function of the Subcarrier Bandwidth at 14 dB SNR

Figure 5.4. Low SINR are observable for relatively low Δf at high velocities.

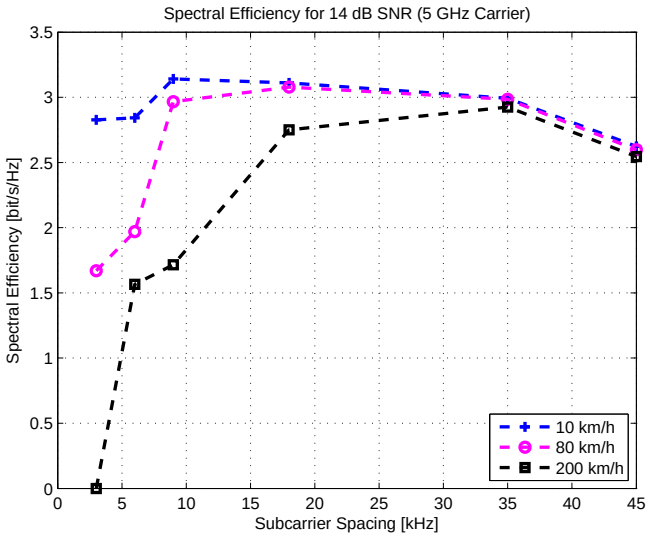

Figure 5.5: Spectral Efficiency as a Function of the Subcarrier Bandwidth at 14 dB SNR at 5 GHz

Solving the aforementioned optimization problem for the finite set of potential subcarrier bandwidths $\Delta f_j = \{3.0, 6.0, 9.0, 18.0, 35.0, 45.0\}$ kHz produces Figure 5.5. For a fixed veloc-

approximately $\tau_{\max} \approx 1.5$ μs.

ity, it can be seen that specific values of Δf_j may be more advantageous than others. The optimal mapping velocity to subcarrier bandwidth at 1 GHz and 5 GHz are shown in Figure 5.6. For 1 GHz the solution to the problem is as follows:

$$\Delta f^*_{1\text{ GHz}} = 9 \text{ kHz} \tag{5.20}$$

Analogously, for 5 GHz:

$$\Delta f^*_{5\text{ GHz}} = \begin{cases} 9 \text{ kHz}, & \text{if } v \leq 60 \text{ km/h} \\ 18 \text{ kHz}, & \text{if } 80 \leq v \leq 140 \text{ km/h} \\ 35 \text{ kHz}, & \text{if } 160 \leq v \leq 200 \text{ km/h} \end{cases} \tag{5.21}$$

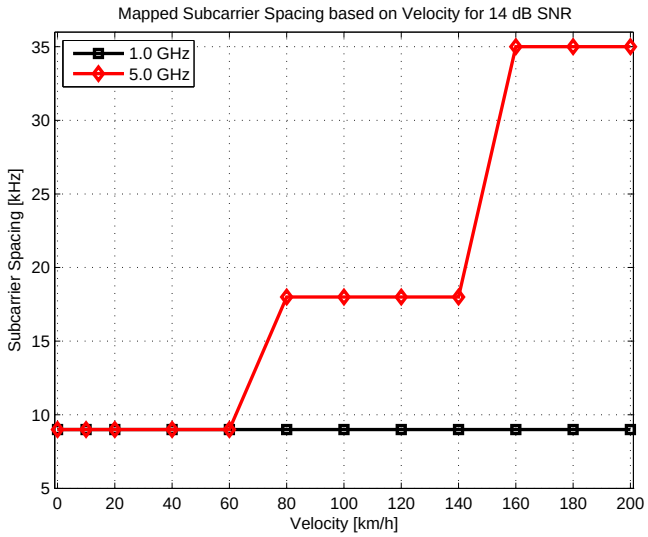

Figure 5.6: Optimal Subcarrier Bandwidth as a Function of Velocity at 14 dB SNR for 1 and 5 GHz Links

Note that the PDP is not changed at different frequencies. The velocities used to obtain Figure 5.6 are finite. To achieve higher accuracy, a frequency-dependent PDP has to be obtained. Nevertheless, this solution can be used as a good approximation in order to design A2G OFDM waveforms. Our results are in line with the common understanding that higher frequency offsets require wider subcarrier spacing (shorter symbol period) to better absorb the ICI.

5.3.2 BER Performance

This section determines the BER of an uncoded, and coded QPSK-modulated OFDM communications system for different waveform and channel parameters. Bose-Chaudhari-Hocquenghem (BCH) codes are utilized. BCH (n, k) codes produce n-bit codewords from k message bits. They are widely used in satellite and wireless data links allowing for a wide range of error correction capability [63]. For further details, we recommend the reader reference [63]. Apart from the impact of interleaving and coding, the effect of MRC on BER is determined. In all cases, the guard interval is set to $N_{CP}T_s = 2$ μs.

Uncoded System

Figure 5.7 shows the results for the uncoded case. The impact of the carrier frequency f_c on the performance is shown in Figure 5.7a. Irrespectively of the carrier frequency, the BER does not differ significantly for $E_b/N_0 \leq 7$ dB (cf. Figure 5.7a). For higher E_b/N_0, in comparison to other cases in Figure 5.7a, the performance for $\Delta f = 18$ kHz at a mobile channel (velocity $v = 40$ km/h) is similar to the theoretical performance of a frequency-selective Rayleigh fading channel. For a BER of $P_b = 4 \cdot 10^{-3}$, one can observe a gain of approximately 1.7 dB when using OFDM with subcarrier spacing of 18 kHz at 1 GHz instead of 5 GHz. We can conclude that greater subcarrier spacing governs BER performance at high SNR (E_b/N_0) regimes. Nevertheless, due to mobility the BER performance flattens and converges to a fixed value for high SNR (for example $P_b \approx 8 \cdot 10^{-3}$ for $\Delta f = 35$ kHz and at $v = 200$ km/h at 5 GHz).

Figure 5.7c reveals that a decrease in the number of effective subcarriers N_{used} does not lead to a significant BER performance improvement. The selection of N_{used} is a trade-off between the required spectrum mask and throughput. Using fewer subcarriers for data transmission, hence, more virtual subcarriers will result in lower out-of-band transmission reducing out of band interference at the cost of lower data rates.

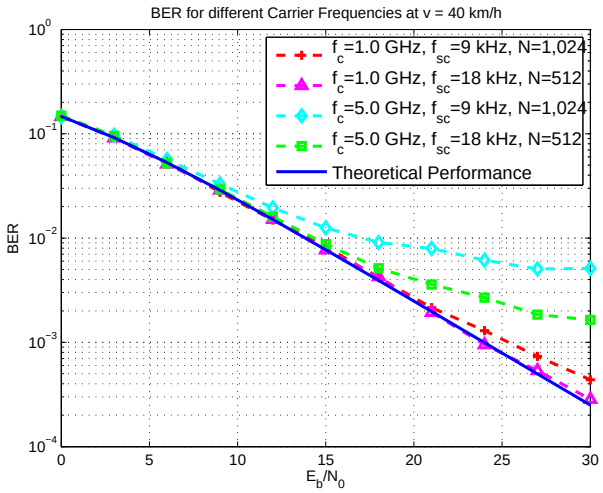

(a) Different Carrier Frequencies

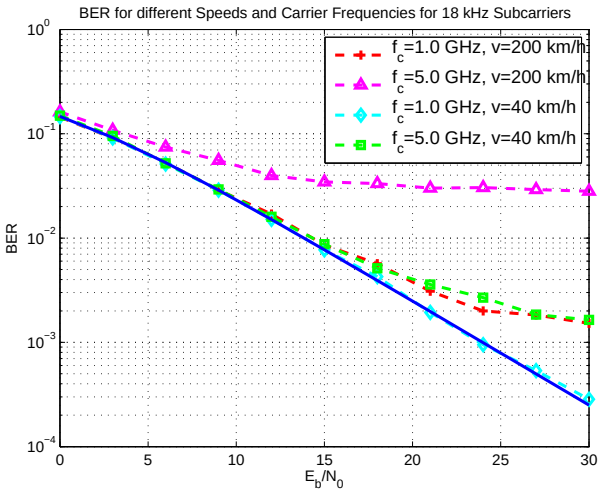

(b) Varying Speed and Carrier Frequency

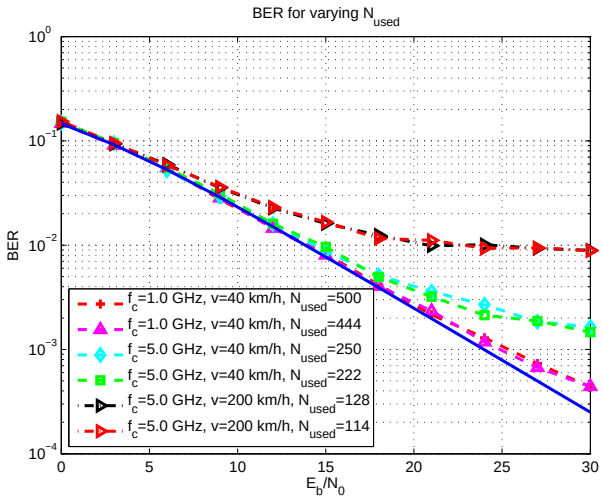

(c) Varying Number of non-zero Subcarriers

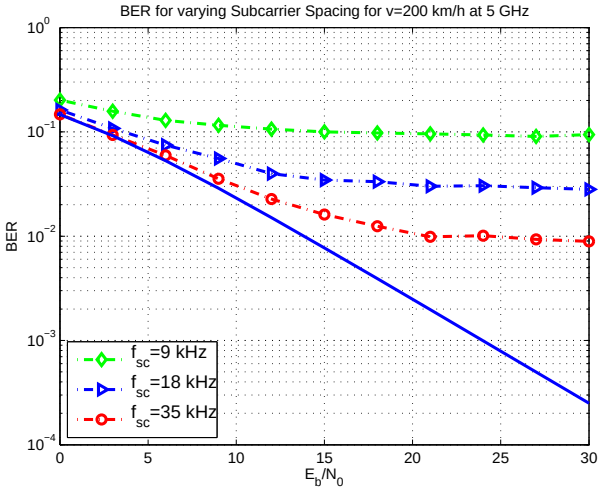

(d) Varying Subcarrier Spacing

Figure 5.7: BER Performance for different OFDM and Channel Parameters as a Function of E_b/N_0

Coded System

In Figure 5.8, the effect of matrix block interleaving[30] and BCH(n, k) codes are illustrated. The code length of BCH codes can be flexibly adjusted to meet design requirements (among others error correction capability t^C). For BCH(15,7), BCH(31,11) and BCH(63,16), t^C

[30] d encoded blocks, each of length n, are arranged in a $d \times n$ matrix for (de)interleaving to reduce the effect of burst errors.

equals 2, 5 and 11. Figures 5.8a through 5.8c show that BCH codes can produce coding gains of up 6 dB for channels with limited mobility (for example 1 GHz links at $v = 40$ km/h) at 10^{-2} BER.

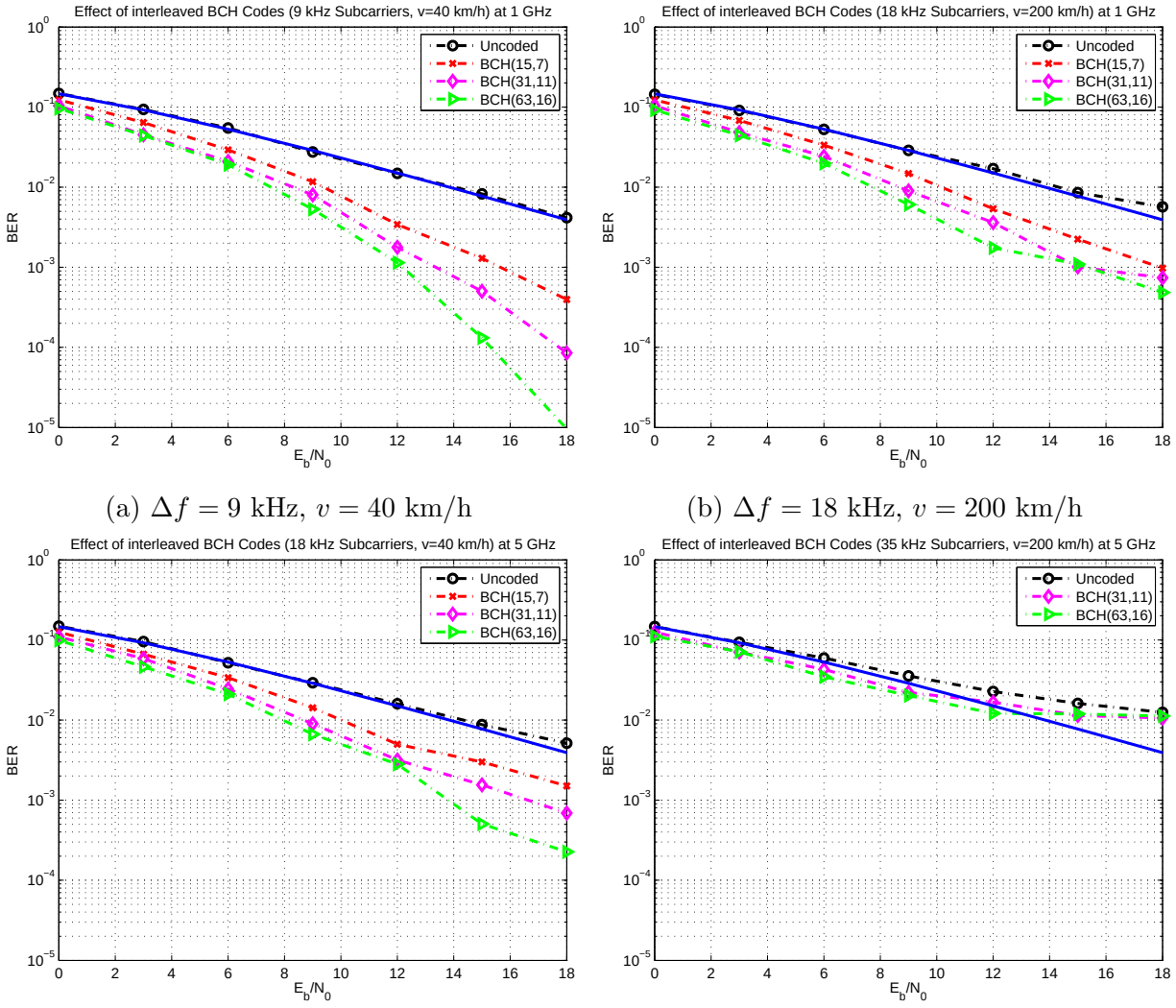

(a) $\Delta f = 9$ kHz, $v = 40$ km/h

(b) $\Delta f = 18$ kHz, $v = 200$ km/h

(c) $\Delta f = 18$ kHz, $v = 40$ km/h

(d) $\Delta f = 35$ kHz, $v = 200$ km/h

Figure 5.8: BER Performance for interleaved and BCH-coded OFDM as a Function of E_b/N_0

Wireless links at high speeds and high carrier frequencies, however, require diversity techniques. Diversity techniques in general are based on the idea of receiving *independent* copies of the same signal [15]. Hence, it is important to avoid correlation between all antenna elements. It is probably easier to achieve higher diversity gains at the GCS than at the UAV. Assuming no correlation between $N_{RX} = 2$ elements, the result of receive diversity using

MRC is shown in Figure 5.9. In this context, Equation (5.13) from Section 5.2.4 is applied to combine the signal from the two antennas.

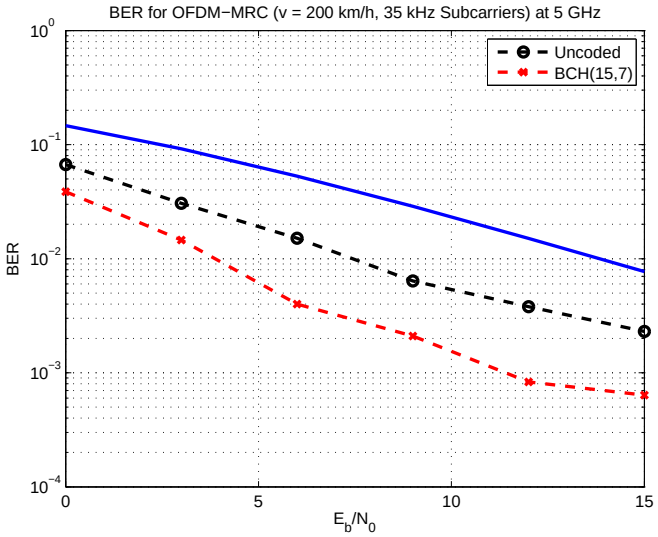

Figure 5.9: Effect of Receive Diversity using MRC for $\Delta f = 35$ kHz, $v = 200$ km/h at 5 GHz

5.4 Waveform Design Recommendation

In Section 5.3.1, optimal subcarrier spacing Δf^* out of a finite set of subcarrier bandwidths Δf_j has been identified for both L (950–1450 MHz [IEEE]) and C-band (4–8 GHz). Note that these bands are likely to be allocated for UAV communications. Based on our results, the subcarrier spacing can be statically fixed to 9 kHz for the L-band and 35 kHz for the C-band. For comparison, Eurocontrol's L-band waveform design of L-DACS1 use a subcarrier bandwidth of 9.76 kHz [46].

The data rate requirement for both UL (cf. Table 5.1) and DL (cf. Table 5.2) have been determined using results from Section 3.2.5. The ratio of UL and DL CNPC data rate requirements (including redundancy links with overhead) equals approximately 1:16. Accounting for *additional* 1 Mbps HD payload video changes the ratio to 1:65. If OFDM is deployed, we suggest in agreement with [46, 78] using OFDM(A)-TDD rather than OFDM(A)-FDD to compensate for UL DL data rate asymmetry. UL and DL control information need to be updated at a minimum rate of 20 Hz (or 50 ms) [39, 78]. We suggest an implementation of

a *fixed* uplink to downlink traffic ratio (instead of a dynamic solution) to simplify network synchronization. An advantage of TDD over FDD is a faster and simpler channel estimation [46]. TDD may also be motivated by the lack of paired spectrum availability (particularly in the L-band) [46]. (OFDMA)-TDD requires in addition to a CP, a UL/DL guard time between transmission and reception. The UL/DL guard time comprises of a time duration attributed to the propagation delay and a time duration for the TX/RX to change from receive to transmit. This interval needs to be sufficiently high to allow the signal to arrive at the receiver before transmission at the receiver in reverse direction occurs. For small cell terrestrial cases, this delay may not be of great issue when TDD is deployed. For the UAS case, however, the delay can reach some ms[31]. For SUAV and MAV cases with communication ranges of 30 km (see Section 4.1.4) the delay may still be dealable (GSM, using TDMA, works for up to 35 km cell radios.).

Each UAV-GCS pair exchanges basic control information (including utilization factor) at a rate of 30.8 kbps for UL and 44.7 kbps for DL (cf. Figure 5.10). The basic control information needs to be packetized and transmitted on an individual basis. Allowing for safe and reliable operation, these links are *not* subject to (spectrum) sharing and are preferably transmitted in the L-band[32]. The SISO-BER performance in the L-band for the specified channel from Section 4.3.2 ($\Delta f = 9$ kHz, $f_c = 1.0$ GHz, $N_{CP}T_s = 2.0$ μs, SNR=14 dB) is approximately $P_b \leq 2 \cdot 10^{-3}$ ($v = 40$ km/h, cf. Figure 5.8a) and $P_b \leq 7 \cdot 10^{-3}$ ($v = 200$ km/h). Depending on the flight of phase and the operating airspace class, S&A weather radar data (and/or S&A spare time video[33]) can be added to the basic DL information.

The effective code rate (obtained from Table 5.1 and 5.2) is approximately 0.687 for UL and 0.646 (0.695) [0.733] for basic control (basic control + weather radar) [basic control + weather radar + spare time video] DL. The BCH(15,7) code from Section 5.3.2 is the code with the closest code rate matching 0.687 and 0.646. With an average bit load $b_L = 2$ bits/Symbol (e.g. QPSK), $P_b = 7 \cdot 10^{-3}$ BW = 5.0 MHz and $\text{BW}_\alpha \approx 4.5$ MHz, the spectral efficiency (including FEC overhead) is 1.134 (1.220) [1.287] for basic control (basic control + weather radar) [basic control + weather radar + spare time video] DL. Further improvement is possible by diversity techniques.

[31]For example, a signal in a TX-RX case with communication range of 100 km has a propagation delay of approximately 0.33 ms.

[32]Note that spectrum in the L-band may not suffice.

[33]These links may be subject to spectrum sharing.

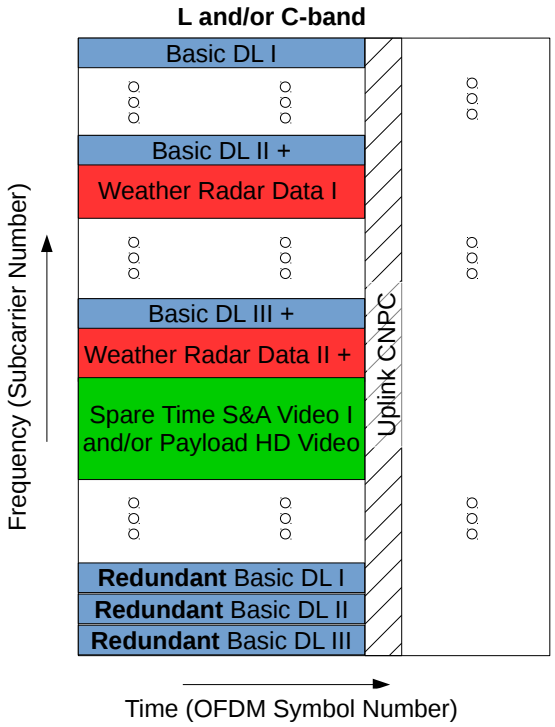

Figure 5.10: OFDM(A)-TDD Resource Grid containing Basic UL/DL Channel, DL S&A Channels and DL Payload Channels

Table 5.1: UL Data Rate Requirement with and without Overhead Accounting for Utilization Factor U and Redundancy Factor R

			Accounting for Redundancy R		**Accounting for Redundancy R & Utilization U**
UL	**Without Overhead** [kbps]	**With Overhead** [kbps]	**Without Overhead** [kbps]	**With Overhead** [kbps]	**With Overhead** [kbps]
Control	2.424	4.606	4.848	9.212	18.424
NavAIDs	0.352	0.669	0.704	1.338	2.676
ATC Voice Relay	4.133	4.798	8.266	9.596	9.596
ATS Data Relay	0.049		0.098		
Total	6.958	10.121	13.916	20.244	30.794
Resulting Overhead Factor	1.455				—

Table 5.2: DL Data Rate Requirement with and without Overhead Accounting for Utilization Factor U and Redundancy Factor R

			Accounting for Redundancy R		**Accounting for Redundancy R & Utilization U**
DL	**Without Overhead** [kbps]	**With Overhead** [kbps]	**Without Overhead** [kbps]	**With Overhead** [kbps]	**With Overhead** [kbps]
Control	4.008	7.615	8.016	15.23	30.46
NavAIDs	0.600	1.140	1.200	2.280	4.560
ATC Voice Relay	4.133	4.798	8.266	9.596	9.596
ATS Data Relay	0.059		0.118		
Basic DL CNPC Total	8.800	13.612	17.600	27.224	44.734
Resulting Basic Overhead Factor	1.547				—
Weather Radar Data	20.6	27.7	20.6	27.7	27.7
Basic + Radar Total	29.4	41.312	38.2	54.924	72.424
Resulting Basic + Radar Overhead Factor	1.405		1.438		—
Video Spare Time	200	270	200	270	270
Total	229.4	311.312	238.2	324.924	342.424
Overall Overhead Factor	1.357		1.364		—

The propagation of signals at different flight phases is to our best knowledge not yet fully understood. Existing literature, e.g. [20], reveals that during departure and landing a much higher delay spread is experienced (than for en-route). Hence, the guard interval is a function of the flight phase. Due to ease of implementation, one should rely on the worst-case scenario. For that purpose, future research needs to study the multipath A2G channel at different altitudes and a characteristic set of ground environments.

To avoid significant interference it may not be possible to use OFDM(A) with cluster size $K = 1$. Instead, a 1/K-reuse scheme needs to be applied. $K = 1$ in combination with interference cancelation techniques, inter-cell interference coordination techniques (e.g. fractional frequency reuse) require high antenna directionality and need further research.

Chapter 6

Spectrum Management

This chapter summarizes concepts for UAV spectrum management. Initially, we introduce what we believe is an appropriate spectrum management infrastructure for future A2G UAV deployment in NAS. That followed, three main UAV spectrum sharing scenarios for individual and cooperative UAS missions are introduced. Each scenario is explained and evaluated for its capability to enable future research.

6.1 Spectrum Management Infrastructure

FCC and NTIA (and partly FAA in aviation) as regulatory bodies in the US are responsible for spectrum allocation and distribution of available spectrum. In the context of UAS, spectrum may be distributed *directly* to (UAS) users and/or distributed *indirectly* through network providers to (UAS) users [61]. In [61], five distinct UAS C2 spectrum management systems have been identified. The first system relies on direct involvement of regulatory bodies in dynamic spectrum assignment of UAS on a competition base, for instance first-come first-served basis. In the second system of [61], direct involvement of FCC and NTIA is prevented through the installation of a spectrum broker as intermediary. The third system extends system two by the introduction of a single, national network provider in addition to direct spectrum assignment for non-networked users. System four adds a single network provider for each region in a nation. The last system establishes regional competition by multiple network providers. We believe that all these systems can be extended to payload information if payload spectrum is allocated. The most appealing system has to

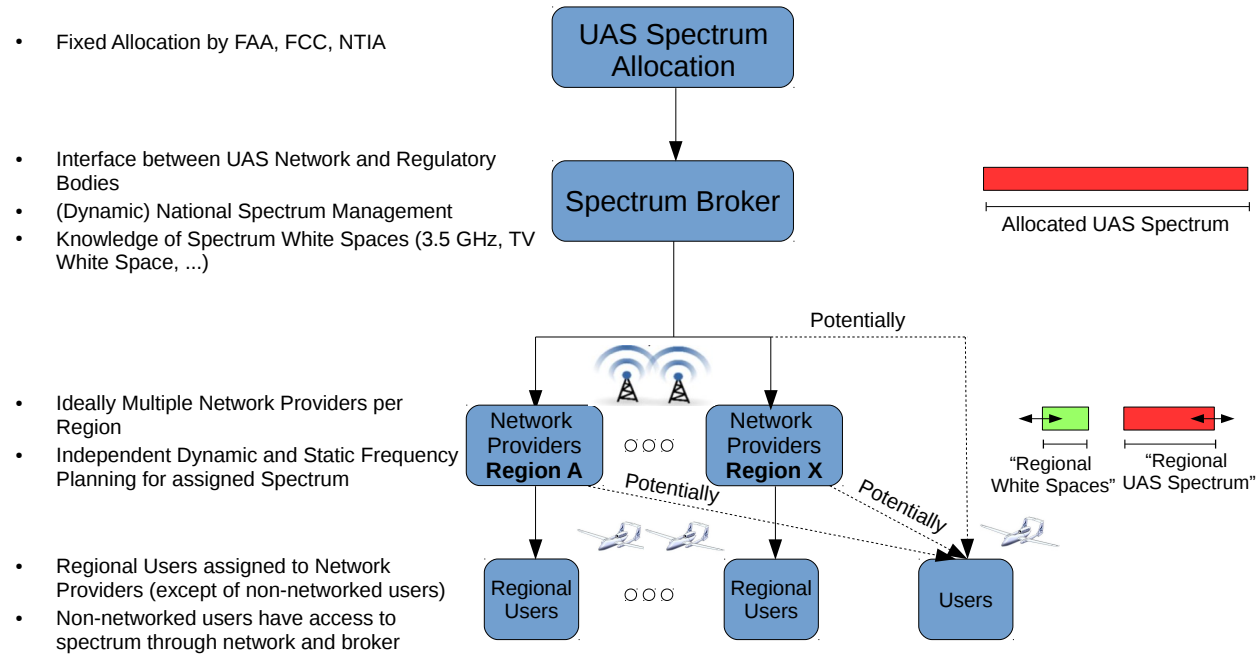

Figure 6.1: (Dynamic) UAS Spectrum Management Infrastructure (modified from [61]) NextGen Institute, "UAS C2 Spectrum Work Group with Industry," Tech. Rep., June 2014. Used under fair use, 2015.

produce an overall system avoiding significant interference, facilitate competition, allow for high frequency utilization and adequately restrict governmental involvement (FAA, etc.) in (dynamic) spectrum management, network creation and standardization.

The most appropriate solution as we believe that meets above requirements is illustrated in Figure 6.1. This solution corresponds in great detail with system five. The regional division enables the *cellular concept* of Section 3.3.1. As a consequence, UAVs are subject to radio handoff procedures. Regulatory bodies will allocate (UAS) spectrum in an international process through ITU. This is also part of the WRC 2015 agenda [38]. A spectrum broker system is established to reduce the involvement of governmental bodies. The broker system manages UAS spectrum and accumulates knowledge about (location-based) spectrum availability (e.g. TV white space, 3.5 GHz) and UAV parameters (locations, range, etc.). *Multiple*, regional network providers in a nation stimulate efficient spectrum utilization through competition. Network providers are responsible for coverage of networked and non-networked UAS users. A single network provider in a region could manage only a specific set of all UAVs in their corresponding cells or all types of UAVs. Depending on the UAV range, flight path, etc. in

a region[34], network providers will lease a rather long-term, quasi-static quantity of spectrum to accommodate UAVs with low depth values (cf. Section 6.2). In addition to quasi-static spectrum, we believe, there is also the need to cover other UAVs through dynamic spectrum access in collaboration with the spectrum broker and other network providers in the same region on a more frequent, temporary lease basis. Due to changes in demand over time, dynamically leased spectrum is attractive to overcome outage for short time ranges. Priority in spectrum access is given to the regional users of network providers. Nevertheless, the provider can procure *non-networked* users with spectrum on a secondary basis if dynamic spectrum leases have not expired, yet. The subarchitecture that needs to be created between spectrum broker and all regional network providers can use a singular centralized broker system or multiple broker systems.

6.2 Cell Changeover

As already mentioned in Section 6.1, we suggest using a cellular-type A2G system, where cells help better managing the available RF spectrum. In the infrastructure context of Section 6.1, a region can be thought of as a combination of various 3D cells (cf. Section 3.3.1). Every cell is a 3D body with minimum altitude $h_{\min}$, maximum altitude $h_{\max}$ and base area. The base area corresponds to a regular hexagon or a circle of radius R_C. The base area cell radius R_C equals the maximum 2D communication range d_{CR} of GCS and UAV. Depending on the (propagation) model used (radio horizon approach vs. approach in Section 4.1 vs. approach in Appendix A), the value of d_{CR} may vary significantly. Routes are either pre-planned (point-to-point or aerial-based) or unplanned [39] (cf. Figure 6.2). The UAV range d_{Rg} in ITAR (International Traffic in Arms Regulations) terminology is defined as the maximum distance a UAV can fly in *one direction* (i.e. point-to-point aerial work) under perfect flight conditions when completely fueled [7]. The total distance covered for all three type of routes in Figure 6.2 are limited by d_{Rg}. The range in this thesis is estimated by: 2 $\times$ upper bound on mission radius (cf. Table 2.5). Note that if more information about the actual UAV is available, d_{Rg} can be accurately estimated or updated (during the flight).

Figure 6.3 shows three distinct cases when a UAV passes (i.e. cell changeover) or remains

[34]In this context, we understand a region as a subarea of a country. This regional approach is likely to be preferred by UAS owners due to more control over the system.

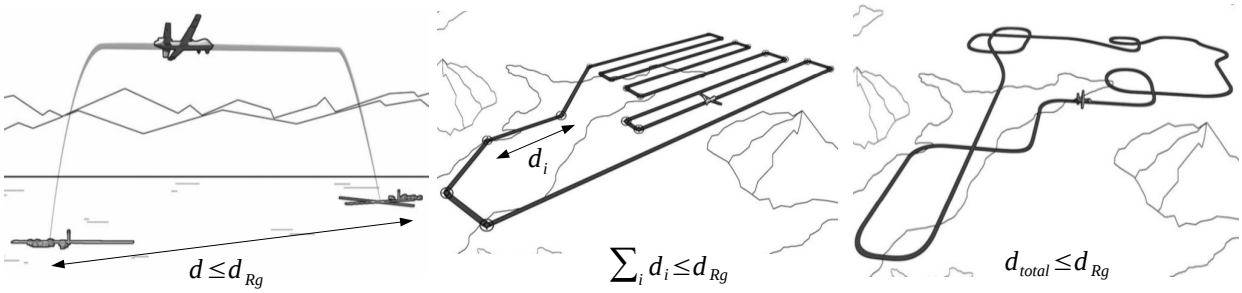

(a) Point-to-Point Aerial Work (b) Planned Aerial Work (c) Unplanned Aerial Work

Figure 6.2: Types of UAV Routes

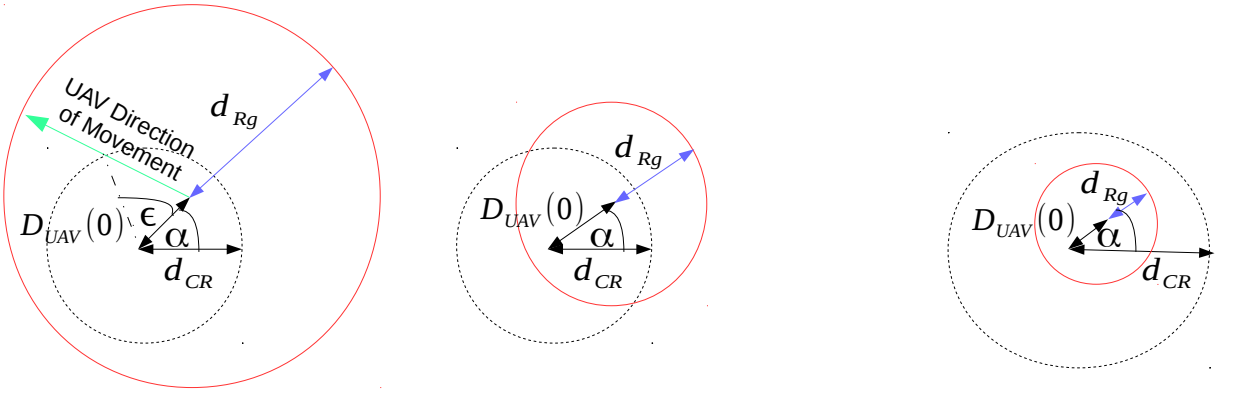

(a) $d_{Rg} > d_{CR} + D_{UAV}(0)$ (b) $d_{CR} - D_{UAV}(0) < d_{Rg} \le d_{CR} + D_{UAV}(0)$ (c) $d_{Rg} \le d_{CR} - D_{UAV}(0)$

Figure 6.3: Cases for Cell Changeovers

(fully/partially) inside its initial cell[35]. The 3rd dimension – the elevation – is omitted because the en-route flight phase is by far the most significant flight phase in time (cf. Section 2.2.2), i.e. the range is mainly determined by the distance covered during the en-route phase. During the en-route phase, height fluctuations of UAVs are negligible making the elevation angle less relevant. The cases (a), (b) and (c) depend on the parameters: GCS-UAV distance $D_{\mathrm{UAV}}(0)$ during take-off (i.e. at time $t = 0$), communication range d_{CR} and UAV range d_{Rg}. Assuming a constant UAV speed v, it may be beneficial to compute case-specific parameters (such as time ratios). This is done (for all cases except of (c)) in the consecutive Subsections 6.2.1 and 6.2.2.

[35]The assumption is $d_{CR} > D_{\mathrm{UAV}}(0)$ to guarantee that the UAV is initially inside its destined cell.

6.2.1 Cell Changeover Parameters

In this section we consider cases (a) and (b). Let t_1 and t_2 be elapsed times the UAV needs to reach the circle boundaries. A_1 and A_2 denote the corresponding areas. Then we can show

$$\frac{t_1}{t_2} = \sqrt{\frac{A_1}{A_2} - \frac{(2d_{CR}D_{\mathrm{UAV}}(0)\cos(\epsilon) - D^2_{\mathrm{UAV}}(0))}{d^2_{Rg}}} = \frac{\sqrt{d^2_{CR} + D^2_{\mathrm{UAV}}(0) - 2d_{CR}D_{\mathrm{UAV}}(0)\cos(\epsilon)}}{d_{Rg}}. \tag{6.1}$$

We define the *depth* D_p as the fractional number of traversed cells (without initial cell). The ceiling function applied on the depth, i.e. $\lceil D_p \rceil$, denotes the number of handoffs (for point-to-point aerial work). The minimum depth for $\epsilon = 0°$ is given by

$$D_p^{\min} = \max\left\{\frac{d_{Rg} - (d_{CR} + D_{\mathrm{UAV}}(0))}{2d_{CR}}, 0\right\}. \tag{6.2}$$

The difference between case (a) and (b) is that the depth for (b) is *always* less than 1 (as opposed to (a)). The depth for case (c) is always 0.

6.2.2 Area Ratio for Case (b)

In case (b), it is also interesting to find the area of the asymmetric "lens" A_L (caused by the intersection of the two circles) and compare the area with the total area of the red circle (i.e. compute ratio $\frac{A_L}{A_2}$). This can be regarded as some sort of probability.

It can be shown (cf. [77]) that A_L corresponds to:

$$\begin{aligned} A_L =& d^2_{Rg}\arccos\left(\frac{D^2_{\mathrm{UAV}}(0) + d^2_{Rg} - d^2_{CR}}{2D_{\mathrm{UAV}}(0)d_{Rg}}\right) + d^2_{CR}\arccos\left(\frac{D^2_{\mathrm{UAV}}(0) + d^2_{CR} - d^2_{Rg}}{2D_{\mathrm{UAV}}(0)d_{CR}}\right) - \\ & \frac{1}{2}\sqrt{(-D_{\mathrm{UAV}}(0) + d_{Rg} + d_{CR})(D_{\mathrm{UAV}}(0) + d_{Rg} - d_{CR})(D_{\mathrm{UAV}}(0) - d_{Rg} + d_{CR})} \\ & \overline{(D_{\mathrm{UAV}}(0) + d_{Rg} + d_{CR})}. \end{aligned} \tag{6.3}$$

6.2.3 Depth and Time Ratios for MAV and SUAV

In practical systems, we believe that $D_{\mathrm{UAV}}(0) \leq 10$ km holds in many cases. d_{Rg} for MAV and SUAV correspond to 16 and 80 km (cf. Table 2.5). 3D cells that accommodate both

MAV and SUAV have a communication range of approximately $d_{CR} = 30$[36] km (cf. Table 4.3). For MAVs on the one hand, case (c) applies, for SUAVs on the other hand, case (a) applies. SUAV simulation results depicting t_1/t_2 and D_p CDFs are shown in Figure 6.4 using a uniform distribution and a truncated version of a Gaussian distribution $\mathcal{N}(\mu_\epsilon, \sigma_\epsilon = 3\frac{1}{3}^\circ)$ to simulate the uncertainty in the path (through statistical modeling of ϵ). After truncation and normalization, the range of the former Gaussian distribution is limited to $[\mu_\epsilon - 3\sigma_\epsilon, \mu_\epsilon + 3\sigma_\epsilon]$.

Since $\alpha = 10^\circ$, the position of the UAV relative to the GCS (GCS in the origin), is in the first quadrant of a 2D axis. Hence, aerial work with path angles $\epsilon = 150^\circ$ and 230° tend to produce greater distances to the cell boundary of the initial cell. This leads to greater t_1/t_2 ratios and therefore smaller average depths. In conclusion, the two quantities introduced in this section characterize UAVs in UAVs that remain in their initial cell or tend to change the communication cell. For that the (current) mechanical range and path angle are utilized. The quantities support a-priori and dynamic spectrum planning.

6.3 Frequency Planning

6.3.1 Static Frequency Planning

With the classification of cell changeovers in Figure 6.3, it is possible to support spectrum or frequency planning of UAVs in 3D cells. The cell radius d_{CR} is fixed to meet minimum performance requirements. To reuse the same frequency, interference between UASs using the same resources is limited by choosing an appropriate 2D interference (avoidance) distance d_{int}[37] such that maximum INR level requirements are satisfied [56]. d_{int} denotes the (minimum) UAV-GCS 2D distance that causes interference that meets (maximum) INR threshold requirement at a GCS by a UAV attributed to a different cell. The smallest frequency reuse pattern K^* is applied that still achieves $D_f - R_c \geq d_{int}$. In case of SUAV and MAV ($d_{CR} = 30$ km, $d_{int} = 85$ km as computed in Section 4.1.4), K^* equals 7. In reference [56], the authors *estimate* the success rate P_S that C independent channels in a (rectangular) deployment area with diameter D_{AOD} suffice (provided that N UAVs are *uniformly* distributed in the

[36]For the radio horizon-based approach introduced in Section 3.3.1, d_{CR} for Cell A equals 65 km.

[37]Note that $D_f - R_c$ in Section 3.3.1 needs to be greater or equal to d_{int}. In aforementioned section, a radio-horizon based approach is used to limit interference by setting $d_{int} > d_R$. In Section 4.1.4, d_{int} values for -5 dB INR have been determined.

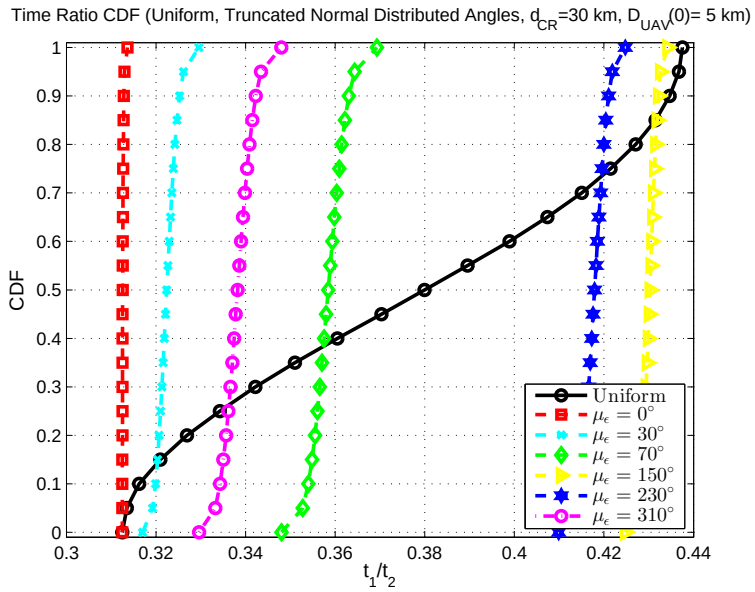

(a) CDF of t_1/t_2 Ratio

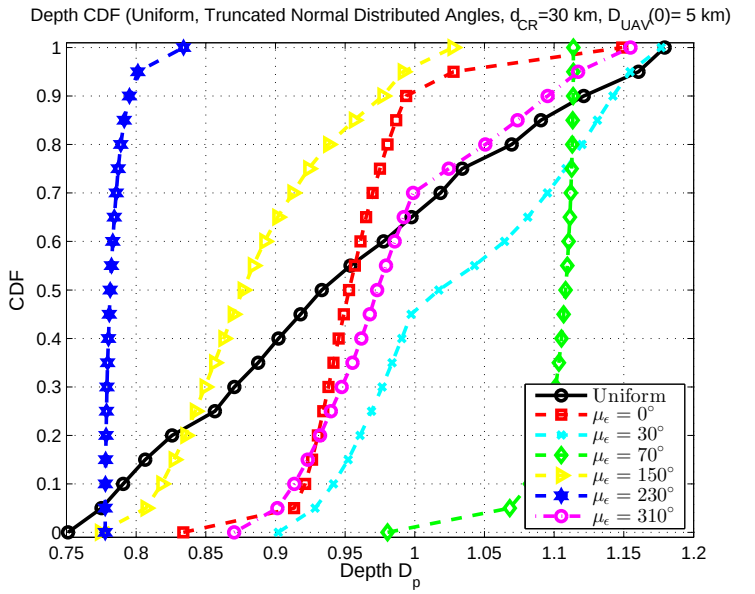

(b) CDF of Depth D_p

Figure 6.4: CDF of t_1/t_2 and D_p ($D_{\text{UAV}}(0) = 5$ km, $d_{CR} = 30$ km, $d_{Rg} = 80$ km, $\alpha = 10°$)

deployment area) as follows:

$$P_S = \sum_{i=1}^{C} \frac{(N-1)!}{(N-i)!(i-1)!} \left(\frac{D_f}{0.5D_{AOD}}\right)^{i-1} \left(1 - \frac{D_f}{0.5D_{AOD}}\right)^{N-i}. \tag{6.4}$$

The main issue with fully static frequency planning as suggested in Equation (6.4) is that UAV characteristics, flight path, and other parameters are not fully taken into account. Instead, we suggest categorizing UAVs based on its depth probability[38] (e.g. $p(0 < D_p \leq 1)$, $p(D_p > 1)$), UAV direction of movement, mission (start) time and mission duration. For instance, the minimum number of channels per cell for a planning period is determined by the number of UAVs with $D_p = 0$ (cf. Figure 6.3 (c)) that overlap in mission time. Note that for MAVs, case (c) applies.

With this approach, it is possible to apply quasi-spectrum planning on a per cell basis and overall frequency planning for a planning duration. The required spectrum can be acquired from the spectrum broker. Required CNPC spectrum (without S&A) can be reliably estimated. Spectrum estimation accounting for S&A and payload, however, is not easy to determine due to their non-continuous usage. In this context, dynamic spectrum allocation becomes more important.

6.3.2 Dynamic Frequency Planning

The static frequency planning may be subject to changes due to dynamic impairments making dynamic frequency/resource planning useful. Since UAV location and status information are continuously updated through CNPC information in at least 50 ms pulses, both broker and network provider have aggregated knowledge of UAV position, range information and direction of movement. This makes it possible to apply dynamic frequency planning.

In a given deployment area, the network provider applies a reuse pattern K^* for a cell accommodating specific UAVs (e.g. SUAV). Suppose that in the deployment area are K^*J cells, where J cells are of "type" $1, 2, ..., K^*$. The number of required channels $\mathbf{G}$ at sampling instance n can be computed by $\mathbf{G}(n) = \Delta\mathbf{M}(n) - \mathbf{C}(n-1)$, where $\Delta\mathbf{M}(n)$ and $\mathbf{C}(n-1)$ are $J \times K^*$ matrices. For each considered cell, a single element of $\Delta\mathbf{M}(n)$ denotes the number of UAVs approaching the considered cell and $\mathbf{C}(n-1)$ quantifies the number of channels[39] available available in that particular cell. If an element of $\mathbf{G}(n)$ is negative (positive), then the absolute value of the element assigns how many channels are available (required). This approach can be easily applied for basic CNPC information (without S&A). For payload information, however, dynamic spectrum allocation needs to be done in a application specific

[38]This probability implicitly considers flight path, UAV start position relative to GCS and UAV range.
[39]It refers to the channels dedicated to UAVs with cell changeovers.

manner.

Channels are acquired by four different means. First, through a handoff procedure; second, the *same* channel may be continuously used during cell changeover only if neighboring cells do not utilize this particular channel. Third, additional spectrum may be acquired from the broker; fourth, (time-multiplexed) spectrum sharing (see Section 6.4) may be applied.

6.4 Spectrum Sharing Scenarios

UAV missions can be either of individual or cooperative nature. Routes are either pre-planned (point-to-point or aerial-based) or unplanned [39] (cf. Figure 6.2). Reference [13] suggests using an adaptive channel assignment approach that maximizes the overall throughput for cooperative UAVs in a master-slave topology. Due to spectrum scarcity, UAVs with throughput intensive (TI) DL communications demands (TI-UAVs) – spare time S&A video and payload data – may need to access spectrum allocated to DL S&A CNPC and/or payload on a secondary basis. In our recent work [49], we distinguish between spectrum sharing for individually and cooperatively operating UAVs (cf. Figure 6.5 (a) and (b)).

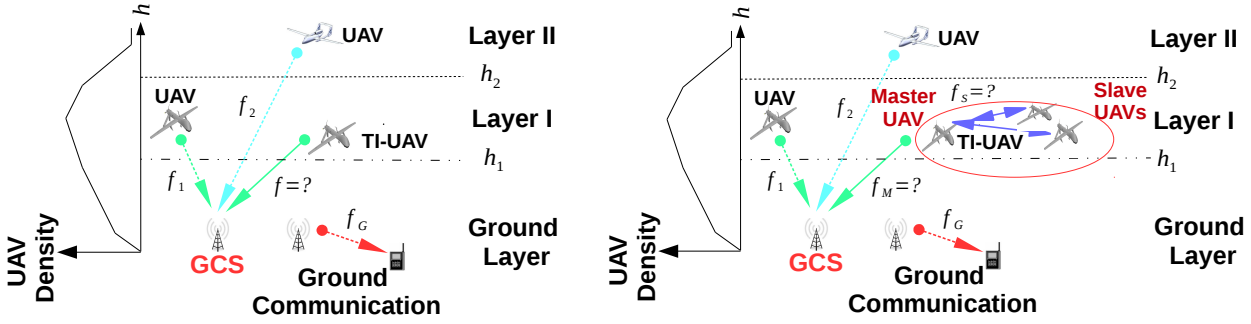

Figure 6.5: Spectrum Sharing Use Case for (a) individual and (b) cooperative UAV Missions

We discuss three spectrum sharing scenarios: The first case considers using CNPC/payload spectrum that is beeing shared by higher-tier UAVs, i.e. UAVs operating at higher altitudes than TI-UAVs. In the second case, spectrum sharing happens at the same tier or altitude either between individually operating or cooperatively operating UAVs. This case is known as *intra-tier* UAV spectrum sharing. In the third case, unused spectrum from

terrestrial communications systems can be opportunistically used for the UAV downlink. In this respect, the ground network would act as the primary user (PU) and the UAV would be the secondary user (SU). Cases 1 and 3 are summarized as *inter-tier* (UAV) spectrum sharing. The spectrum sharing scenarios 1 and 2 are *UAV-UAV spectrum sharing* cases (i.e. *intra-network cases*) that are similar in their concept. The spectrum sharing scenario 3, however, involves two networks – ground and aerial networks. It is therefore an *inter-network* spectrum sharing case.

6.5 Intra-Network UAV Spectrum Sharing

In Section 6.4, two scenarios for intra-network UAV spectrum sharing involving either the same tier or distinct tiers are identified. The first case is an intra-network, intra-tier UAV spectrum sharing case and the second case is an intra-network, inter-tier UAV spectrum sharing case. In the next two subsections, both scenarios are introduced in the way we believe they might be relevant.

If leased spectrum is underutilized, i.e. white-spaces occur for a long time, TI-UAVs can be signalled to use underutilized spectrum. This is typically not the case if a proper quasi-static frequency planning according to 6.3.1 is conducted. If a TI-UAV is using the same resource channel at the same time as any other UAV in the same cell, significant interference at the GCS is expected.

UAVs with very sophisticated autonomous capabilities may not require the transmission of DL S&A video at very high rates. The TI-UAV can in this case share the channel with an (autonomous) UAV in an alternating way through information caching and time-multiplexing. This spectrum sharing technique does require signalling overhead but is typically less complex than inter-network spectrum sharing.

6.6 Inter-Network Spectrum Sharing

In Section 6.4, we have identified one scenario for inter-network spectrum sharing involving two tier networks – ground and UAV network. The primary user network is located at the ground and the secondary network is the UAV network.

This sharing scenario makes use of the spatial availability of spectrum at the ground, the high NLoS probability (cf. Section A.3) and the augmented shadowing effect of A2G channels for low elevation angles. The ground network that is considered has to operate at a band that is being supported by UAV radios. Potential bands could be bands in the TV white space or 3.5 GHz. Identifying these bands is beyond the scope of this thesis.

The ground network should define exclusion zones with radius R_{PU}^{G}. Inside these exclusion zones, the utilization of ground frequencies should be omitted. The value of R_{PU}^{G} depends on the PU interference avoidance strategy. A database is needed to support this scenario. It has to provide information about channel usage at geographic locations, the dimension of exclusion zones and other parameters. The database needs to be frequently updated and has to be accessible to the network providers, which would then signal the available frequency and transmission time slot to the UAV.

In reference [21], a mathematical model of mobile radios accessing spectrum on a secondary basis is provided. In the following, we utilize this concept and apply it to the ground-based spectrum sharing case. The 2D density of the PU, i.e. the considered ground network, in $\mathcal{R}^2$ is λ_{PU}. In reference [21], the authors derived expressions of time-fractional channel availability for mobile SUs, such as UAVs, moving at a constant velocity v_{SU} along a a straight line in $\mathcal{R}^2$ (cf. Figure 6.6). They use an M/G/∞ queue to model the arrival process of the PUs as customers and the service time of the PUs as the elapsed time required by the SU to traverse the exclusion zone. For further details on the system model and derivations, we recommend the reader Section III.A of [21].

The expected outage period $E[O]$ (cf. Figure 6.6) equals [21]

$$E[O] = \frac{e^{\lambda_{PU}\pi(R_{PU}^{G})^2} - 1}{2R_{PU}^{G}\lambda_{PU}v_{SU}}, \tag{6.5}$$

and the expected available period $E[A]$ is [21]

$$E[A] = \frac{1}{2R_{PU}^{G}\lambda_{PU}v_{SU}}, \tag{6.6}$$

The fraction of time f_{SU}^{O} the SU is in outage can be calculated by [21]

$$f_{SU}^{O} = 1 - e^{-\lambda_{PU}\pi(R_{PU}^{G})^2}. \tag{6.7}$$

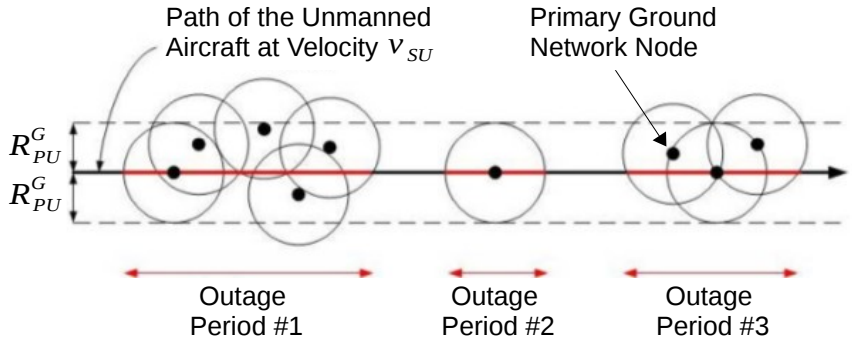

Figure 6.6: 2D Ground Spectrum Sharing Model (modified from [21]) T. X. Brown and N. M. Balasubramanya, "Dynamic Outage, Availability, and Interference Models for Mobile Cognitive Radios," in Proceedings of the Global Communications Conference, GLOBECOM 2011, 5-9 December 2011, Houston, Texas, USA, 2011, pp. 1–6. [Online]. Available: `http://dx.doi.org/10.1109/GLOCOM.2011.6134256`. Used under fair use, 2015.

Considering TV white space[40] spectrum usage for MAV ($v_{SU} = 40$ km/h) and SUAV ($v_{SU} = 120$ km/h) is impractical, because the sum of average available and outage distances[41], i.e. $(E[O] + E[A])v_{SU}$, clearly exceeds the range d_{Rg} for each UAV type. UAVs with high endurance and high speed capability (such as HALE aircrafts) might be better suited for the TV white space scenario.

Ground networks with smaller exclusion zones (e.g. $R_{PU}^{G} = 40$ km) and greater densities (e.g. $\lambda_{PU} = 2.0 \cdot 10^{-4}$ km^{-2}) than the TV white space case produce a SUAV channel availability $E[A] = 30.6$ mins and a fractional outage time of only $f_{SU}^{O} = 64.1\%$. The distance that can be covered during $E[A]$ mins lies within the range of practical SUAVs. Availability can further be increased through the use of N independent channels. In this case, the fractional availability for N channels then equals $1 - (f_{SU}^{O})^{N}$.

To make the use of ground frequencies possible, high interference power levels in exclusion zones need to be avoided. To achieve this, beam stearing will become very important. Furthermore, in the SUAV MAV case, ground networks with small exclusion zones can be utilized.

[40] We assume the existence of 168 stations for a specific channel. Using the total US area of 9.8 Mio. km^2, gives us $\lambda_{PU} = 1.7 \cdot 10^{-5}$ km^{-2}. The exclusion zone radius is fixed to $R_{PU}^{G} = 150$ km.

[41] For MAV (SUAV): $E[O] = 11.5$ h ($E[O] = 3.8$ h), $E[A] = 4.9$ h ($E[A] = 1.6$ h)

Chapter 7

Further Research

This thesis focused on UAV communications. Research in this area is very limited. The thesis conducted initial research in addressing the expected issue in spectrum scarcity.

First, the thesis determined CNPC spectrum needs based on recent estimates in UAV quantity. Spectrum needs are approximately two times higher than ITU estimates. As part of the standardization process, regulatory entities need to identify the operating bands for CNPC and payload communication. Based on band availability, contiguous or non-contiguous CNPC and payload bands may be identified.

Second, due to lack of spectrum availability, the thesis conducted preliminary research in OFDM waveforms for a SUAV and MAV communication channel. The subcarrier spacing for a SUAV and MAV communication channel has been determined. Nevertheless, much more research in suitable waveforms needs to be done. Most importantly, this is coupled with a much better understanding of UAV wideband channel modeling. The channel behavior (probably for the L- and C-band) has to be understood better at different flight phases, at distinct elevation angles and different environments. Furthermore, the impact of GCS parameters, amongst others, height, antenna pattern and channel correlation in case of antenna diversity techniques, need to be studied as well. With this knowledge, the suitability of one waveform over another can be appropriately determined. In the OFDM context, for instance, this will enable an appropriate CP length adjustment. Moreover, with this knowledge the applicability of inter-cell interference coordination techniques for the UAV context can be studied.

Third, the thesis proposes concepts for efficient spectrum management. Utilizing, a-priori information is vital for pre-allocating spectrum, particularly CNPC spectrum without S&A, on a lease basis. Dynamic spectrum allocation and spectrum sharing scenarios are corrective procedures that come into place when spectral needs differ from the a-priori planned case. Further research should find efficient algorithms for a-priori spectrum and frequency planning.

Bibliography

[1] "A Short History of Unmanned Aerial Vehicles (UAVs)," http://www.draganfly.com/news/2009/03/04/a-short-history-of-unmanned-aerial-vehicles-uavs/, accessed: 2015-01-02.

[2] "AeroVironment to Deploy Small UAS for Federal Communications Commission Post-Disaster Communications Demonstration," http://www.unmannedsystemstechnology.com/, accessed: 2014-12-03.

[3] Airspace. [Online]. Available: http://www.faa.gov/regulations_policies/handbooks_manuals/aviation/pilot_handbook/media/PHAK-Chapter14.pdf

[4] "Communication Systems/Wave Propagation," https://upload.wikimedia.org/wikibooks/en/b/b7/Surface_wave.gif, accessed: 2014-12-27.

[5] "Military UAS Applications," https://www.uavs.org/military, accessed: 2014-12-22.

[6] "Radio Horizon," http://continuouswave.com/whaler/reference/radioHorizon.html, accessed: 2014-12-07.

[7] "UAVs and ITAR: Why Range matters," http://www.wiggin.com/15501, accessed: 2015-1-7.

[8] "Unmanned Aircraft Systems," http://www.faa.gov/uas/, accessed: 2014-13-12.

[9] Video Compression Guidelines. [Online]. Available: http://vimeo.com/help/compression

[10] "Unmanned Aerial Vehicles," 2007.

[11] "CARE innovative action preliminary study on integration of unmanned aerial vehicles into future air traffic managemen," Industrieanlagen-Betriebsgesellschaft mbH, Tech. Rep., February 2011.

[12] 3GPP, 3GPP, Tech. Rep. TR 25.943, December 2004.

[13] I. Abualhaol and M. M. Matalgah, "Throughput optimization of cooperative UAVs using adaptive channel assignment," in *Wireless Communications and Networking Conference, 2006. WCNC 2006. IEEE*, vol. 4, April 2006, pp. 2279–2284.

[14] Ad Hoc Autonomy Levels for Unmanned Systems Working Group Participants, "Autonomy Levels for Unmanned Systems (ALFUS) Framework," vol. 1, no. 2, 2012.

[15] R. Adve, "Receive Diversity." [Online]. Available: http://www.comm.utoronto.ca/~rsadve/Notes/DiversityReceive.pdf

[16] A. Al-Hourani, S. Kandeepan, and A. Jamalipour, *Globecom 2014*.

[17] A. Al-Hourani, S. Kandeepan, and S. Lardner, "Optimal LAP Altitude for Maximum Coverage," *Wireless Communications Letters, IEEE*, vol. PP, no. 99, pp. 1–1, 2014.

[18] R. Austin, *Unmanned Aircraft Systems: UAVs Design, Development and Deployment*. Wiley, May 2010.

[19] J. D. Blom, "Unmanned Aerial Systems: A Historical Perspective," vol. Occasional Paper 37, September.

[20] C. Blümm, C. Heller, B. Fourestie, and R. Weigel, "Wideband aeronautical channel sounding and modeling for C-band telemetry," in *PIMRC*. IEEE, 2013, pp. 264–269.

[21] T. X. Brown and N. M. Balasubramanya, "Dynamic Outage, Availability, and Interference Models for Mobile Cognitive Radios," in *Proceedings of the Global Communications Conference, GLOBECOM 2011, 5-9 December 2011, Houston, Texas, USA*, 2011, pp. 1–6. [Online]. Available: http://dx.doi.org/10.1109/GLOCOM.2011.6134256

[22] J. Cai, W. Song, and Z. Li, "Doppler spread estimation for mobile OFDM systems in rayleigh fading channels," *IEEE Trans. Consumer Electronics*, vol. 49, no. 4, pp. 973–977, 2003. [Online]. Available: http://dx.doi.org/10.1109/TCE.2003.1261183

[23] Y. S. Cho, J. Kim, W. Y. Yang, and C. G. Kang, *MIMO-OFDM Wireless Communications with MATLAB*. Wiley, October 2010.

[24] S. T. Chung and A. Goldsmith, "Degrees of freedom in adaptive modulation: a unified view," *Communications, IEEE Transactions on*, vol. 49, no. 9, pp. 1561–1571, Sep 2001.

[25] B. Clough, "Unmanned Aerial Vehicles: Autonomous Control Challenges, A Researcher's Perspective," in *Cooperative Control and Optimization*, R. Murphey and P. Pardalos, Eds. Dordrecht/Boston: Springer, 2002, ch. 3, pp. 35–53.

[26] S. Colaner, "Google's Project Loon Reaches New Heights," http://www.tomshardware.com/news/google-project-loon-balloons-data,28176.html, accessed: 2014-12-05.

[27] K. Dalamagkidis, K. Valavanis, and L. Piegl, *On Integrating Unmanned Aircraft Systems into the National Airspace System: Issues, Challenges, Operational Restrictions, Certification, and Recommendations, Intelligent Systems, Control and Automation: Science and Engineering*, 2nd ed. Dordrecht/New York: Springer, 2012, vol. 36.

[28] S. Das, E. de Carvalho, and R. Prasad, "Performance analysis of ofdm systems with adaptive sub carrier bandwidth," *Wireless Communications, IEEE Transactions on*, vol. 7, no. 4, pp. 1117–1122, April 2008.

[29] Department of Defense, "Department of Defense Report to Congress on Future Unmanned Aircraft Systems Training, Operations, and Sustainability," Tech. Rep., April 2012.

[30] G. Dyer, T. Gilbert, S. Henriksen, and E. Sayadian, "Mobile propagation measurements using CW and sliding correlator techniques," in *Antennas and Propagation Society International Symposium, 1998. IEEE*, vol. 4, June 1998, pp. 1896–1899 vol.4.

[31] FAA, "National Airspace System Ooverview," https://www.faa.gov/air_traffic/nas_redesign/regional_guidance/eastern_reg/nynjphl_redesign/documentation/feis/appendix/media/Appendix_A-National_Airspace_System_Overview.pdf, accessed: 2015-01-03.

[32] Q. Feng, J. McGeehan, E. Tameh, and A. Nix, "Path loss models for air-to-ground radio channels in urban environments," in *Vehicular Technology Conference, 2006. VTC 2006-Spring. IEEE 63rd*, vol. 6, May 2006, pp. 2901–2905.

[33] L. Geiver, "GoogleX, GoPro, Amazon Prime Air join new sUAV Coalition," http://www.uasmagazine.com/articles/865/googlex-gopro-amazon-prime-air-join-new-suav-coalition, accessed: 2014-12-03.

[34] S. Gupta, M. Ghonge, and P. Jawandhiya, "Review of Unmanned Aircraft System (UAS)," *International Journal of Advanced Research in Computer Engineering and Technology (IJARCET)*, vol. 2, no. 4, pp. 1645–1658, 2014.

[35] S. Henriksen, "Unmanned Aircraft System Control and ATC Communications Bandwidth Requirements," NASA, Tech. Rep. 2008-214841, February 2008.

[36] J. Holis and P. Pechac, "Elevation Dependent Shadowing Model for Mobile Communications via High Altitude Platforms in Built-Up Areas," *Antennas and Propagation, IEEE Transactions on*, vol. 56, no. 4, pp. 1078–1084, April 2008.

[37] C. Howard, "UAV command, control & communications," July 2013.

[38] ITU, "World Radiocommunication Conference 2015 (WRC-15), institution = International Telecommunication Union, year = 2012," Tech. Rep.

[39] ITU, "Characteristics of unmanned aircraft systems and spectrum requirements to support their safe operation in non-segregated airspace," International Telecommunication Union, Tech. Rep. M.2171, December 2009.

[40] ITU, "Propagation data and prediction methods required for the design of terrestrial broadband radio access systems operating in a frequency range from 3 to 60 GHz," International Telecommunication Union, Tech. Rep. P.1410, February 2012.

[41] ITU-R, "Calculation of Free-Space Attenuation," International Telecommunication Union, Tech. Rep. P.525-2, September 1994.

[42] ITU-R, "Specific attenuation model for rain for use in prediction methods," International Telecommunication Union, Tech. Rep. P.838-1, October 1999.

[43] ITU-R, "Attenuation by atmospheric gases," International Telecommunication Union, Tech. Rep. P.676-5, January 2001.

[44] ITU-R, "Propagation data and prediction methods required for the design of terrestrial line-of-sight systems," International Telecommunication Union, Tech. Rep. P.530-11, January 2006.

[45] ITU-R, "Characteristics of precipitation for propagation modelling," International Telecommunication Union, Tech. Rep. P.837-6, February 2012.

[46] R. Jain and F. Templin, "Requirements, challenges and analysis of alternatives for wireless datalinks for unmanned aircraft systems," *IEEE Journal on Selected Areas in Communications*, vol. 30, no. 5, pp. 852–860, 2012. [Online]. Available: http://dx.doi.org/10.1109/JSAC.2012.120602

[47] John A. Volpe National Transportation Systems Center, "Unmanned Aircraft System (UAS) Service Demand 2015 - 2035," U.S. Department of Transportation, Tech. Rep. DOT-VNTSC-DoD-13-01, September 2013.

[48] Joint Air Power Competence Centre (JAPCC), "Strategic Concept of Employment for Unmanned Aircraft Systems in NATO," 2010.

[49] J. Kakar, V. Marojevic, and J. H. Reed, "Analysis of Spectrum Sharing for Unmanned Aerial Systems," *SDR WinnComm*, March 2015.

[50] R. Kerczewski, J. Wilson, and W. Bishop, "Frequency spectrum for integration of unmanned aircraft," in *Digital Avionics Systems Conference (DASC), 2013 IEEE/AIAA 32nd*, Oct 2013, pp. 6D5–1–6D5–9.

[51] J. Kunisch, I. de la Torre, A. Winkelmann, M. Eube, and T. Fuss, "Wideband Time-Variant Air-to-Ground Radio Channel Measurements at 5 GHz," *European Conference on Antennas and Propagation (EUCAP)*, pp. 1386–1390, April 2011.

[52] W. Lee, *Mobile Communications Design Fundamentals*, ser. Wiley Series in Telecommunications and Signal Processing. Wiley, 2010. [Online]. Available: http://books.google.com/books?id=cWIJuIqqXPQC

[53] J. Maddalon, K. Hayhurst, D. Koppen, J. Upchurch, H. Verstynen, and T. Morris, "Perspectives on Unmanned Aircraft Classification for Civil Airworthiness Standards," NASA, Tech. Rep. 23681-2199, February 2013.

[54] D. W. Matolak, "Air-Ground Channels & Models: Comprehensive Review and Considerations for Unmanned Aircraft Systems," *IEEE Aerospace Conference*, pp. 1–17, March 2012.

[55] D. W. Matolak, "AG Channel Sounding for UAS in the NAS," February 2014.

[56] M. McHenry, Y. Zhao, and O. Haddadin, "Dynamic Spectrum Access radio performance for UAS ISR missions," in *MILITARY COMMUNICATIONS CONFERENCE, 2010 - MILCOM 2010*, Oct 2010, pp. 2345–2350.

[57] Y. S. Meng and Y. H. Lee, "Measurements and Characterizations of Air-to-Ground Channel over Sea Surface at C-Band with Low Airborne Altitudes," *IEEE Transactions on Vehicular Technology*, vol. 60, no. 4, pp. 1943–1948, May 2011.

[58] J. H. W. Michael J. Luddy and A. Lackpour, "Beyond Line-of-Sight Communications with Smart Antennas (BLoSSA)."

[59] D. Moltchano, "Distance distributions in random networks," 2011.

[60] W. G. Newhall, R. Mostafa, C. Dietrich, C. R. Anderson, K. Dietze, G. Joshi, and J. H. Reed, "Wideband air-to-ground radio channel measurements using an antenna array at 2 GHz for low-altitude operations," *Military Communications Conference*, vol. 2, pp. 1422–1427, October 2003.

[61] NextGen Institute, "UAS C2 Spectrum Work Group with Industry," Tech. Rep., June 2014.

[62] R. Olsen and B. Segal, "New techniques for predicting the multipath fading distribution on VHF/UHF/SHF terrestrial line-of-sight links in Canada," *Electrical and Computer Engineering, Canadian Journal of*, vol. 17, no. 1, pp. 11–23, Jan 1992.

[63] J. Proakis, *Digital Communications*, ser. McGraw-Hill Series in Electrical and Computer Engineering. Computer Engineering. McGraw-Hill, 2001.

[64] T. S. Rappaport, *Wireless Communications: Principles and Practice*, 1st ed. Piscataway, NJ, USA: IEEE Press, 1996.

[65] M. Rice, A. Davis, and C. Bettweiser, "Wideband Channel Model for Aeronautical Telemetry," *IEEE Transactions on Aerospace and Electronic Systems*, vol. 40, no. 1, pp. 57–69, August 2004.

[66] P. E. Ross, "When will we have Unmanned Commercial Airliners?" *IEEE Spectrum*, November 2011.

[67] T. Simonite, "Air Traffic Control for Drones," *MIT Technology Review*, October 2014.

[68] R. S. Stansbury, M. A. Vyas, and T. A. Wilson, "A Survey of UAS Technologies for Command, Control, and Communication (C3)," *Journal of Intelligent and Robotic Systems*, vol. 54, no. 1-3, pp. 61–78, 2009. [Online]. Available: http://dblp.uni-trier.de/db/journals/jirs/jirs54.html#StansburyVW09

[69] M. B. Stefania Sesia, Issam Toufik, Ed., *LTE – The UMTS Long Term Revolution.* Wiley, February 2009, ch. 5, pp. 111–113.

[70] H. Thompson, "Distribution of distance to nth neighbour in a population of randomly distributed individuals," vol. 37, no. 2, p. 391394, April 1956.

[71] N. Tripathi and J. H. Reed, *Cellular Communications: A Comprehensive and Practical Guide.* New Jersey: Wiley, 2009.

[72] Unmanned Aircraft Systems Study Group (UASSG), "Command and Control (C2) link provision, link certification and requirement for Annex 10 SARPs (brainstorming)," ICAO, Tech. Rep. UASSG/10-SN No. 6, September 2012.

[73] U.S. Department of Defense, Office of the Secretary of Defense, "Unmanned systems roadmap 2007–2032." 2007.

[74] K. P. Valavanis and G. J. Vachtsevanos, *Handbook of Unmanned Aerial Vehicles.* Springer Netherlands, 2015.

[75] J.-J. van de Beek, P. O. Börjesson, P. Ödling, and S. K. Wilson, "Orthogonal frequency-division multiplexing (OFDM)," 1999.

[76] S. N. Venkatasubramanian, "Propagation channel model between unmanned aerial vehicles for emergency communications," Master's Thesis, Aalto University, January 2013.

[77] E. W. Weisstein, "Circle-Circle Intersection," http://mathworld.wolfram.com/Circle-CircleIntersection.html, accessed: 2015-2-7.

[78] W. Wilson, "Strawman design for terrestrial unmanned aircraft control links," in *Integrated Communications, Navigation and Surveilance Conference (ICNS), 2011*, May 2011, pp. K4–1–K4–11.

[79] E. Yanmaz, R. Kuschnig, and C. Bettstetter, "Achieving air-ground communications in 802.11 networks with three-dimensional aerial mobility," in *Proceedings of the IEEE INFOCOM 2013, Turin, Italy, April 14-19, 2013*, 2013, pp. 120–124. [Online]. Available: http://dx.doi.org/10.1109/INFCOM.2013.6566747

Appendix A

Large-Scale Fading

A.1 Path Loss Model in built-up Areas

In literature, various authors have two main ways of computing macroscopic A2G path loss L in dB. We call these two ways M1 and M2. On the one hand (M1), in references [16, 17, 36] for example, the idea is to describe the path loss as the sum of free space path loss (FSPL) and excessive path loss η_ϵ for distinct propagation groups ϵ, i.e. $L = L_{\mathrm{FSPL}} + \eta_\epsilon$. Or in detail for [17, 36]:

$$L = \begin{cases} L_{\mathrm{FSPL}}(d) + \underbrace{\mathcal{N}(\mu_{\mathrm{LoS}}, \sigma_{\mathrm{LoS}})}_{\eta_{\mathrm{LoS}}}, & \text{if } \epsilon = \mathrm{LoS} \\ L_{\mathrm{FSPL}}(d) + \underbrace{\mathcal{N}(\mu_{\mathrm{NLoS}}, \sigma_{\mathrm{NLoS}}) + \mathcal{N}(\mu_{\mathrm{NLoS}}(\theta), \sigma_{\mathrm{NLoS}}(\theta))}_{\eta_{\mathrm{NLoS}}}, & \text{if } \epsilon = \mathrm{NLoS} \end{cases} \tag{A.1}$$

and for [16]:

$$L = L_{\mathrm{FSPL}}(d) + \mathcal{N}(\mu_\epsilon, \sigma_\epsilon(\theta)) \tag{A.2}$$

where $L_{\mathrm{FSPL}}(d) = 20\log(d) + 20\log(f_c) + 20\log\left(\frac{4\pi}{c}\right) \approx 20\log(d_{\mathrm{km}}) + 20\log(f_{\mathrm{MHz}}) + 32.45$. $d = \frac{\Delta h}{\sin(\theta)}$ (as opposed to chapter 4) is the 3D distance between airborne and ground station. Equations (A.1) and (A.2) can easily be explained by two phases of propagation: (free-space) propagation from the airborne station to the first ground obstacle in case of NLoS and propagation from that obstacle to the ground station. In Equation (A.1), η_{LoS} does only

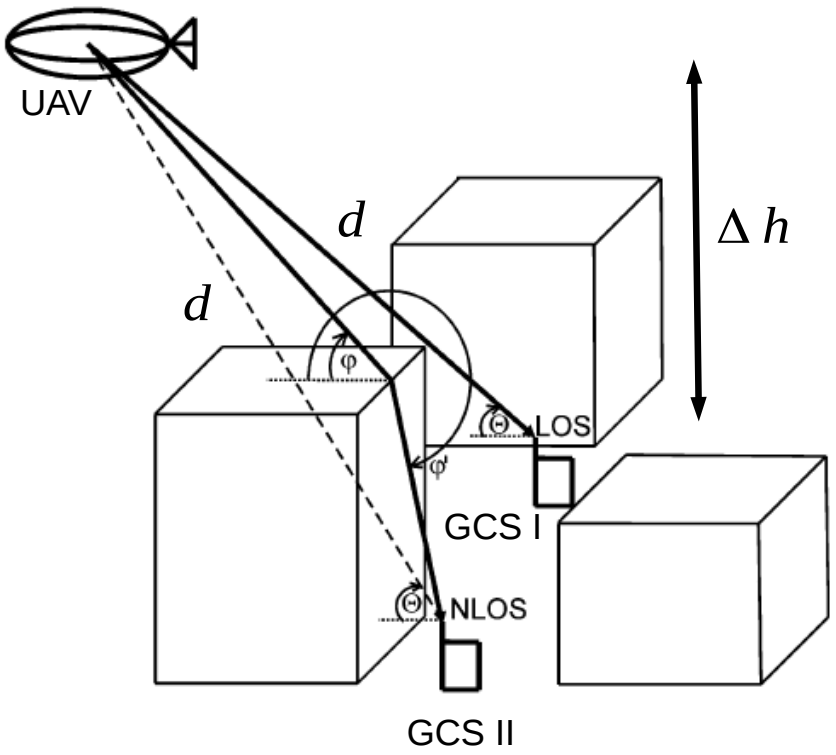

Figure A.1: Geometry of Basic LoS and NLoS Scenarios (modified from [36]) J. Holis and P. Pechac, "Elevation Dependent Shadowing Model for Mobile Communications via High Altitude Platforms in Built-Up Areas," Antennas and Propagation, IEEE Transactions on, vol. 56, no. 4, pp. 1078–1084, April 2008. Used under fair use, 2015.

account for location-based log-normal shadowing[42] and not for additional shadowing that depends on the elevation angle θ between airborne station and ground station (cf. Figure A.1).

On the other hand (M2), an other way the path loss L is simulated in [32, 57, 60, 76, 79] is the so-called log-distance path loss model, in which the path loss exponent n[43] varies for different environments. The log-distance path loss model is given by

$$L = L_{\mathrm{FSPL}}(d_0) + 10n \cdot \log\left(\frac{d}{d_0}\right) + \chi, \qquad \text{for } d \geq d_0, \tag{A.3}$$

The author of [32] uses the relationship $-10\log\big[\sin(\theta)\big] \approx -0.3115 + 0.2656e^{(90-\theta)/23.8}$ (for

[42]Log-normal shadowing is typically of zero mean, i.e. $\mu_{\mathrm{LoS}}, \mu_{\mathrm{NLoS}} \equiv 0$.

[43]Path loss exponent values depend on the environment. For example $n = 2$ for free space, $n = 2.7 - 3.5$ for urban areas and $n = 3 - 5$ for shadowed urban areas [23].

$\theta > 10°$) to approximate the path loss (without shadowing) for three distinct propagation groups ϵ^*(LoS, OLoS[44] and NLoS) at elevation angles $\theta > 10°$ as follows:

$$L = \begin{cases} L_{\text{FSPL}}(d_0) - 0.58 + 0.5496e^{(90-\theta)/24} & \text{if } \epsilon^* = \text{LoS}, \\ L_{\text{FSPL}}(d_0) + \alpha_0 + \alpha_1 e^{(90-\theta)/\beta} & \text{if } \epsilon^* = \text{OLoS}, \\ L_{\text{FSPL}}(d) + \eta_0 - \eta_1 e^{-(90-\theta)/\nu} & \text{if } \epsilon^* = \text{NLoS}. \end{cases} \tag{A.4}$$

The path loss parameters for OLoS and NLoS are given in Table A.1.

Table A.1: Parameter Values for Mean Path Loss in Equation (A.4) [32] Q. Feng, J. McGeehan, E. Tameh, and A. Nix, "Path loss models for air-to-ground radio channels in urban environments," in Vehicular Technology Conference, 2006. VTC 2006-Spring. IEEE 63rd, vol. 6, May 2006, pp. 2901–2905. Used under fair use, 2015.

	OLoS			**NLoS**		
	α_0	α_1	β	η_0	η_1	ν
$f_c = 200$ MHz	2.11	0.4125	22.07	9.08	6.4058	12.01
$f_c = 1.0$ GHz	3.76	0.3724	21.38	12.68	10.2576	7.42
$f_c = 2.0$ GHz	4.77	0.3530	21.04	15.15	12.6238	7.32
$f_c = 2.5$ GHz	5.12	0.3895	21.58	16.16	12.0436	7.52
$f_c = 5.0$ GHz	6.23	0.4787	22.65	20.43	14.6048	10.50

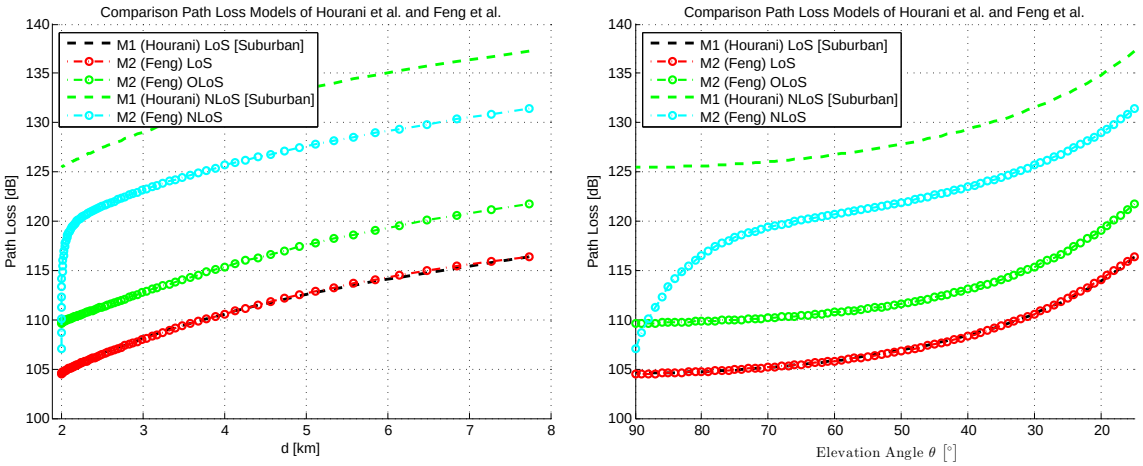

(a) Path Loss for as a Function of d_{km} (b) Path Loss for as a Function of θ

Figure A.2: Path Loss for M1 and M2 ($f_c = 2.0$ GHz, $\Delta h = d_0 = 2.0$ km)

[44]In [32], obstructed LoS (OLoS) is introduced to account for attentuation of the direct path by foliage only. In the other introduced path loss model OLoS and LoS are not differentiated.

Figure A.2 shows the path loss L as a function of the distance and the elevation angle θ ($f_c = 2.0$ GHz, $\Delta h = 2.0$ km) for M1 (using Equation (A.2)) and M2. The LoS path loss for M1 and M2 is identical. In case of M1, μ_ϵ from Hourani et al. [16] is explicitly used to calculate the (mean) path loss. M1 NLoS produces greater values for the path loss. The slope, however, in Figure A.2a for M1 and M2 NLoS is similar.

A.2 Shadowing in A2G Channels in built-up Areas

For the first path loss model in A.1, Holis et al. [36] derived a generic, frequency-dependent expression for $\mu_{\text{NLoS}}(\theta)$ and $\sigma_{\text{NLoS}}(\theta)$ applicable to HAPs[45] in built-up areas. That is:

$$\mu_{\text{NLoS}}(\theta), \sigma_{\text{NLoS}}(\theta)) = \frac{g + \theta}{h + i\theta}, \tag{A.5}$$

where values for g, h and i differ for $\mu_{\text{NLoS}}(\theta)$, $\sigma_{\text{NLoS}}(\theta)$ and different carrier frequencies. Table A.2 lists all values for g, h and i. Figure A.3 plots $\mu_{\text{NLoS}}(\theta)$ and $\sigma_{\text{NLoS}}(\theta)$ for $f_c = \{2.0, 3.5, 5.0\}$ GHz. Hourani et al. [16] uses the path loss model M1 to compute the path loss for LAPs. The shadowing model is different than that of Holis et al.. $\eta_\epsilon \sim \mathcal{N}(\mu_\epsilon, \sigma_\epsilon(\theta))$ is modeled by a *constant* mean[46] and a standard deviation

$$\sigma_\epsilon(\theta) = \vartheta_\epsilon e^{-\psi_\epsilon \theta}, \tag{A.6}$$

where the values for ϑ_ϵ and ψ_ϵ ($\epsilon = \{\text{LoS, NLoS}\}$) are given in Table II of [16]. Figure A.4 plots mean and standard deviation for suburban and urban high-rise ground environments.

For the second path loss model M2 in A.1, Feng et al. [32] uses the expression

$$\sigma_s = \rho(90 - \theta)^\gamma \tag{A.7}$$

to compute the standard deviation of random variable χ. ρ and γ values for LoS fluctuate for different frequencies and UAV altitudes (cf. Table A.3), whereas for OLoS and NLoS ρ and γ only depend on the frequency f_c (cf. Table A.4). In this case, a plot is also provided

[45] High altitude platforms (HAP) are quasi-stationary unmanned vehicles in the stratosphere at an altitude of between 17 and 22 km.

[46] The mean is constant but depends on four ground environments introduced in Section A.3 and the carrier frequency f_c. For further detail, see Table II of [16].

Table A.2: Parameter Values for Equation (A.5) [36] J. Holis and P. Pechac, "Elevation Dependent Shadowing Model for Mobile Communications via High Altitude Platforms in Built-Up Areas," Antennas and Propagation, IEEE Transactions on, vol. 56, no. 4, pp. 1078–1084, April 2008. Used under fair use, 2015.

		$0° < \theta < 10°$			$10° \leq \theta < 90°$		
		g	h	i	g	h	i
$f_c = 2.0$ GHz	$\mu_{\text{NLoS}}(\theta)$	2.55	0.0594	0.0406	-94.20	-3.44	0.0318
	$\sigma_{\text{NLoS}}(\theta)$	-12.96	-1.076	0.0780	-89.55	-8.87	0.0927
$f_c = 3.5$ GHz	$\mu_{\text{NLoS}}(\theta)$	2.70	0.059	0.0376	-92.90	-3.14	0.0302
	$\sigma_{\text{NLoS}}(\theta)$	-12.24	-1.006	0.0788	-89.06	-8.63	0.0921
$f_c = 5.5$ GHz	$\mu_{\text{NLoS}}(\theta)$	2.636	0.0554	0.0352	-92.80	-2.955	0.0285
	$\sigma_{\text{NLoS}}(\theta)$	-12.40	-0.998	0.0769	-89.54	-8.474	0.0900

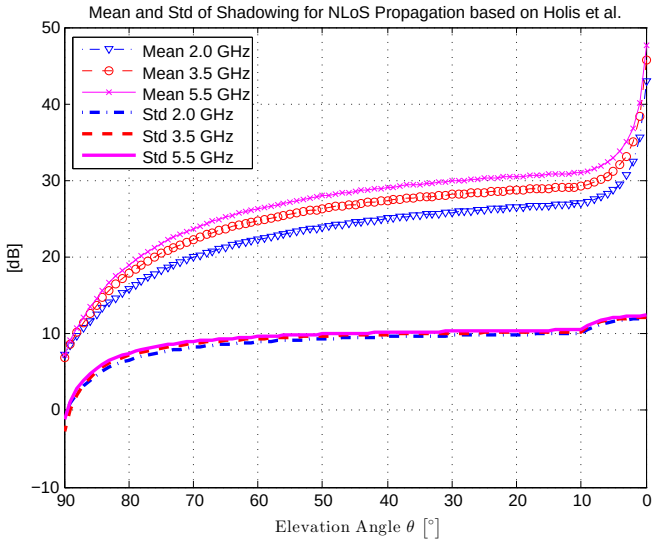

Figure A.3: Plot of $\mu_{\text{NLoS}}(\theta)$ and $\sigma_{\text{NLoS}}(\theta)$ for varying f_c

in Figure A.5.

A.3 Probability of Propagation Group

In the previous two sections, A.1 and A.2, it has been shown that both macroscopic path loss and shadowing effects differ for varying propagation groups (ϵ and ϵ^*). In case of M1, ϵ is limited to LoS and NLoS, whereas in case of M2, ϵ^* includes besides LoS and NLoS also OLoS. To determine the importance of elements of a propagation group for a given elevation angle θ_0, it is important to determine the conditional probability density function (PDF)

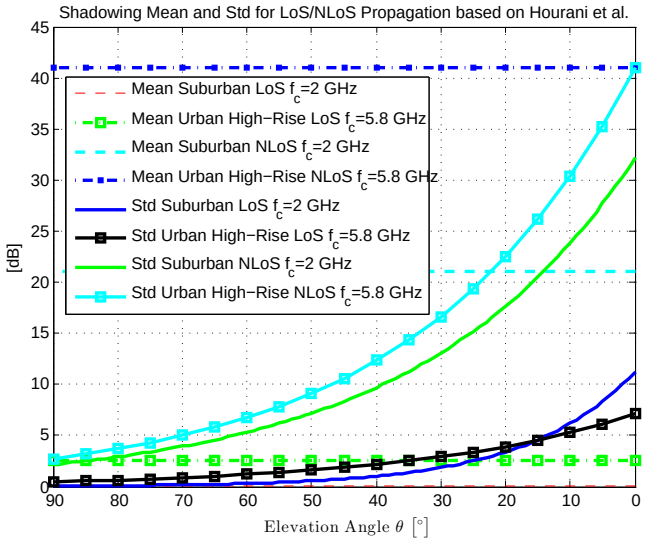

Figure A.4: Plot of μ_ϵ and $\sigma_\epsilon(\theta)$ for varying f_c and varying Ground Environments

Table A.3: Parameter Values for Equation (A.7) attributed to LoS Shadowing [32] Q. Feng, J. McGeehan, E. Tameh, and A. Nix, "Path loss models for air-to-ground radio channels in urban environments," in Vehicular Technology Conference, 2006. VTC 2006-Spring. IEEE 63rd, vol. 6, May 2006, pp. 2901–2905. Used under fair use, 2015.

Altitude	100 m		200 m		500 m		1,000 m		2,000 m	
	ρ	γ	ρ	γ	ρ	γ	ρ	γ	ρ	γ
$f_c = 200$ MHz	0.0143	0.9941	0.0153	0.9131	0.0214	0.7308	0.0418	0.4746	0.0513	0.3656
$f_c = 1.0$ GHz	0.0154	0.9751	0.0218	0.8135	0.0186	0.7512	0.0307	0.5455	0.0353	0.4730
$f_c = 2.0$ GHz	0.0187	0.9268	0.0338	0.6935	0.0375	0.5367	0.0536	0.3426	0.0499	0.2975
$f_c = 2.5$ GHz	0.0148	0.9843	0.0272	0.7475	0.0306	0.5901	0.0389	0.4256	0.0398	0.3179
$f_c = 5.0$ GHz	0.0086	1.1222	0.0140	0.8926	0.0181	0.7236	0.0184	0.6186	0.0160	0.5574

$p(\epsilon|\theta)$ and $p(\epsilon^*|\theta)$. This function permits a weight on LoS and NLoS (and OLoS for M2) propagation behavior.

Simulation results for $p(\epsilon^*|\theta)$ exist that are applicable to ground environments similar to Bristol, UK [32]. In [17, 36], the authors pursue a more flexible approach by deploying ITU-R P. 1410 [40] parameters ζ_0, ζ_1 and ζ_2 to quantify $p(\epsilon|\theta)$ for different ground environments.

Suppose the ground environment considered has a total area of A_{tot} and is given by Figure A.6. In this environment, N_b buildings with building area $A_b = b^2$ exist. Based on this configuration, ζ_0, ζ_1 and ζ_2 are defined as follows [40]:

ζ_0: Ratio of land area covered by buildings to total land area, i.e. $\zeta_0 = \frac{N_b \cdot A_b}{A_{\text{tot}}}$

Table A.4: Parameter Values for Equation (A.7) attributed to OLoS and NLoS Shadowing [32] Q. Feng, J. McGeehan, E. Tameh, and A. Nix, "Path loss models for air-to-ground radio channels in urban environments," in Vehicular Technology Conference, 2006. VTC 2006-Spring. IEEE 63rd, vol. 6, May 2006, pp. 2901–2905. Used under fair use, 2015.

	OLoS		**NLoS**	
	ρ	γ	ρ	γ
$f_c = 200$ MHz	0.3334	0.3967	0.7489	0.4638
$f_c = 1.0$ GHz	0.5568	0.3598	1.5036	0.3200
$f_c = 2.0$ GHz	0.6877	0.3619	2.1139	0.2508
$f_c = 2.5$ GHz	0.7224	0.3643	2.3197	0.2361
$f_c = 5.0$ GHz	0.8937	0.3713	2.7940	0.2259

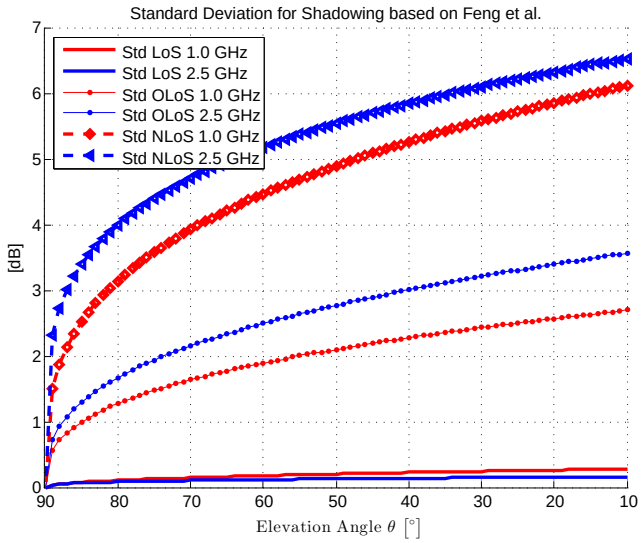

Figure A.5: Plot of σ_s for LoS, OLoS and NLoS

ζ_1: Mean number of buildings per unit area [buildings/km^2], i.e. $\zeta_1 = \frac{N_b}{A_{\text{tot}}}$

ζ_2: Scale parameter of Rayleigh distribution to describe variation in building height h. The Rayleigh pdf is given by $p(h) = \frac{h}{{\zeta_2}^2} e^{-h^2/(2{\zeta_2}^2)}$. The variable ζ_2 is the most probable building height.

In Table A.5, four environments are described ITU-R parameters ζ_0, ζ_1 and ζ_2. The considered operating environment in Bristol [32] is a 1.4 km×1.4 km area with a mean building height of $E[h] = 11.7$ m. 28% of the area is covered by buildings, i.e. $\zeta_0 = 0.28$. For that reason, this area in Bristol can be seen as an urban ground environment.

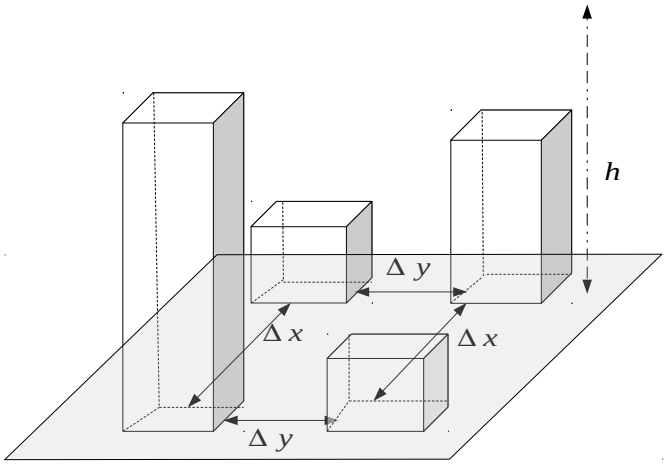

Figure A.6: Ground Environment with $N_b = 4$ Buildings

Table A.5: ITU-R Parameters for selected Environments [40] ITU, "Propagation data and prediction methods required for the design of terrestrial broadband radio access systems operating in a frequency range from 3 to 60 GHz," International Telecommunication Union, Tech. Rep. P.1410, February 2012. Used under fair use, 2015.

Environment	ζ_0	ζ_1 [buildings/km^2]	ζ_2 [m]
Suburban	0.1	750	8
Urban	0.3	500	15
Dense Urban	0.5	300	20
Urban High-Rise	0.5	300	50

Holis et al. [36] suggests to model $p(\epsilon = \text{LoS}|\theta)$, or simply $p(\text{LoS}|\theta)$, by

$$p(\text{LoS}|\theta) = c_1 - \frac{c_1 - c_2}{1 + \left(\frac{\theta - c_3}{c_4}\right)^{c_5}}, \tag{A.8}$$

where values for $c_1, ..., c_5$ are given by Table II in [36] for all four environments from Table A.5. Hourani et al., on the other hand, expresses in [17] $p(\text{LoS}|\theta)$ by the sigmoid term

$$p(\text{LoS}|\theta) = \frac{1}{1 + a_1 \cdot e^{-a_2(\theta - a_1)}}, \tag{A.9}$$

and in [16] by

$$p(\text{LoS}|\theta) = b_1\big(\theta - \theta_o\big)^{b_2} \qquad \text{for } \theta > \theta_o = 15^\circ. \tag{A.10}$$

a_1 and a_2 have been computed by Equation (5) of reference [17] (see results in Table A.6)

Table A.6: Computed Parameters a_1 and a_2 of Equation (A.8)

Environment	a_1	a_2
Suburban	5.0188	0.3511
Urban	9.6101	0.1592
Dense Urban	11.9480	0.1359
Urban High-Rise	27.1562	0.1228

and b_1 and b_2 are attainable in Table II of [16]. Note that $p(\text{NLoS}|\theta)$ is the complementary probability of $p(\text{LoS}|\theta)$, i.e. $p(\text{NLoS}|\theta) = 1 - p(\text{LoS}|\theta)$.

Figure A.7 shows a plot of $p(\text{LoS}|\theta)$ based on Equation (A.8) (dashed curves), (A.9) (solid curves) and (A.10) (solid curves with square markers) for all four selected ground environments from Table A.5.

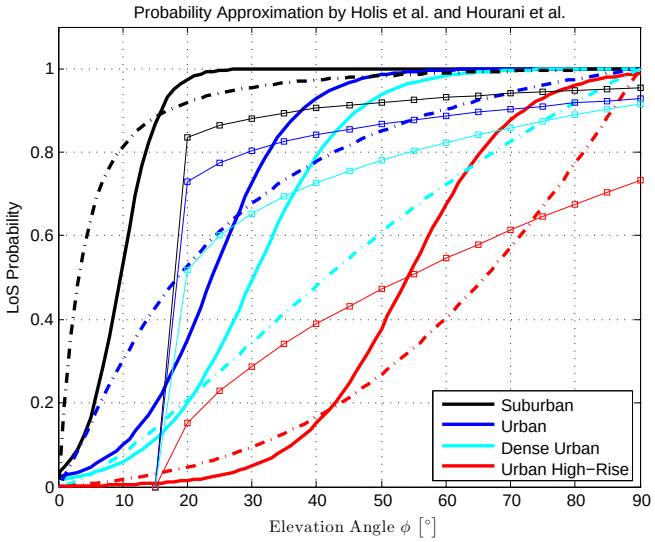

Figure A.7: $p(\text{LoS}|\theta)$ for Suburban, Urban, Dense Urban and Urban High-Rise Ground Environment

The solid curves are direct approximations of ITU-R Recommendation P.1410-2 and are more accurate than the curves with square markers. However, curves based on Equation (A.10) are rather easy to compute to determine closed-form expressions [16].